REYST

Calcite Mineral Scaling Potentials of High-Temperature Geothermal Wells

Alvin I. Remoroza

REYKJAVÍK ENERGY GRADUATE SCHOOL OF SUSTAINABLE SYSTEMS

REYST report 10-2010

Calcite Mineral Scaling Potentials of High-Temperature Geothermal Wells

Alvin I. Remoroza

Faculty of Science
University of Iceland
2010

Calcite Mineral Scaling Potentials of High-Temperature Geothermal Wells

Alvin I. Remoroza

60 ECTS thesis submitted in partial fulfillment of a
Magister Scientiarum degree in Geology (Geochemistry)

Advisor
Prof. Stefán Arnórsson

External Examiner
Ingvi Gunnarsson

Faculty of Science
School of Engineering and Natural Sciences
University of Iceland
Reykjavik, June 2010

Calcite Mineral Scaling Potentials of High-Temperature Geothermal Wells
60 ECTS thesis submitted in partial fulfillment of a *Magister Scientiarum* degree in Geology (Geochemistry)

Faculty of Science
School of Engineering and Natural Sciences
University of Iceland
Sturlugötu 7
101 Reykjavik
Iceland
Telephone: 525 4000

Bibliographic information:
Remoroza, A.I., 2010, *Calcite Mineral Scaling Potentials of High-Temperature Geothermal Wells*, Master's thesis, Faculty of Science, University of Iceland, pp. 99.

Printing: Háskólaprent ehf.
Reykjavik, Iceland, June 2010

Abstract

A comparative assessment of the calcite precipitation potential of geothermal fluids from some of the Hengill-Hellisheidi geothermal wells in Iceland, Pataan wells in Northern Negros, Philippines, and Mahanagdong wells in Leyte, Philippines are presented in this paper. The wells from these geothermal fields represent the varying characteristics of geothermal fluid discharges in different settings, ranging in composition from dilute to high salinities, and from different host rocks, i.e. basaltic and andesitic.

Water and gas analyses from the wells were used to calculate aquifer fluid compositions using the speciation program WATCH version 2.1. The total fluid enthalpy approaching that of saturated steam when the total discharge SiO_2 approaches zero and Na/K and quartz temperature analysis are taken to indicate that "excess" enthalpy is mostly caused by phase segregation in the producing aquifers of Hellisheidi, Mahanagdong and Pataan wells. Plots of Na/K versus H_2S temperatures and quartz versus H_2S temperatures of closed system and phase segregation models substantiate the conclusion that "excess" enthalpy is mostly caused by phase segregation in producing aquifer. Phase segregation model was therefore used to calculate aquifer fluid compositions.

The selected phase segregation temperature correspond to saturation vapour pressure haftway between the sampling vapour pressure and the saturation vapour pressure of the selected aquifer temperature. Selected aquifer temperature was based on quartz temperature.

The mean differences between quartz and cation geothermometers for individual wells are within 5% (13 ^oC) except for very high enthalpy wells HE29 and MG40, and for most of the Pataan wells. No wells exceeded 10% mean percentage differences. The mean percentage difference for all the wells is 4 % (11 ^oC).

Evaluation of mineral-gas equilibria indicate that H_2S aquifer fluid concentrations of Hellisheidi and Pataan wells are controlled by pyrite-pyrrhotite-magnetite or pyrite-pyrrhotite-prehnite-epidote mineral assemblage. Mahanagdong wells are systematically above the equilibrium magnetite-hematite-pyrite mineral assemblage by about 2000J/mol which is within the limit of error according to the data on enthalpy reported by Holland and Powell (1998) on these minerals. Hellisheidi's H_2 concentrations are found to be controlled by pyrite-pyrrhotite-magnetite or pyrite-pyrrhotite-prehnite-epidote mineral assemblage while Mahanagdong and Pataan are controlled by magnetite-hematite mineral assemblage. CO_2 concentrations of Hellisheidi are consistently lower than equilibrium while Mahanagdong and Pataan wells are slightly above or at equilibrium with clinozoisite-calcite-quartz-prehnite or clinozoisite-calcite-quartz-grossular mineral assemblage. One cause of the low CO_2 values at Hellisheidi may be insufficient supply of this gas to the fluid.

Aquifer fluid composition calculations show Hellisheidi's pH range is alkaline to slightly alkaline (7-7.4). Mahanagdong's pH is near neutral around 5.5 (5.3 – 5.9). Pataan wells have slightly acidic pH (4.9 – 5.6). Hellisheidi wells have higher concentrations of aqueous H2 (up to 8 ppm) compared to Mahanagdong and Pataan wells (less than 0.5 ppm). Hellisheidi wells also have higher concentrations of H2S of up to 250 ppm compared to Mahanagdong (<140 ppm) and Pataan (<200 ppm) wells. Pataan wells have the highest

CO2 concentration of up to 9700 ppm, followed by Mahanagdong with up to 5300 ppm. Hellisheidi wells are the lowest, with less than 900 ppm.

Generally, the aquifer fluids are very close to equilibrium with calcite, and when all uncertainties were considered such as analytical imprecision and selection of aquifer temperatures, departure from saturation is not significant. The average departure from calcite saturation of Hellisheidi aquifer fluids is only 0.05 SI units, Mahanagdong and Pataan are both 0.2 SI units. Well PT02 from Pataan is the most oversaturated with 0.74 SI units.

The calculated saturation index for calcite increases with increasing value of the calculated aquifer pH. This is considered to be due to error in the calculated aquifer water pH. Many factors affect the calculated pH and it is not possible to identify the main sources of apparent variation in pH and calcite saturation index but it seems to be significant, particularly in the case of Hellisheidi.

Mahanagdong and Pataan aquifer fluids approach anhydrite equilibrium whereas Hellisheidi waters are considerably anhydrite undersaturated.

The Hellisheidi waters are close to the mineral-gas equilibrium curve for the redox reactions involving pyrite, magnetite, H_2S and H_2, with an average of 0.03 log units above the curve. Mahanagdong and Pataan aquifer waters are systematically with higher H_2S/H_2 ratios than those corresponding to equilibrium, by 0.2 and 0.55 log units on average, respectively.

Hellisheidi waters are also close to mineral-gas equilibrium curve for the redox reactions involving pyrite, pyrrhotite, H_2S and H_2 yet systematically below the equilibrium curve on average by 0.25 log units. Mahanagdong and Pataan aquifer waters are systematically with higher H_2S/H_2 ratios than those corresponding to equilibrium, by 0.96 and 1.3 log units on average, respectively. Clearly the H_2S/H_2 ratios in the aquifer waters in the Philippine geothermal fields are not controlled by pyrite-pyrrhotite buffer.

An overall pattern in the variation of the saturation index (SI) with temperature upon boiling and degassing of Hellishedi wells is observed. The SI initially increases then, after it reaches a peak, decreases to negative values. The initial increase in SI reflects an increase in pH due to CO_2 and H_2S degassing. The extent of degassing increases the level of calcite SI except for degassed well HE03 which shows the opposite. This well receives degassed fluid.

The majority of the wells in Mahanagdong followed the general pattern exhibited by Hellisheidi wells except MG40, MG29, MG14, and MG03. MG40 is a high “excess” enthalpy and acidic well. MG03 and MG14 were postulated to receive fluid from the upflow zone but have been affected by brine injection returns. The reservoir chloride levels of MG03 and MG14 are shifted towards the composition of the injected brine. Well MG29, on the other hand, is located on the western periphery of the Mahanagdong geothermal system and could be affected by intrusion of cooler peripheral waters. The highest positive departure from the initial saturation in Mahanagdong is from MG19, with 0.40 (at 251 oC) SI units above the initial saturation at degassing coefficient of 1.0. MG19 is thought to deposit calcite scale in the well.

Comparing MG01 CO_2 and H_2S concentrations on samples taken in 2009 and 1994 show that they have been partially degassed or mixed with degassed injected brine. Aquifer aqueous CO_2 concentration decreased from 8000 to 1200 ppm and H_2S concentration decreased from 92 to 15 ppm. Activity of free Ca^{2+} affects calcite saturation because it increased (from 10 to 16 ppm) in 1994 to 2009 samples. Boiling of MG01 aquifer fluid sampled in 1994 produces an increase in calcite saturation of 0.51 SI units above the initial saturation which is high compared to the more recent sample with only 0.07 SI units departure from the initial saturation.

The case of well MG19 is similar with MG01, with the present fluid discharge partially degassed or mixed with injected brine and Ca2+ concentration has increased. Calcite mineral SI trend of MG19 practically remains the same after almost 15 years of production.

Pataan aquifer fluids show similar trends to those of Hellisheidi and most of the Mahanagdong wells with PT08 having the highest departure of 0.6 SI units (at 223 ^oC) above the initial saturation, followed by PT05, PT10 and PT07 with 0.40 (at 246 ^oC), 0.31(at 258 ^oC) and 0.28 (at 252 ^oC) SI units above the the initial saturation, respectively. PT05 was postulated to be nearest to the upflow region followed by PT08 and PT07. Well PT05 has the highest dissolved aqueous CO_2 concentration at 9700 ppm, followed by PT08 and PT07 at 7800 and 6700 ppm, respectively. Wells PT02 and PT04 have the lowest positive departure from the initial saturation at 0.10 (at 262 ^oC) and 0.15 (at 262 ^oC) SI units above the initial saturation, respectively.

The effect of fluid mixing particularly the injected separated water from the separators and aquifer fluids from Hellisheidi and Pataan areas were investigated. Pataan separated water is slightly acid, pH of 5.3 and higher in dissolved CO_2 than Hellisheidi. Hellisheidi separated water on the other hand is very alkaline with pH of 9.3 and has higher H_2S concentration than Pataan. Pataan separated water is being injected at temperature of 160 ^oC, which is used in both Pataan and Hellisheidi mixing simulations. The composition of the fluid mixtures were simulated using the aqueous modeling code PHREEQC-2. The mixed fluid compositions were then inputted into WATCH 2.1 to simulate boiling and degassing.

The results show that calcite saturation of the mixed fluids dropped to below the initial saturation of aquifer fluids. Increasing the separated water proportion in the mixture decreases the calcite saturation index of the mixed fluid for the case of Hellisheidi wells. In Pataan wells, however, increasing the separated water proportion in the mixture increases the calcite SI of the mixed fluid. Pataan wells and well HE11 from Hellisheidi show that mixing injected separated water by more than 30% of the initial aquifer fluids will bring the saturation to or above the initial saturation upon adiabatic boiling.

I would like to dedicate this work to my wife, Cherrie, and son, Atom, who had to endure hardship during my long absence due to my pursuit of knowledge in energy science and engineering.

Table of Contents

List of Figures

List of Tables

Acknowledgements

I would like to extend my great appreciation and deepest gratitude to…

Edda Lilja Sveinsdóttir and REYST Academic Council for giving me a chance to finish my research work despite my rather complicated situation. Special thanks to Edda Lilja for all the administrative and moral support that she unconditionally gave me.

Orkuveita Reykjavikur (Reykjavik Energy) through Einar Gunnlaugsson for funding my research work.

Ingvi Gunnarsson of Reykjavik Energy who helped in well sampling and laboratory analyses.

Prof. Behdad Moghtaderi and Elham Doroodchi of Priority Reseach Centre for Energy, The University of Newcastle, Australia, for giving considerations and allowing me to take leave of absence to finish my research in Iceland.

The management and staff of Energy Development Corporation. Special mention to Marivic Olivar for providing the Pataan well data and Erlindo C. Angcoy for providing the Mahanagdong well data as well as their indirect help through their publications and reports.

The first batch of REYST students who have been warm and accommodating and made my stay in Iceland uniquely memorable. They have been great in providing all kinds of support (moral, technical, etc.).

My supervisor, Prof. Stefan Arnórsson, not only for his useful advice but also for his patience and very kind consideration. Without his understanding and consideration, I would not have the chance to finish this research.

1 Introduction

Numerous studies on the effect of calcite formation on the operation of geothermal power plants and facilities have been published since the utilization of geothermal resources for power generation and space heating (Arnórsson, 1978, Arnórsson, 1989, Rahmani, 2007, Satman et al., 1999, Siega et al., 2005, Stáhl et al., 2000, Sanchez et al., 2005 and many others).

It is commonly known that precipitation of calcium carbonate minerals (mostly calcite and rare aragonite) is enhanced by depressurization boiling and controlled by the reaction

$$Ca^{++} + 2HCO_3^- = CaCO_{3(s)} + H_2O + CO_{2\,(aq)} \text{ or } Ca^{++} + 2HCO_3^- = CaCO_{3(s)} + H_2CO_3 \quad (1)$$

(Sanchez et al., 2005, Satman et al., 1999, Siega et al., 2005). Ultimately, however, the potential for precipitation and scaling are dependent on saturation of the initial aquifer fluid and the processes it will undergo like boiling, phase segregation, mixing, and others (Arnorsson et al., 2007).

This thesis will do comparative studies and assess the calcite precipitation potential of geothermal fluids from some of the Hengill-Hellisheidi geothermal wells in Iceland, Pataan wells in Northern Negros, Philippines and Mahanagdong wells in Leyte, Philippines.

Wells that are suspected and/or have been known to be affected by calcite scale formation are wells from Pataan and wells MG01 and MG19 from Mahanagdong. One well from Mindanao Geothermal Production Field, MD01, is also included in the pool of well data.

There are two sets of data for wells MG01 and MG19—one set is from Angcoy (2010) and the other set is from Olivar (personal comm.) which was taken before commercial production in the area. They are compared for changes in the aquifer fluid and calcite saturation after 15 years of production.

2 Geothermal Fields

Hellisheidi is a high-temperature geothermal field located in the southern sector of the Hengill central volcano in SW Iceland. It is part of the Hengill area which contains three geothermal fields, including the Nesjavellir and Hveragerdi geothermal fields, Figure 2.1 (Bjornsson et al., 2003, Franzson et al., 2005, Mutonga, 2007, Bjornsson, 2004 and many others). Geothermal systems in Iceland were classified by Bödvarsson (1961) as high and low-temperature. They have been described by Arnorsson (1995b and 1995a). Chemistry of geothermal waters in Iceland has been reported by several authors (Arnorsson, 1979, Arnórsson, 1983, Arnórsson et al., 1978, Arnórsson et al., 1983a, Arnórsson et al., 1983b, Gudmundsson and Arnórsson, 2005, Stefánsson and Arnórsson, 2002).

Pataan geothermal wells are situated in the northern part of the Negros Island in central Philippines and are part of the Northern Negros Geothermal Field (Figure 2.2). A total of 11 wells were drilled in the area, five of which have not been used for production (Olivar, 2007).

Mahanagdong is located in the southern part of the Greater Tongonan Geothermal Field in the island of Leyte, Philippines (Figure 2.3). This geothermal field is widely studied, as cited by Angcoy (2010) from exploration to exploitation and monitoring.

The wells from these geothermal fields should represent the varying characteristics of geothermal fluid discharges in different geological settings, ranging in composition from dilute to high salinities, and from different host rocks, i.e. basaltic and andesitic.

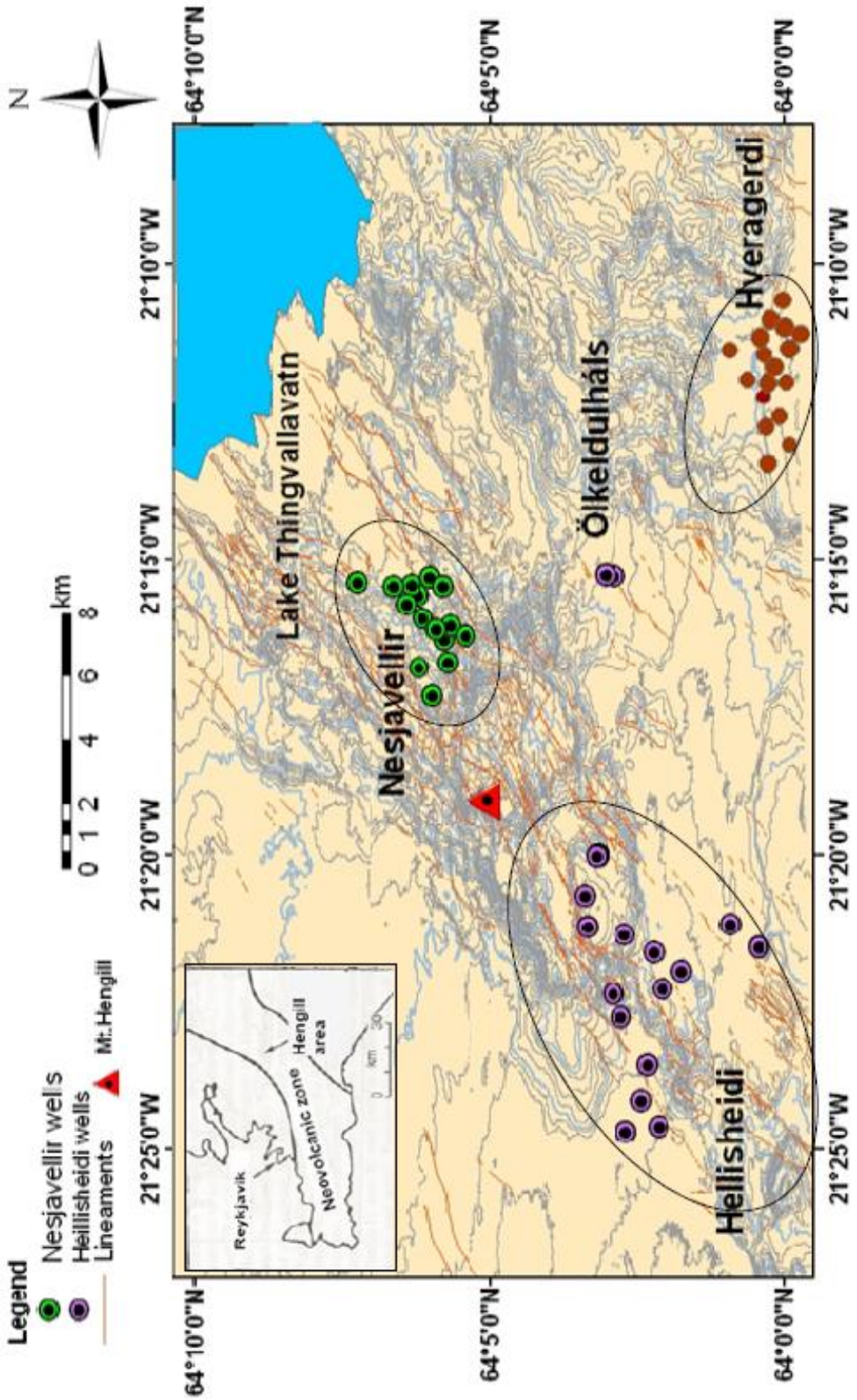

Figure 2.1 The Hengill Area showing the three high temperature geothermal fields of Hellisheidi, Nesjavellir and Hveragerdi (Mutonga, 2007).

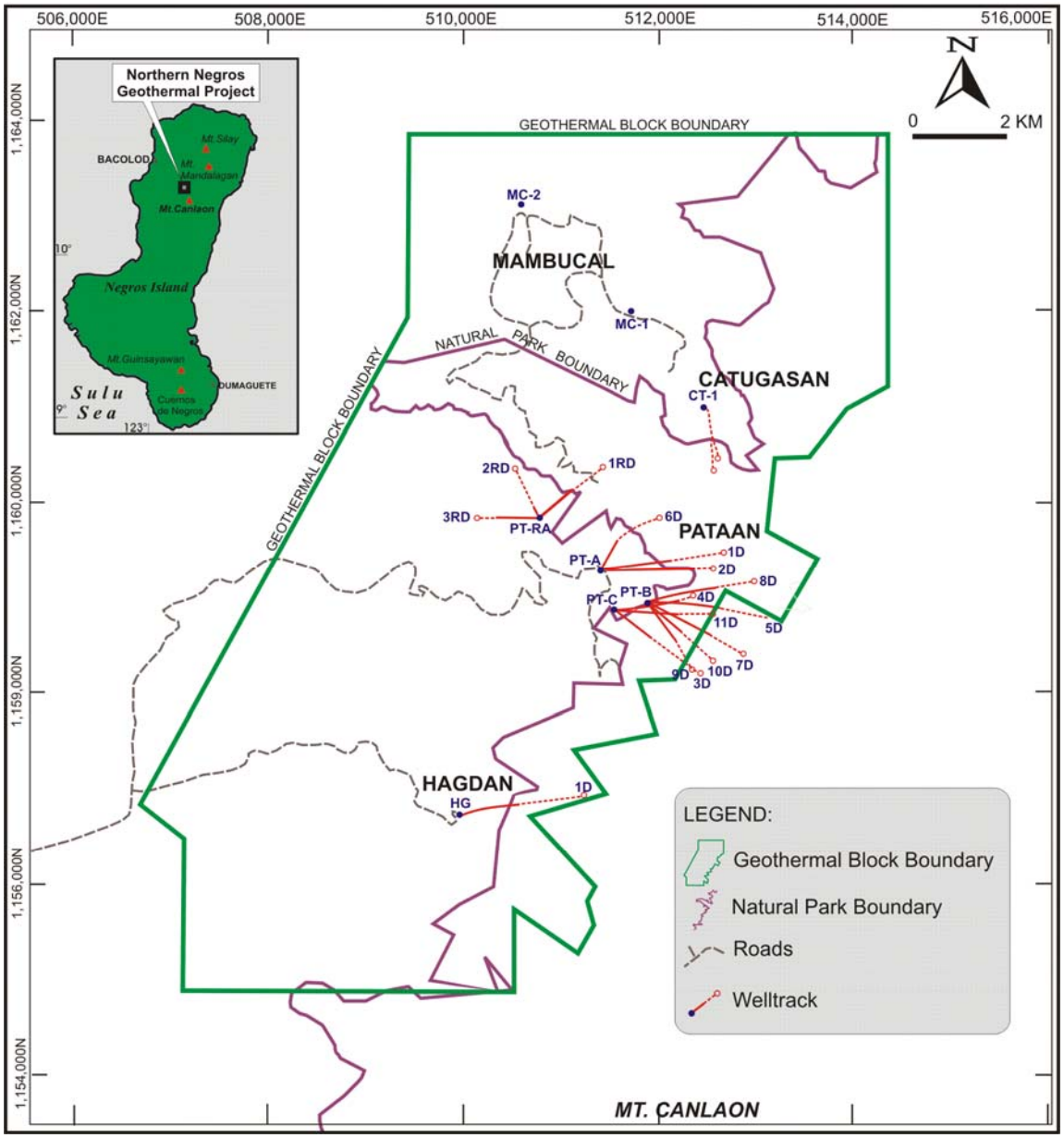

Figure 2.2 Location map of Pataan wells, Northen Negros Geothermal Field (Olivar, 2007).

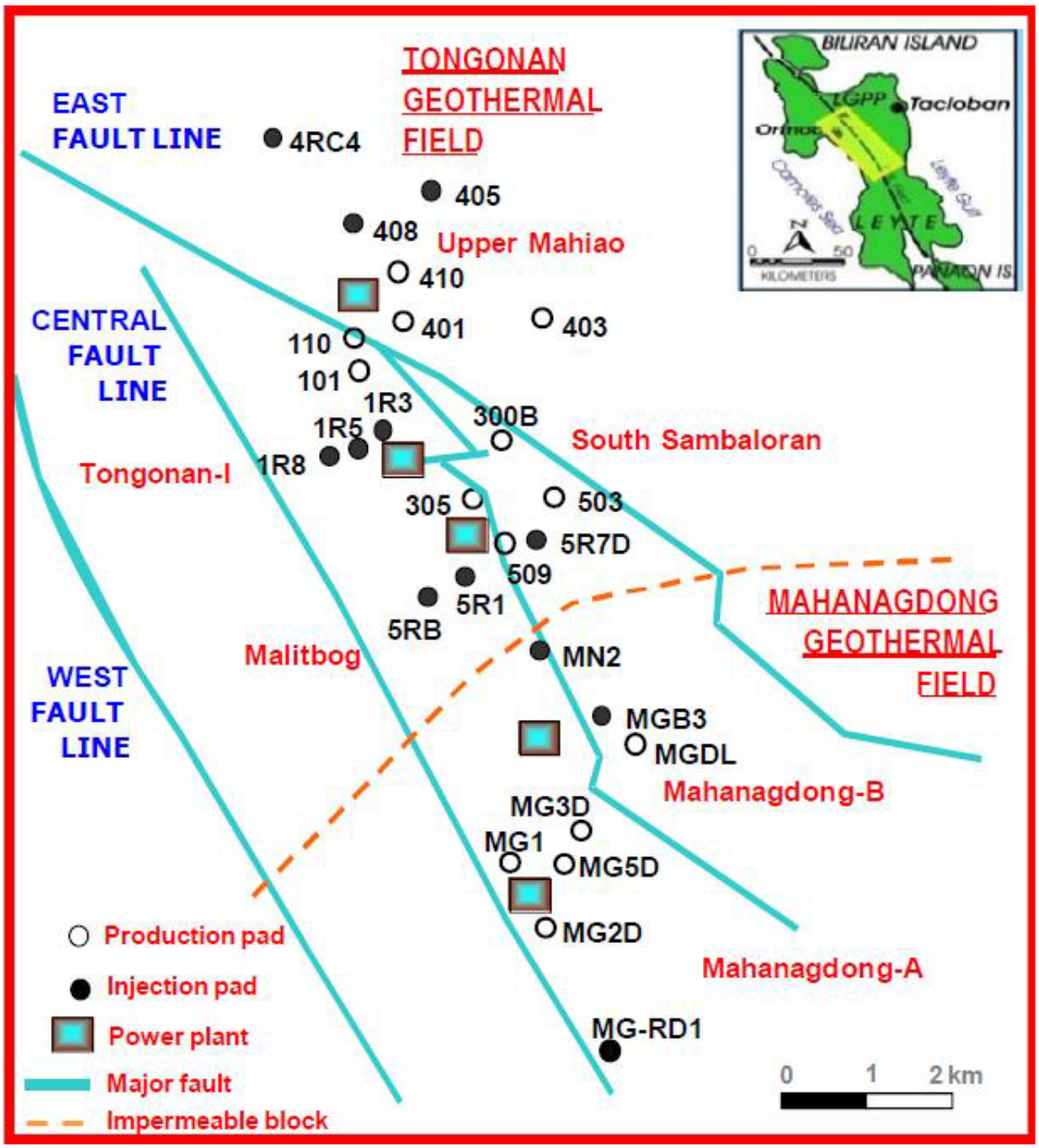

Figure 2.3 Location map of the Leyte Geothermal Production Field showing Greater Tongonan and Mahanagdong Geothermal Fields (Angcoy, 2010).

3 Sampling and Analysis

3.1 Collection of Water and Steam Samples from Wet-Steam Wells

Comprehensive water and gas sampling techniques for geothermal wells have been described by Arnorsson et al (2006) and references therein.

Webre-separator installed at the two-phase line near the wellhead was used to separate and collect steam and liquid water samples at the same sampling pressure. It was ensured that the vapor coming out of the steam outlet was dry before collecting using pre-evacuated gas bulbs.

Steam samples were collected using double-ended gas bulbs. A pre-weighed and evacuated gas bulb containing 35% NaOH solution was used to collect steam samples from the Philippine fields for non-condensible (CO_2 and H_2S are captured by the strong base) and residual gases (H_2, CH_4, Ar and N_2 occupied the head space) analyses. In the case of Hellisheidi wells, 50% v/w KOH solution was used instead of 35% NaOH. For Mahanagdong and Pataan, another gas bulb was used for collection of steam condensate for water-soluble NH_3 analysis.

CO_2 and H_2S in the hydroxide solution were analyzed by titration while the residual gases in the head space of the gas sampling bulbs were analyzed on a gas-chromatograph. NH_3 in the steam condensate was analyzed by ion-selective electrode method (Pataan and Mahanagdong wells). At Hellisheidi, CO_2 was also determined by ion chromatography.

Liquid water samples collected from the webre-separator were cooled in a stainless steel cooling coil submerged in a water bath. Generally, there were three sets of liquid water samples collected for each well depending on the sample treatments. They were filtered and air-free, filtered and acidified (5ml HNO3 to 1000 ml sample for Mahanagdong and Pataan, 0.5ml 5ml HNO3 to 1000 ml sample for Hellisheidi), and unfiltered and air-free.

For Hellisheidi and Mahanagdong wells, liquid water analyses pertinent to these studies included 1) on-site determination pH, H_2S and total carbonate carbon and 2) analysis of major elements and some minor and trace elements using Spectro Ciros^{TM} Inductively Coupled Plasma-Atomic Emission Spectrometer (ICP-AES) and Reagent Free Ion Chromatograph (RFICTM, Dionex 2000). Water analyses of Pataan wells were based from EDC laboratory procedures manual (Angcoy, 2010) which include: 1) pH by electrometric method, 2) total carbonate carbon by titration, 3) H_2S by iodometry, 4) Cl by argentometric-potentiometric method, 5) total SiO_2 by spectrophotometry (heteropoly blue), 6) metals (Na, K, Ca, Mg, Fe, Li) by Atomic Absorption Spectrometry (AAS), 7) B by titrimetry (mannitol) and 8) SO_4^{-2} by colorimetry (barium chromate/bromophenol blue).

The effect of silica polymerization on pH was reported by Gunnarsson and Arnórsson (2005) and therefore expected to have differences between *in-situ* pH measurement and laboratory result if considerable time has elapsed before measurement. The magnitude of pH differences are dependent on the weak-acids and buffers present in the fluid (Angcoy, 2010, Zhong-He and Ármansson, 2006). The comparison showed that on-site pH measurement is systematically lower by about 0.2 pH units compared with laboratory measurements for the case of Mahanagdong geothermal wells (Angcoy, 2010). The difference is considerably higher for the Hellisheidi wells.

3.2 Analytical Results

Measured discharge enthalpies and analyses of separated water from Hellisheidi, Pataan, and Mahanagdong geothermal wells are listed in Table 3.1. Separated gas analyses are listed in Table 3.2. Water and gas analyses from Hellisheidi geothermal wells are from Stefansson et al (2009), Mahanagdong wells are from Angcoy (2010) and Pataan wells are from Olivar (personal comm.). It should be noted that the separated water pH measurement from Hellisheidi and Mahanagdong wells were done on-site and pH from Pataan were measured in the laboratory. Also, water and gas samples from Hellisheidi and Mahanagdong were taken during normal production discharges of the wells whereas Pataan water and gas samples were taken before commercial production or during discharge testing of the wells.

Separated water from Hellisheidi wells are highly alkaline (8.47-9.24) while that from Pataan and Mahanagdong are slightly acidic to near-neutral. Pataan has the most saline separated water >10,000 ppm Cl, Hellisheidi has diluted water with < 500 ppm Cl and Mahanagdong in the middle with 2,000<Cl< 7,500 ppm. Dissolved H2S is high in Hellisheidi (20 – 80 ppm) compared to Mahanagdong (0.3 -2.7 ppm) and Pataan (2-10 ppm). However, dissolved CO2 in Hellisheidi (4-35 ppm) is lowest compared to Mahanagdong (17-74 ppm) and Pataan (30-68 ppm). Ca2+ concentrations in Pataan are high ranging from 490 -1050 ppm compared to Mahanagdong (8-216 ppm) and Hellisheidi (< 1 ppm)

Separated vapour from Pataan wells has the highest CO2 concentration (431-1073 mmol/kg) while Hellisheidi has the lowest concentration (10-155 mmol/kg) and Mahanagdong at the middle (132-628 mmol/kg). Hellisheidi has high H2 gas concentration (up to 34 mmol/kg) compared to Mahanagdong (< 2 mmol/kg) and Pataan (<1 mmol/kg).

Table 3.1 Measured discharge enthalpies and separated water analyses of well fluid discharges.

Well	Date	SP#	WHP^	H	pH	Temp	H_2S	CO_2	SO_4	Cl	F	SiO_2	Na	K	Ca	Mg	Fe	Al	Li	B	NH_3
		bar-g	bar-g	kJ/kg		°C	ppm	ppm	ppm	ppm	ppm	ppm	ppm	ppm	ppm	ppm	ppm	ppm	ppm	ppm	ppm
HE07	8-Oct-08	8.50	20.00	1372	9.13	17	76.09	7.38	7.54	199	1.1	659	201	32.7	0.35	0.012	0.011	1.740	0.19	1.23	
HE12	8-Oct-08	9.50	17.00	1746	8.66	19	77.42	10.98	13.71	196	1.26	816	188	35.5	0.28	0.005	0.030	1.900	0.19	1.36	
HE17	8-Oct-08	10.00	20.80	2319	8.47	17	68.03	10.55	5.52	207	1	796	177	36.2	0.27	0.002	0.009	1.680	0.17	1.47	
HE11	8-Oct-08	9.50	18.00	2047	8.74	17	55.69	22.94	8.57	158	1.08	754	168	31.8	0.17	0.001	0.024	2.030	0.15	1.04	
HE29	9-Oct-08	8.80	15.00	2399	8.71	21	57.49	11.88	3.92	104	1.89	931	128	25.7	0.23	0.002	0.005	2.170	0.18	5.92	
HE05	9-Oct-08	8.80	16.20	1194	9.24	20	37.74	33.12	19.21	77	2.08	698	157	27.9	0.32	4E-04	0.011	2.010	0.21	0.40	
HE06	10-Sep-08	9.10	17.00	1548	8.82	21	56.88	34.50	10.35	107	0.91	633	160	24.9	0.37	6E-04	0.004	1.950	0.07	0.68	
HE03	10-Oct-08	9.80	13.00	1396	8.81	19	24.28	4.28	11.43	354	0.84	670	246	45.9	0.72	3E-04	0.016	1.210	0.23	1.01	
HE18	10-Oct-08	9.40	15.20	1385	8.97	19	57.90	18.85	8.78	144	1.16	682	165	27.6	0.31	0.001	0.006	1.930	0.13	0.84	
MG40D	27-Jul-09	8.20		2265	3.98	23	0.34	17.00	73.20	7159	2.66	881	3486	983	216	17.04	227	0.770	12.1	66.40	134.00
MG39D	26-Dec-08	10.30		1195	7.07	24.4	1.98	48.00	31.80	4051	1.66	734	2421	474	22.5	0.024	0.126	0.360	8.45	57.50	3.06
MG29D	10-Jan-09	8.60		1370	7.21	22.9	2.21	26.30	56.50	3568	1.96	739	2116	440	40	0.038	0.007	0.189	7.64	32.50	6.54
MG23D	26-Dec-08	10.70		1212	6.65	22.8	1.88	43.40	47.20	3081	1.64	634	1827	333	30.3	0.022	0.251	0.393	4.69	42.90	2.85
MG22D	7-Jan-09	10.00		1163	6.56	23.8	1.22	35.10	23.90	4278	1.42	744	2464	504	39.3	0.027	0.024	0.254	8.06	59.70	2.51
MG18D	26-Dec-08	9.40		1460	6.48	23.6	2.26	40.10	61.20	3653	1.66	635	2216	351	24.1	0.029	1.722	0.377	5.7	51.30	5.17
MG16D	7-Jan-09	10.40		1379	6.08	24.3	1.45	61.50	22.20	4396	1.57	754	2551	516	38	0.033	0.014	0.354	8.38	61.70	2.80
MG14D	9-Jan-09	9.90		1438	6.4	24.1	2.05	51.80	70.50	5672	1.32	683	3232	679	94.8	0.341	0.006	0.246	10.3	54.30	11.40
MG13D	7-Jan-09	10.00		1327	6.86	24.8	2.68	61.80	123.00	3741	2.3	819	2259	467	7.6	0.017	0.133	0.362	7.69	56.80	3.93
MG07D	7-Jan-09	10.30		1177	6.27	24.1	0.42	38.30	23.70	4219	1.42	716	2424	480	40.3	0.028	0.254	0.284	7.75	58.60	2.38
MG03D	9-Jan-09	9.60		1840	6.22	23.7	1.83	55.40	70.60	3749	1.15	581	2183	369	40.4	0.236	0.002	0.222	5.84	42.10	11.40
MG01	19-Jan-09	12.80		1072	7.8	24.9	1.33	44.60	85.70	2286	1.74	560	1446	212	17.1	0.019	nil	0.517	3.93	32.10	3.54
MG19	13-Jan-09	10.40		1204	6.57	21.4	0.35	74.20	31.90	3556	1.42	696	2071	416	26.1	0.016	0.005	0.389	7.78	49.40	3.20
MD01D*	5-Jun-95	2.08	15.05	1423	7.53		6.13	72.00	112.00	6707	0.83	734	4095	500	74.5	0.14	0.080		11.9	118.95	0.64
MG01*	5-Nov-94	6.20	30.40	1133	7.59		2.22	61.06	30.70	3407	1.41	728	2058	325	13	0.12	0.120		7.03	49.56	3.21
MG19*	20-Dec-95	11.43	29.93	1193	6.81		4.26	87.12	31.03	3455	1.54	698	1907	360	14	0.07	0.100		7.84	44.54	3.86
PT02D	16-Aug-97	2.62	7.14	1114	7.18		4.77	30.20	30.60	10448	6.01	816	5901	1014	494	3.21	0.510		22.7	201.00	7.75
PT04D	8-Oct-97	4.34	4.52	1241	6.24		9.68	62.70	17.20	12049		828	6471	1139	502	2.38	0.000		22.6	213.00	9.84
PT05D	26-Jun-01	4.15	5.22	1342	6.64		9.27	67.70	29.40	18207	7.83	939	9257	1577	1056	2.03	0.800		37.5	281.00	12.70
PT07D	7-May-02	3.97	7.90	1202	6.33		4.70	60.60	24.44	13327		779	7115	1250	614	1.56	0.880			234.00	6.70
PT08D	29-Oct-02	3.31	7.20	1192	7.17		5.40	52.70	25.60	12551		789	6903	985	631	3.21	0.740		27.1	235.00	5.34
PT10D	3-Oct-05	8.70	11.30	1202	6.29		4.43	63.20	12.80	10614	6.7	773	5646	1109	432	1.69	0.290			200.00	7.00

Notes: Hellisheidi wells (prefix HE) data are from Stefansson et al (2009)
Mahanagdong wells (prefix MG) discharge chemistry data are from Angcoy (2010) if not specified
Pataan wells (prefix PT) discharge chemistry data are from Olivar (personal comm.)
pH in Hellisheidi and Mahanagdong are taken on-site unless otherwise specified
*well discharge chemistry data are from Olivar (personal comm.) and pH taken in laboratory, # Sampling pressure, ^ Well head pressure

Table 3.2 Separated gas analyses of the well fluid discharges.

Well	Date	CO_2	H_2S	Ar	N_2	CH_4	H_2	NH_3
		mmol/kg	mmol/kg	mmol/kg	mmol/kg	mmol/kg	mmol/kg	mmol/kg
HE-03	8-Oct-08	9.56	3.11	0.019	1.150	0.074	0.770	
HE-05	8-Oct-08	80.86	6.17	0.148	8.880	0.660	0.610	
HE-06	8-Oct-08	155.23	19.19	0.029	1.640	0.216	13.860	
HE-07	8-Oct-08	29.74	24.12	0.054	3.300	0.247	12.980	
HE-11	9-Oct-08	99.36	27.92	0.091	6.740	0.356	21.380	
HE-12	9-Oct-08	52.84	33.65	0.146	10.060	0.342	24.680	
HE-17	10-Sep-08	71.83	47.14	0.136	10.350	0.283	33.980	
HE-18	10-Oct-08	64.82	18.09	0.066	4.920	0.446	12.120	
HE-29	10-Oct-08	55.58	27.29	0.030	1.480	0.177	17.960	
MG40D	27Jul09	232.10	24.26	0.063	3.898	0.623	1.592	8.855
MG39D	26Dec08	226.60	4.95	0.010	0.763	0.239	0.028	2.299
MG29D	10Jan09	258.50	7.32	0.063	4.408	0.468	0.648	4.560
MG23D	26Dec08	246.95	5.45	0.027	2.012	1.579	0.343	2.024
MG22D	07Jan09	231.00	4.79	0.009	0.794	0.343	0.090	1.568
MG18D	26Dec08	331.10	11.11	0.111	10.911	0.454	0.569	3.427
MG16D	07Jan09	628.10	7.70	0.028	2.963	1.188	0.983	1.546
MG14D	09Jan09	421.85	15.57	0.012	1.345	0.545	1.016	6.325
MG13D	07Jan09	335.50	7.48	0.007	0.745	0.513	0.199	2.684
MG07D	07Jan09	177.10	4.73	0.001	0.072	0.050	0.009	1.595
MG03D	09Jan09	504.35	13.86	0.080	6.520	0.924	1.361	4.741
MG01	19Jan09	132.00	2.31	0.017	1.411	0.321	0.039	0.968
MG19	13Jan09	309.65	4.51	0.043	3.374	0.665	0.069	2.569
MD-01D*	5-Jun-95	148.21	6.72	0.002	0.113	0.003	0.042	0.303
MG-01*	5-Nov-94	508.20	7.73	0.000	0.785	0.778	0.041	1.100
MG-19*	20-Dec-95	584.65	7.66	0.127	8.235	0.826	0.072	1.667
PT-02D	16-Aug-97	794.75	9.35	0.075	9.114	3.575	0.308	9.350
PT-04D	8-Oct-97	726.00	10.40	0.056	9.147	3.919	0.253	0.000
PT-05D	26-Jun-01	623.70	15.29	0.823	64.680	3.337	0.203	1.188
PT-07D	7-May-02	430.65	8.27	0.006	1.106	0.537	0.035	0.699
PT-08D	29-Oct-02	504.46	5.96	0.424	37.143	5.105	0.221	0.677
PT-10D	3-Oct-05	1072.50	17.49	0.121	17.248	6.435	0.229	1.227

Notes: Hellisheidi wells (prefix HE) data are from Stefansson et al (2009)

Mahanagdong wells (prefix MG) discharge chemistry data are from Angcoy (2010) unless otherwise specified

Pataan wells (prefix PT) discharge chemistry data are from Olivar (personal comm.)

*well discharge chemistry data are from Olivar (personal comm.)

4 Data Handling

Separated water and gas analyses from the wells are used to infer aquifer fluid compositions with the help of a speciation program WATCH developed by Arnosson et al (1982), version 2.1 (Bjarnason, 1994).

Several models of boiling and phase segregation of aquifer fluid have been postulated to explain "excess discharge enthalpy of a geothermal well (Arnorsson et al., 2007). Plot of SiO_2 versus discharge enthalpy is shown in Figure 4.1 for all the wells considered in this study. If the aquifer temperature is fairly constant, the plot showing discharge enthalpy approaching that of saturated steam when SiO_2 approaches zero indicates that the excess discharge enthalpy can be explained by phase segregation rather than conductive heating of the fluid by host rock (Arnorsson et al., 2007). The use of geothermometers to validate phase segregation model are discussed in the succeeding sections.

In phase segregation model, one has to choose the temperature at which water and steam segregate. In this study, the phase segregation temperature is calculated as the saturation temperature of the phase segregation vapour pressure. Segregation pressure is calculated as the midpoint between the sampling pressure and the saturation vapour pressure of the selected aquifer temperature. Selected aquifer temperature is based on quartz solubility data according to Gunnarsson and Arnorsson (2000). The procedure is somewhat iterative as one is to assume first the aquifer temperature then check if one will get comparable quartz geothermometer temperature from the calculated aquifer fluid composition. One must then adjust the selected aquifer temperature appropriately and calculate for the new segregation pressure until the selected aquifer temperature equals quartz geothermometer temperature.

The calculation of the aquifer fluid composition was done in two-step run by the speciation program WATCH. Separated water and gas analyses, measured discharge enthalpy and measured pH were used in the first WATCH run which use arbitrary reference temperature equal to the segregation temperature.

The output of the first WATCH run was then used as input in the second WATCH run. The segregation pressure was set as the sampling pressure and pH was the output from the first run with the corresponding temperature equal to the segregation temperature. Flowing fluid enthalpy was set to liquid enthalpy at the selected aquifer temperature. The model reference temperature was then set to the selected aquifer temperature. The output of the second WATCH run is the calculated aquifer fluid composition assuming liquid enthalpy at the aquifer.

Fluid mixing of the aquifer fluids with injected mixed brine will be simulated using geochemical model PHREEQC (Parkhurst and Appelo, 1999) using the graphical windows interface developed by Vincent Post (http://www.falw.vu/~ posv/ phreeqc/index.html). The mixed fluid is then inputted into WATCH for simulations of boiling and degassing.

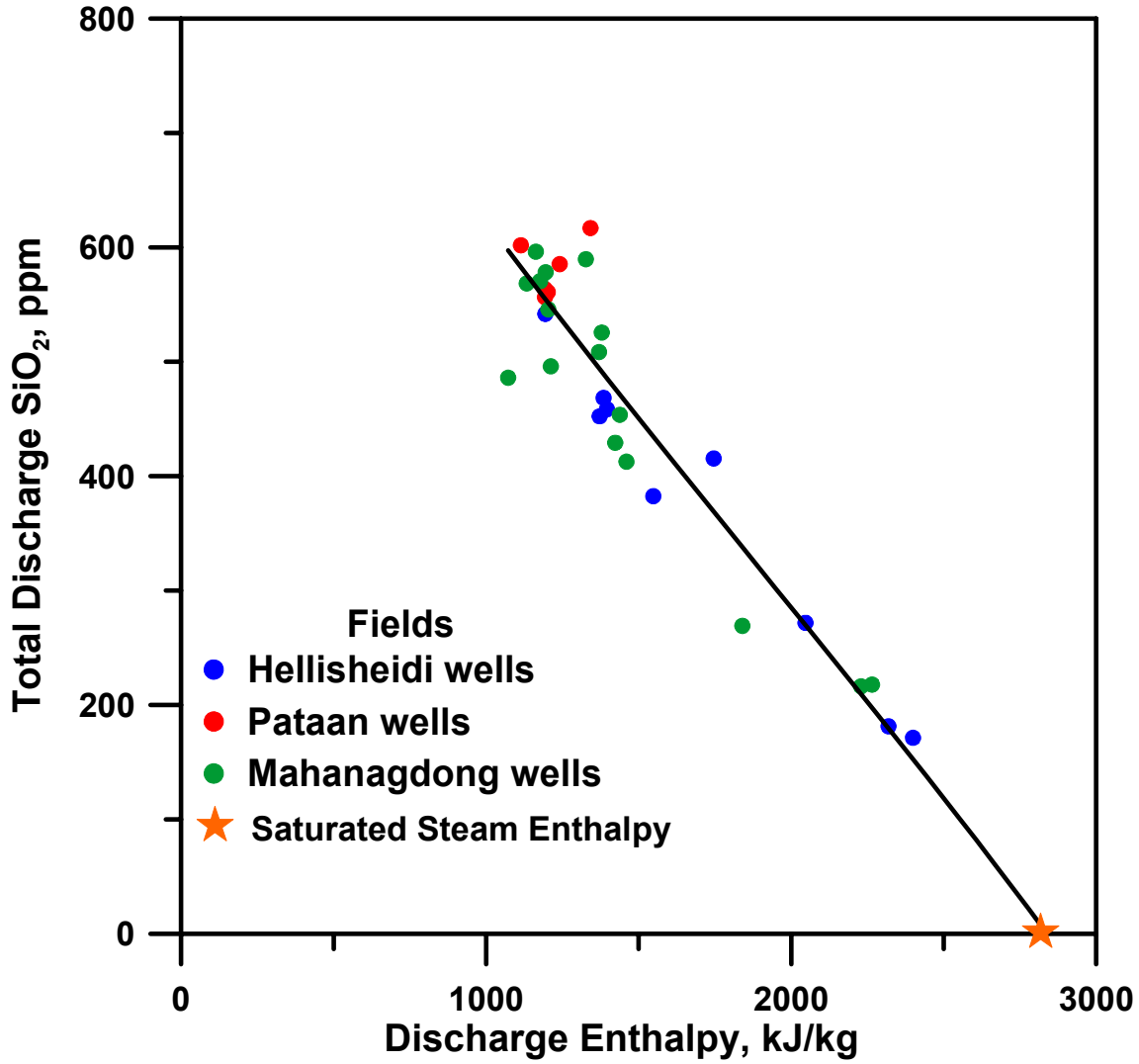

Figure 4.1Total discharge SiO_2 as function of total discharge enthalpy. As the concentration of SiO_2 approaches zero, the total discharge enthalpy approaches that of saturated steam, suggesting that the initial aquifer fluid undergoes phase segregation before entering production wells

4.1 Aquifer Temperatures

Na/K versus quartz equilibrium temperatures of the wells using the closed system and phase segregation models (model 2 and 3 of Arnorsson et al (2007), respectively) are shown in Figure 4.2. Na/K and quartz temperature agree well in the phase segregation model while Na/K temperatures are generally higher than quartz for the closed system model. Based from this observation and the plot from Figure 4.1 it is taken to indicate that "excess" enthalpy is mostly caused by phase segregation in the producing aquifers of Hellisheidi, Mahanagdong and Pataan wells; thus, phase segregation model is used to calculate aquifer compositions.

Arnorsson (2010, unpublished work) formulated a new Na/K geothermometer for Icelandic waters which is used to calculated Na/K temperatures for Hellisheidi wells,

$$T_{NaK} = 757 - 780.208X + 374.098X^2 - 91.985X^3 + 8.874X^4 \quad (2)$$

Where $$X = \log\left(\frac{Na}{K}\right) \quad (3)$$

Na = mole Na, K = mole K

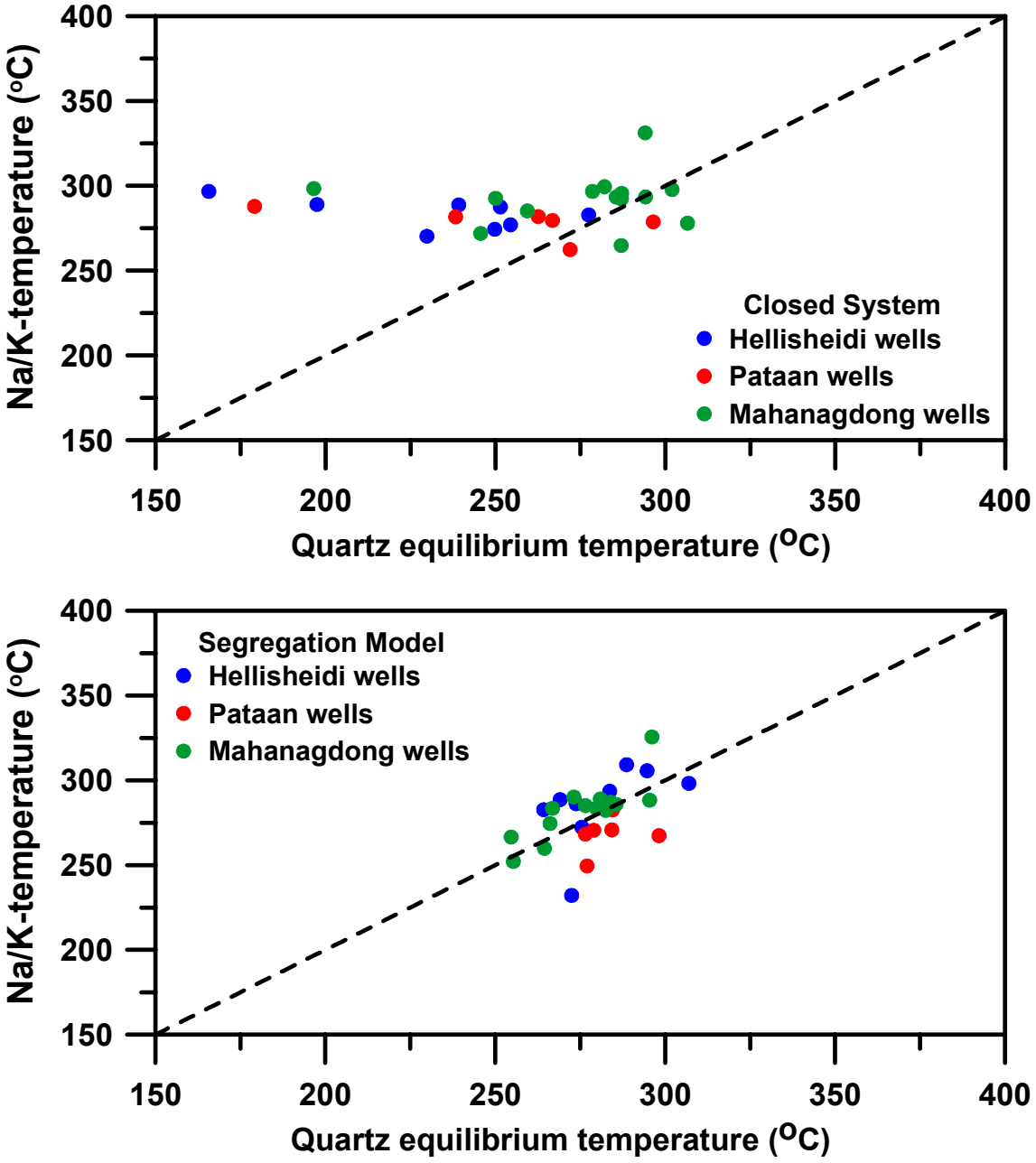

Figure 4.2 Na/K versus quartz equilibrium temperatures according to the closed system model (above) and phase segregation model (below).

Table 4.1 summarizes the results of geothermometer temperatures based on the calculated aquifer composition calculated using the phase segregation model. The mean

percentage differences for quartz and cation geothermometers for individual wells were within 5% except for very high enthalpy wells HE29 and MG40 and for most of the Pataan wells (note that the pH are not taken *in-situ*). No wells exceeded 10% mean percentage differences. The mean percentage difference for all the wells is 4 %. The mean standard deviation of calculated geothermometer temperatures for the wells is 11 ^{o}C. The mean difference between the selected aquifer temperature and quartz geothermometer temperature is less than 1%.

Table 4.1 Aquifer temperatures based on quartz, cation and H_2S geothermometers.

Well	Date	$T_{selected}$	T_{QTZ} *	T_{NaK_A} **	T_{NaK_G} ^	T_{NAK_F} ^^	T_{NaKCa_TF} ^^^	T_{AVE}	Stdev	M#	m##	T_{H2S}
						°C						°C
HE03	10-Oct-08	270	272	279	288	277	261	275	10	3.60	0.74	232
HE05	9-Oct-08	275	275	273	283	272	256	272	10	3.62	0.00	272
HE06	10-Sep-08	265	264	257	270	258	246	259	9	3.44	0.38	283
HE07	8-Oct-08	267	269	263	274	263	251	264	9	3.27	0.75	289
HE11	8-Oct-08	282	284	281	289	279	271	281	7	2.38	0.71	294
HE12	8-Oct-08	292	295	280	289	278	266	282	11	3.93	1.02	306
HE17	8-Oct-08	288	289	291	297	287	271	287	10	3.37	0.35	309
HE18	10-Oct-08	272	274	266	277	265	254	267	9	3.35	0.73	286
HE29	9-Oct-08	303	307	288	295	285	263	288	16	5.61	1.31	298
MG40	27Jul09	301	296	321	331	326	287	312	19	6.21	1.68	332
MG39	26Dec08	283	283	272	292	282	279	282	7	2.61	0.00	300
MG29	10Jan09	282	281	279	298	289	273	284	10	3.40	0.36	301
MG23	10Jan09	268	266	263	285	274	263	270	9	3.50	0.75	290
MG22	26Dec08	284	284	277	297	287	276	284	9	2.99	0.00	305
MG18	07Jan09	267	264	247	272	260	260	261	9	3.47	1.13	302
MG16	26Dec08	286	286	276	296	286	276	284	8	2.97	0.00	303
MG14	07Jan09	275	273	280	299	290	274	283	11	3.92	0.73	316
MG13	09Jan09	295	295	278	298	288	296	291	8	2.74	0.00	311
MG07	07Jan09	280	280	273	293	284	273	281	8	2.96	0.00	298
MG03	07Jan09	258	255	254	278	267	258	262	10	3.81	1.17	300
MG02	09Jan09	269	267	273	293	283	274	278	10	3.67	0.75	296
MG01	19Jan09	257	255	239	265	252	249	252	10	3.79	0.78	267
MG19	13Jan09	277	277	275	295	285	275	281	9	3.09	0.00	291
MD01	5-Jun-95	260	261	220	249	235	241	241	15	6.37	0.38	261
MG01	5-Nov-94	272	275	247	272	260	265	264	11	4.26	1.10	282
MG19	20-Dec-95	278	275	266	288	277	276	277	8	2.80	1.08	275
PT02	16-Aug-97	277	277	256	280	268	251	266	13	4.75	0.00	303
PT04	8-Oct-97	283	284	259	282	271	255	270	13	4.85	0.35	292
PT05	26-Jun-01	298	298	255	279	267	252	270	19	6.96	0.00	305
PT07	7-May-02	279	279	259	282	271	255	269	12	4.44	0.00	286
PT08	29-Oct-02	276	277	236	262	249	239	253	17	6.74	0.36	276
PT10	3-Oct-05	284	285	272	293	283	263	279	12	4.20	0.35	305
Mean									10.85	3.97	0.53	

*T_{QTZ}-quartz geothermometer by Arnorrson (2000)

**Na-K geothermometer by Arnorsson et (1998); for Hellisheidi geothermometer by Arnorsson (2010, unpublished work)

^Na-K geothermometer by Giggenbach et al (1983)

^^Na-K geothermometer by Fournier(1979)

^^^Na-K-Ca geothermometer by Fournier and Truesdell (1973)

Mean percentage difference of quartz and cation geothermometers

mean percentage difference between the selected aquifer temperature and quartz geothermometer

Tselected is the selected aquifer temperature used in the calculation of liquid aquifer composition

Tave is the average geothermometer temperatures

Stdev is the standard deviation of the calculated geothermometer temperatures

T_{H2S} is the H_2S equilibrium temperature

4.2 Mineral Assemblage-H_2S Equilibria

Equilibrium constants derived by Arnórsson et al. (2010), as cited by Angcoy (2010), for several mineral assemblages that potentially could control the concentrations of H_2S, H_2 and CO_2 in the aquifer fluid are listed in Table 4.2. Also shown in Table 4.2 are the respective reactions and temperature equations for the equilibrium constants. The equilibrium constants were derived from thermodynamic data on oxide and silicate minerals as given by Holland and Powell (1998), but those on pyrite and pyrrhotite minerals by Robie and Hemmingway (1995). Data on the dissolved gases were retrieved from data on Henry's Law coefficients given by Fernandez-Prini et al (2003) and the pure gases according to Robie and Hemingway (1995).

Figure 4.3 shows the concentrations of H_2S as plotted against equilibrium reaction curves that could potentially control its concentration in the aquifer fluid. H_2S aquifer fluid concentrations of Hellisheidi and Pataan wells are controlled by pyrite-pyrrhotite-magnetite mineral assemblage (reaction 4 in Table 4.2). One well from Hellisheidi (HE03) was significantly below the curve but was found to be highly degassed. Hellisheidi aqueous H_2S concentrations can also be controlled by pyrite-pyrrhotite-prehnite-epidote mineral assemblage (reaction 1). The data points of Mahanagdong wells are systematically above the equilibrium magnetite-hematite-pyrite mineral assemblage (reaction 5), by about 2000J/mol. According to the data on enthalpy reported by Holland and Powell (1998) on these minerals, it is within the limit of error. Temperatures have been calculated for the two H_2S mineral equilibria in Table 4. Na/K versus H_2S temperatures and quartz versus H_2S temperatures of closed system and phase segregation models were plotted in Figures 4.4 and 4.5, respectively. Both plots show scattered data for closed system model. It also show, however, that H_2S temperatures are systematically higher than quartz temperatures on the phase segregation model but they agree well nonetheless. The results for the three areas substantiate the conclusion that "excess" enthalpy is mostly caused by phase segregation in producing aquifer.

H_2 aquifer fluid concentrations of all wells are plotted in Figure 4.6. Hellisheidi's H_2 aquifer fluid concentrations are controlled by pyrite-pyrrhotite-magnetite (reaction 9) or pyrite-pyrrhotite-prehnite-epidote (reaction 6) mineral assemblage. Mahanagdong and Pataan H_2 aquifer fluid concentrations on the other hand are controlled by magnetite-hematite mineral assemblage (reaction 10).

Hellisheidi CO_2 concentrations are consistently lower than equilibrium while Mahanagdong wells are slightly above or at equilibrium with the mineral assemblage clinozoisite-calcite-quartz-prehnite or clinozoisite-calcite-quartz-grossular (Figure 4.7). One cause of the low CO_2 values at Hellisheidi may be insufficient supply of this gas to the fluid.

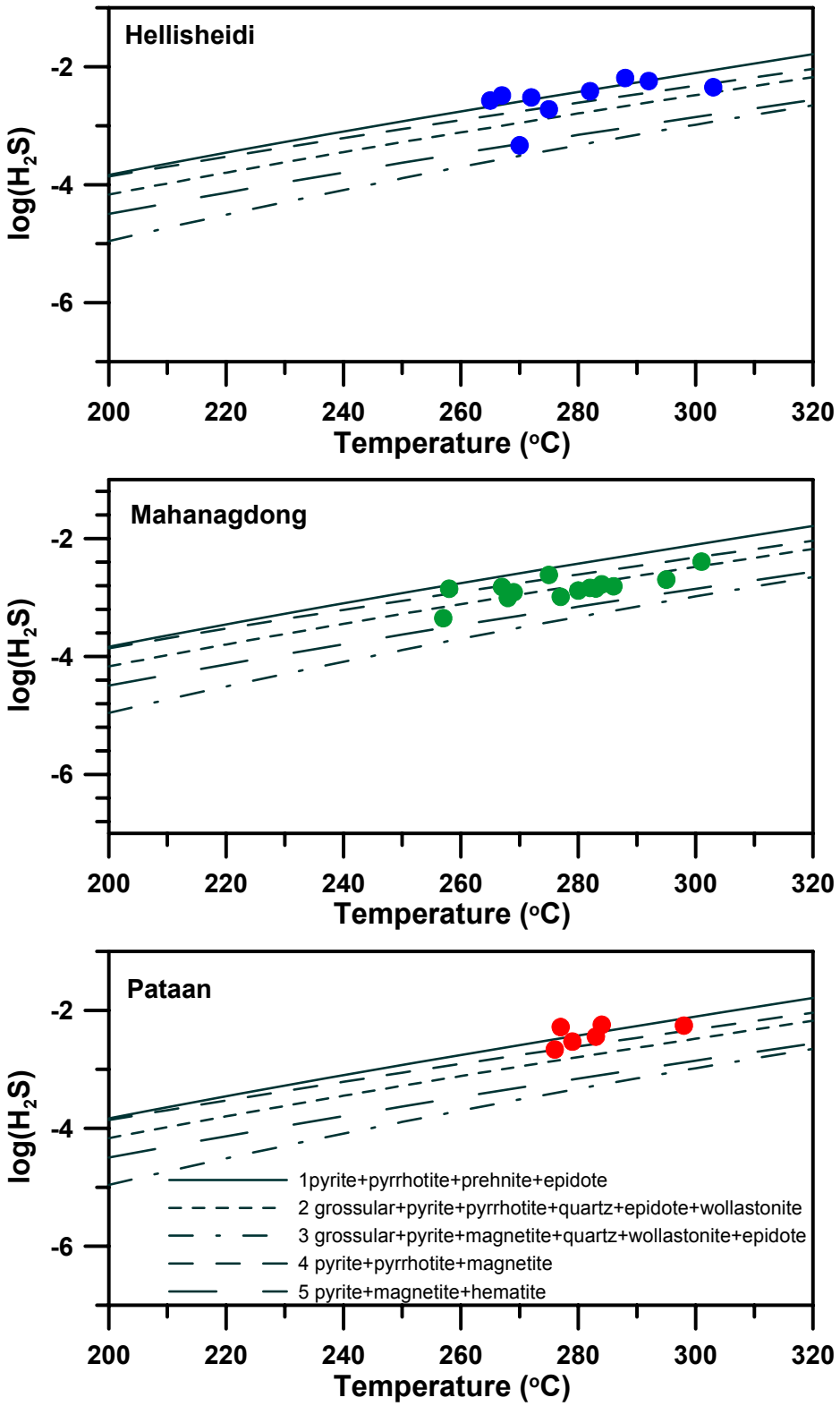

Figure 4.3 Aquifer fluid concentrations of H_2S in Hellisheidi, Mahanagdong, and Pataan wells. The equilibrium curve numbers refers to the reactions in Table 4.2.

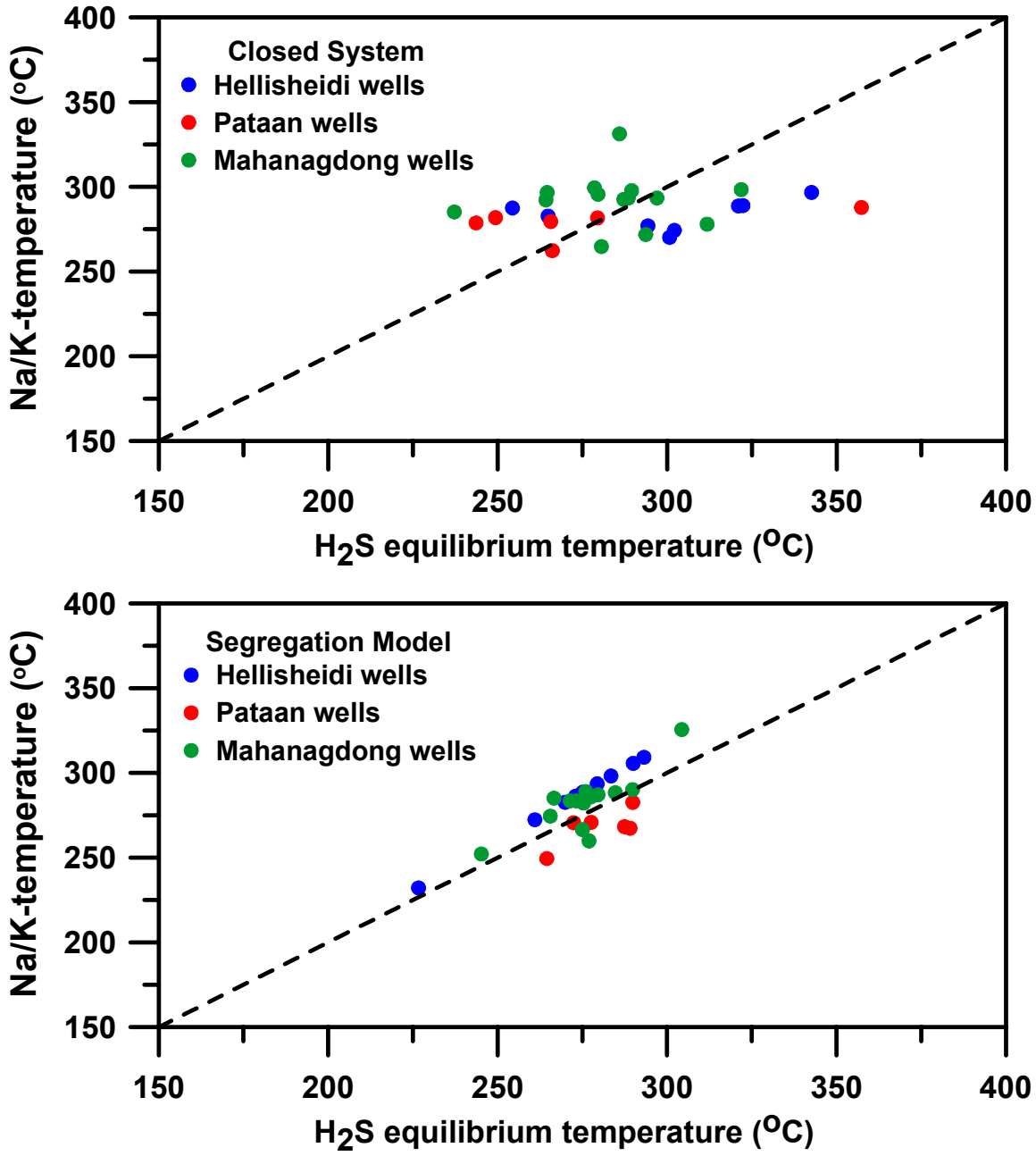

Figure 4.4 Na/K versus H_2S equilibrium temperatures of a closed system model (above) and phase segregation model (below).

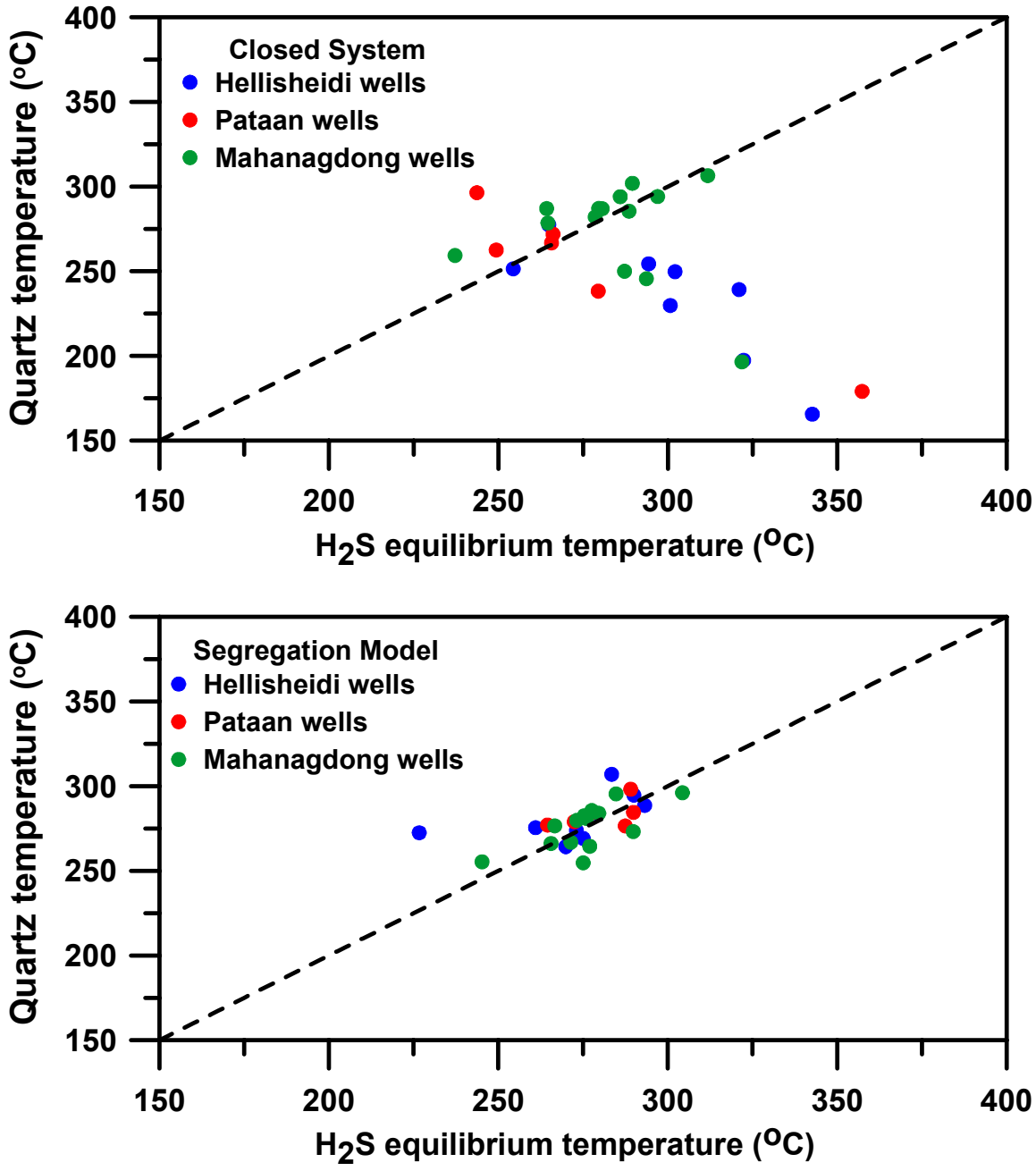

Figure 4.5 Quartz versus H_2S equilibrium temperatures of a closed system model (above) and phase segregation model (below).

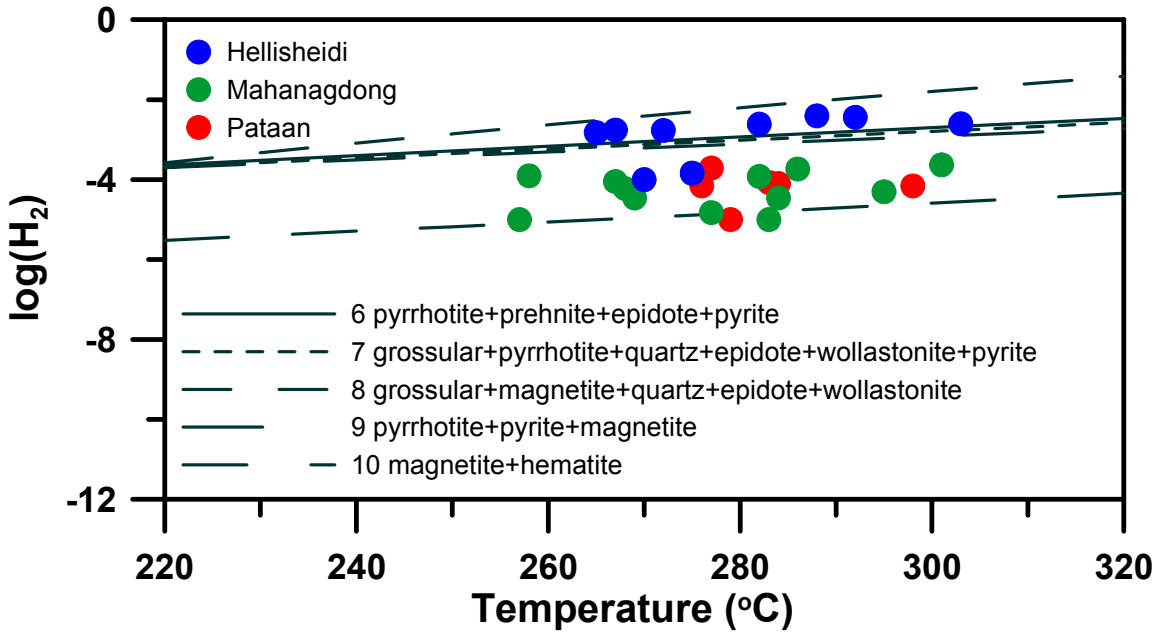

Figure 4.6 Aquifer fluid H_2 concentrations in Hellisheidi, Mahanagdong, and Pataan wells. The equilibrium curve numbers refers to the reactions in Table 4.2.

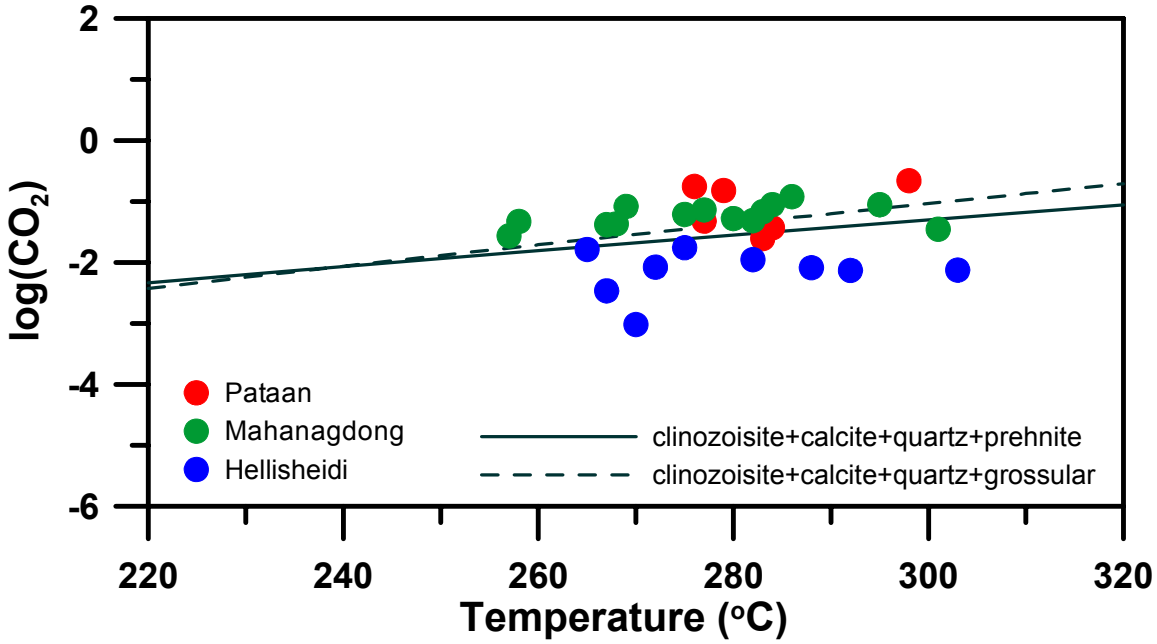

Figure 4.7 Aquifer fluid CO_2 concentrations in Hellisheidi, Mahanagdong, and Pataan wells.

Table 4.2 Reactions and log K-temperature equations for equilibrium constants for pure minerals (Karingith et ali, 2010)[a]

1	H_2S:	$\frac{1}{3}pyr + \frac{1}{3}pyrr + \frac{2}{3}pre + \frac{2}{3}H_2O_l \leftrightarrow \frac{2}{3}epi + H_2S_{aq}$	$log[H_2S] = 13.608 + \frac{592324}{T^2} - \frac{9346.7}{T} - 0.043552T + 2.9164x10^{-5}T^2 + 5.139logT$
2	H_2S:	$\frac{2}{3}gro + \frac{1}{3}pyr + \frac{1}{3}pyrr + \frac{2}{3}qtz + \frac{4}{3}H_2O_l \leftrightarrow \frac{2}{3}epi + \frac{2}{3}wol + H_2S_{aq}$	$log[H_2S] = 13.659 + \frac{555082}{T^2} - \frac{9256.6}{T} - 0.04361T + 2.861x10^{-5}T^2 + 5.148logT$
3	H_2S:	$2gro + \frac{1}{4}pyr + \frac{1}{2}mag + 2qtz + 2H_2O_l \leftrightarrow 2epi + 2wol + H_2S_{aq}$	$log[H_2S] = -0.836 - \frac{216659}{T^2} - \frac{2847.3}{T} + 0.008524T - 2.366x10^{-6}T^2 + 0.152logT$
4	H_2S:	$\frac{1}{4}pyr + \frac{1}{2}pyrr + H_2O_l \leftrightarrow \frac{1}{4}mag + H_2S_{aq}$	$log[H_2S] = 13.589 + \frac{590215}{T^2} - \frac{9024.5}{T} - 0.044882T + 2.978x10^{-5}T^2 + 5.068logT$
5	H_2S:	$\frac{1}{2}pyr + \frac{1}{2}mag + H_2O_l \leftrightarrow hem + H_2S_{aq}$	$log[H_2S] = 35.516 - \frac{4156.9}{T} + 0.01267T - 13.914logT$
6	H_2:	$\frac{4}{3}pyrr + \frac{2}{3}pre + \frac{2}{3}H_2O_l \leftrightarrow \frac{2}{3}epi + \frac{2}{3}pyr + H_{2aq}$	$log[H_2] = -1.643 - \frac{110535}{T^2} - \frac{802.06}{T} - 4.184x10^{-4}T + 7.574x10^{-6}T^2 - 0.56logT$
7	H_2:	$\frac{2}{3}gro + \frac{4}{3}pyrr + \frac{2}{3}qtz + \frac{4}{3}H_2O_l \leftrightarrow \frac{2}{3}epi + \frac{2}{3}wol + \frac{2}{3}pyr + H_{2aq}$	$log[H_2] = -1.546 - \frac{138877}{T^2} - \frac{769.11}{T} - 4.872x10^{-4}T + 6.932x10^{-6}T^2 - 0.528logT$
8	H_2:	$6gro + 2mag + 6qtz + 4H_2O_l \leftrightarrow 6epi + 6wol + H_{2aq}$	$log[H_2] = 1.444 - \frac{273812}{T^2} - \frac{3962.1}{T} + 2.401x10^{-3}T + 1.304x10^{-6}T^2 + 0.979logT$
9	H_2:	$\frac{3}{2}pyrr + H_2O_l \leftrightarrow \frac{3}{4}pyr + \frac{1}{4}mag + H_{2aq}$	$log[H_2] = -1.572 - \frac{168874}{T^2} - \frac{232.45}{T} - 3.0275x10^{-3}T + 9.517x10^{-6}T^2 - 0.652logT$
10	H_2:	$2mag + H_2O_l \leftrightarrow 3hem + H_{2aq}$	$log[H_2] = 824.146 + \frac{3212081}{T^2} - \frac{51505}{T} + 0.11297T - 294.895logT$
11	CO_2:	$czo + cal + \frac{3}{2}qtz + H_2O_l \leftrightarrow \frac{3}{2}pre + CO_{2aq}$	$log[CO_2] = -0.89 + \frac{7251.5}{T^2} - \frac{1710.6}{T} + 4.188x10^{-3}T + 2.683x10^{-6}T^2 - 0.064logT$
12	CO_2:	$\frac{2}{5}czo + cal + \frac{3}{5}qtz \leftrightarrow \frac{3}{5}gro + \frac{1}{5}H_2O_l + CO_{2aq}$	$log[CO_2] = -1.449 - \frac{40536}{T^2} - \frac{2135.9}{T} + 6.5639x10^{-3}T + 2.725x10^{-6}T^2 - 0.193logT$

a-The equations for the reaction 5 and 10 are from the present study cal:calcite, czo:clinozoisite, epi:epidote, gro:grossular, mag:magnetite, pre:prehnite, pyr:pyrite, pyrr:pyrrhotite, qtz:quartz, wol:wollastonite

5 Aquifer Fluid Compositions

Aquifer fluid compositions of individual wells are shown in Table 5.1. The initial aquifer fluid compositions were calculated using geochemical speciation program WATCH version 2.1 and the model used is the open system phase segregation model.

The pH of wells from Hellisheidi is higher than Mahanagdong and Pataan. Hellisheidi's pH range is alkaline to slightly alkaline (7-7.4). Mahanagdong's pH is near neutral around 5.5 (5.3 – 5.9) except for MG40 (pH =4.3) which is a very high enthalpy well. MG40 could be affected by steam condensates or other acidic fluids as it also has the highest concentration of Fe and Mg in Mahanagdong. Pataan wells have slightly acidic pH (4.9 – 5.6).

Hellisheidi wells have higher H_2 aquifer fluid concentrations (up to 8 ppm) compared to Mahanagdong and Pataan wells (less than 0.5 ppm). Hellisheidi wells also have higher H_2S aquifer fluid concentrations of up to 250 ppm compared to Mahanagdong (<140 ppm) and Pataan (<200 ppm) wells. Pataan wells have the highest CO_2 aquifer fluid concentration of up to 9700 ppm followed by Mahanagdong with up to 5300 ppm and Hellisheidi wells have the lowest with less than 900 ppm.

Pataan's Ca^{2+} concentrations are high at 320-680 ppm compared to Mahanagdong (6-148 ppm) and Hellisheidi (0.13-0.58 ppm).

Table 5.1 Aquifer fluid composition based on the phase segregation model.

Well	Date	Temp*	pH	B	SiO_2	Cl	Na	K	Mg	Ca	F	SO_4	Al	Fe	CO_2	H_2S	NH_3	H_2	CH_4	N_2
		°C		ppm																
HE03	8-Oct-08	270	7.43	0.80	532	281	195	36	0.000	0.58	0.67	9.09	0.961	0.013	60	28		0.20	0.15	4.20
HE05	8-Oct-08	275	7.01	0.31	542	60	122	22	0.000	0.25	1.61	14.90	1.56	0.009	873	80		0.29	2.55	59.81
HE06	8-Oct-08	265	6.83	0.54	506	86	128	20	0.001	0.29	0.73	8.28	1.559	0.003	805	110		3.02	0.37	4.96
HE07	8-Oct-08	267	7.19	0.98	522	158	159	26	0.010	0.39	0.87	5.97	1.378	0.009	190	162		3.49	0.53	
HE11	9-Oct-08	282	7.00	0.78	566	119	126	24	0.001	0.13	0.81	6.44	1.524	0.018	541	156		4.91	0.65	21.46
HE12	9-Oct-08	292	7.15	1.00	597	143	138	26	0.004	0.20	0.92	10.04	1.391	0.022	365	235		7.28	0.80	41.06
HE17	10-Sep-08	288	6.98	1.07	580	151	129	26	0.002	0.20	0.73	4.02	1.225	0.007	393	253		7.94	0.53	33.46
HE18	10-Oct-08	272	7.07	0.67	536	113	130	22	0.001	0.25	0.91	6.91	1.518	0.005	431	133		3.42	1.00	19.22
HE29	10-Oct-08	303	7.28	4.01	630	70	87	17	0.001	0.16	1.28	2.65	1.468	0.003	366	182		5.02	0.39	5.72
MG40	27-Jul-09	301	4.33	45.31	601	4885	2379	671	11.628	147.40	1.82	49.95	0.525	189	1540	138	131.24	0.47	1.44	15.83
MG39	26-Dec-08	283	5.80	44.08	563	3106	1856	363	0.019	17.25	1.27	24.38	0.276	0.097	3012	49	11.96	0.02	0.03	6.50
MG29	10-Jan-09	282	5.53	24.54	558	2694	1598	332	0.029	30.21	1.48	42.66	0.143	0.005	2152	50	22.79	0.24	1.38	22.79
MG23	10-Jan-09	268	5.71	34.66	512	2489	1476	269	0.017	24.48	1.33	38.13	0.318	0.203	1910	34	8.83	0.12	4.34	9.66
MG22	26-Dec-08	284	5.43	45.50	567	3261	1878	384	0.021	29.95	1.08	18.22	0.194	0.018	3927	57	8.80	0.07	2.21	8.92
MG18	7-Jan-09	267	5.61	40.96	507	2916	1769	280	0.023	19.24	1.33	48.86	0.301	1.374	1852	52	14.45	0.18	0.90	37.50
MG16	26-Dec-08	286	5.33	46.79	572	3334	1934	391	0.025	28.81	1.19	16.84	0.268	0.011	5293	53	8.15	0.37	3.56	15.52
MG14	7-Jan-09	275	5.44	42.49	534	4438	2529	531	0.267	74.18	1.03	55.17	0.192	0.005	2719	83	30.19	0.29	1.24	53.42
MG13	9-Jan-09	295	5.92	41.57	599	2738	1653	342	0.012	5.57	1.68	90.01	0.265	0.097	3933	69	15.16	0.10	2.16	5.48
MG07	7-Jan-09	280	5.51	45.39	555	3268	1878	372	0.022	31.22	1.10	18.36	0.22	0.197	2326	45	8.27	0.01	0.25	60.55
MG03	7-Jan-09	258	5.41	34.37	474	3060	1782	301	0.193	32.98	0.94	57.64	0.181	0.002	2083	49	20.05	0.25	1.34	16.50
MG02	9-Jan-09	269	5.35	41.73	515	2992	1722	341	0.026	23.57	1.32	22.94	0.268	0.116	3665	42	9.20	0.07	3.24	8.93
MG01	19-Jan-09	257	5.56	27.31	476	1945	1230	180	0.016	14.55	1.48	72.92	0.44	0.118	1213	15	5.92	0.02	1.04	7.94
MG19	13-Jan-09	277	5.75	38.68	545	2784	1621	326	0.013	20.43	1.11	24.98	0.312	0.004	3239	36	12.20	0.03	2.50	22.15
MD01	5-Jun-95	260	6.14	80.37	496	4531	2767	338	0.095	50.33	0.56	75.67		0.054	1171	46	1.57	0.02	0.02	0.55
MG01	5-Nov-94	272	5.51	36.68	539	2521	1523	241	0.088	9.62	1.04	22.72		0.089	7988	92	8.26	0.03	4.54	7.98
MG19	20-Dec-95	278	5.63	34.43	540	2671	1487	278	0.054	10.82	1.19	23.99		0.077	6864	71	9.78	0.04	3.54	55.91
PT02	16-Aug-97	277	5.57	134.18	545	6975	3940	677	2.143	329.80	4.01	20.43		0.341	2147	180	65.42	0.39	36.41	161.81
PT04	8-Oct-97	283	5.25	51.71	568	8265	4439	781	1.632	344.37	0.00	11.80		0	1094	123	6.94	0.17	20.84	84.86
PT05	26-Jun-01	298	4.95	181.58	607	11766	5982	1019	1.312	682.41	5.06	19.00		0.517	9677	189	7.21	0.14	18.78	635.37
PT07	7-May-02	279	4.86	161.72	552	9210	4917	864	1.078	424.35	4.36	16.87		0.608	6675	101	8.63	0.02	3.05	10.91
PT08	29-Oct-02	276	4.91	160.89	546	8593	4726	674	2.197	432.02	0.00	17.52		0.507	7799	74	7.56	0.14	28.78	365.58
PT10	3-Oct-05	284	5.49	147.14	569	7808	4154	816	1.244	317.81	0.00	9.42		0.213	1659	196	11.53	0.16	35.61	166.52

*Selected aquifer temperature

5.1 Classification of Geothermal Waters

Chloride-bicarbonate-sulfate ternary diagram (Giggenbach, 1991) of all the wells under study is shown in Figure 5.1. The plot shows that Hellisheidi wells are distributed between peripheral water and mature water while most of Mahanagdong and Pataan wells are halfway towards the mature water type.

Na-K-Mg ternary diagram of the wells in Figure 5.2 shows that they are discharging partially mixed/equilibrated to fully equilibrated waters with respect common hydrothermal minerals (Giggenbach, 1988).

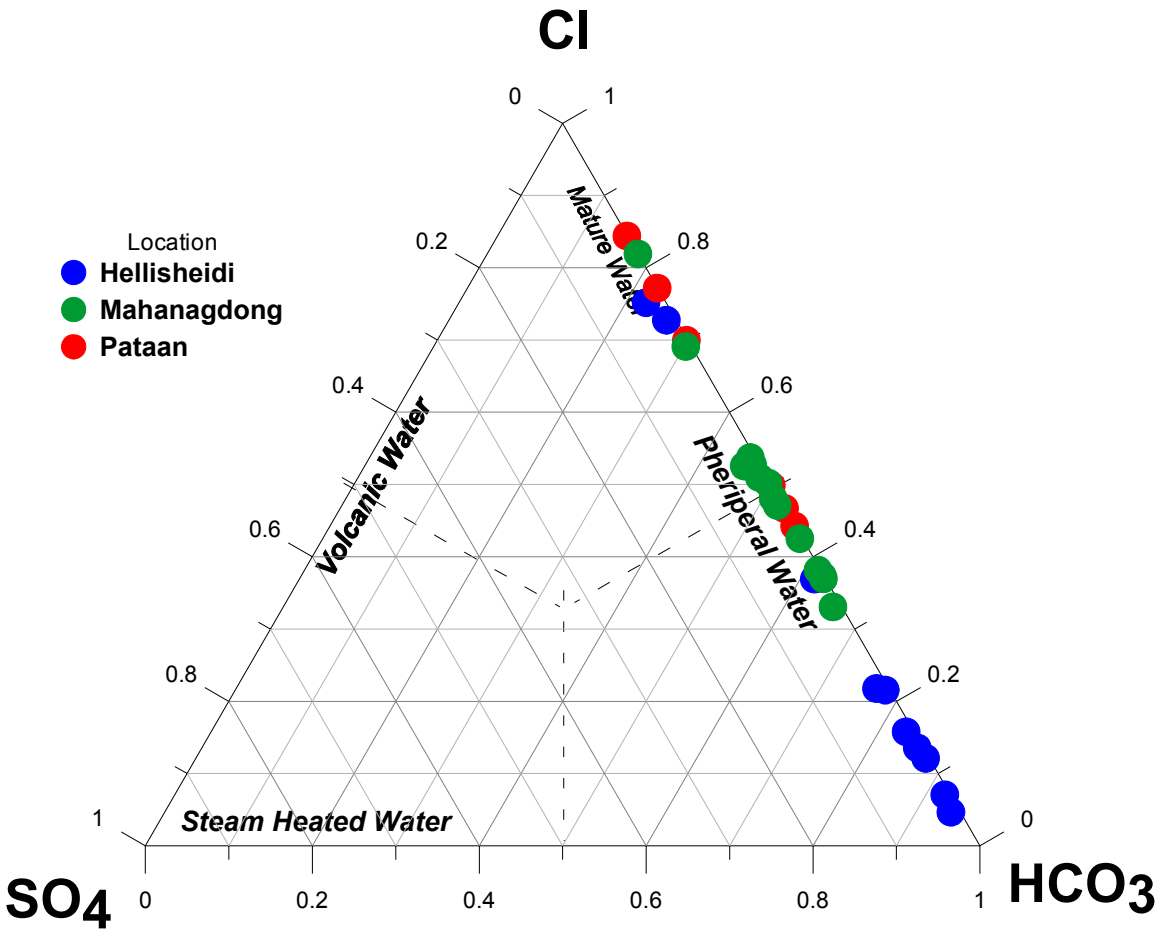

Figure 5.1 Cl-HCO_3-SO_4 ternary diagram of waters from Hellisheidi, Mahanagdong and Pataan wells.

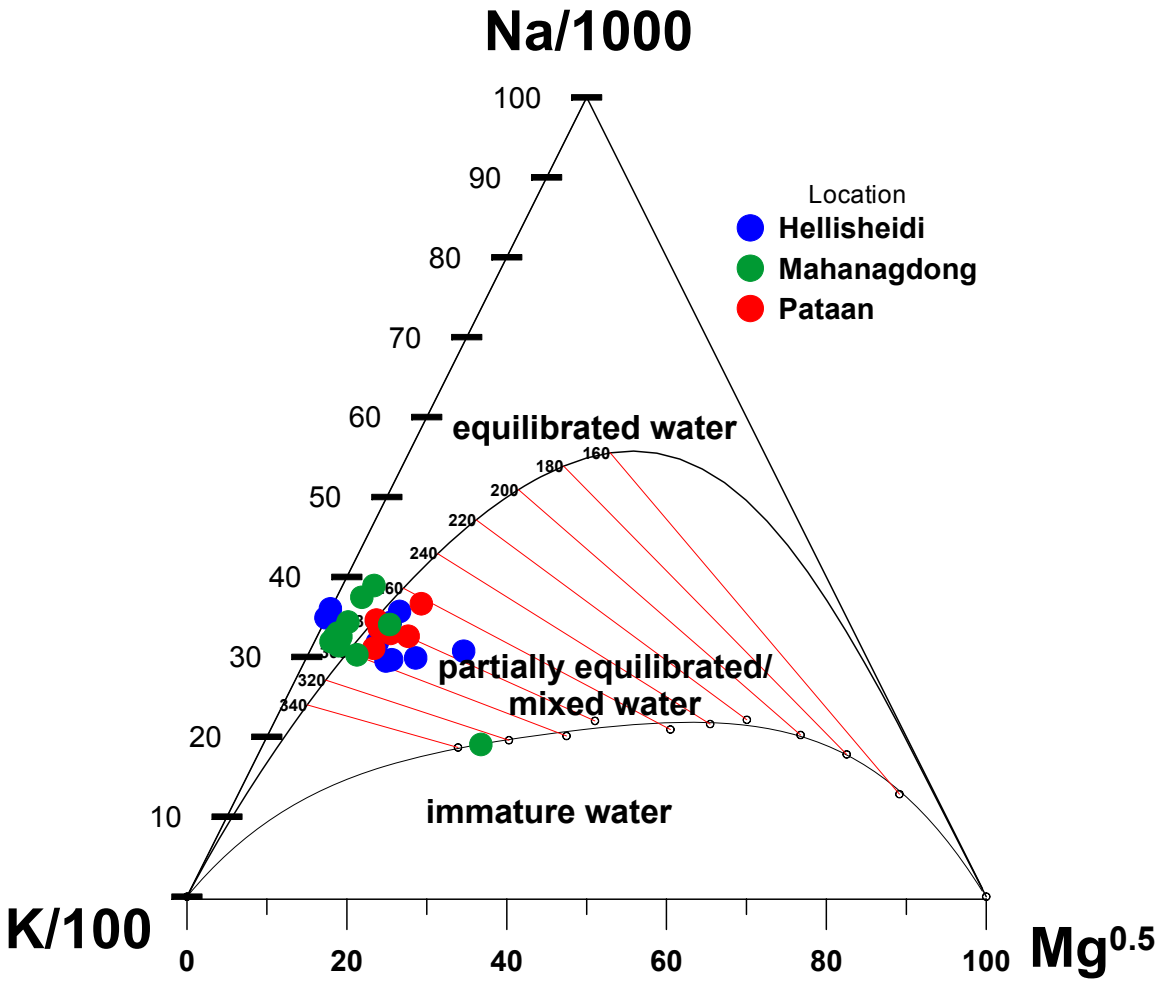

Figure 5.2 Na-Cl-K ternary diagram of geothermal waters from Hellisheidi, Mahanagdong and Pataan wells. This shows partially equilibrated/mixed and fully equilibrated fluid discharges of the wells

6 Results and Discussions

6.1 Mineral Saturation

Saturation index (SI) is used to assess the departure of mineral saturation from the equilibrium and is expressed as

$$SI = \log \frac{Q}{K}$$

where Q is the reaction qoutient/activity product of mineral dissolution reaction and K is the equilibrium constant.

Logarithm of activity product/reaction qoutient, log Q, are calculated based from the species activities calculated using WATCH speciation program except for anhydrite mineral saturation which are directly taken from WATCH logQ and logK WATCH output. WATCH uses the thermodynamic data provided by (Arnórsson et al., 1982). Gas solubility constants were taken from Fernandez-Prini (2003). Activities of $H_4SiO_4^o$ were based from the work of Gunnarsson and Arnórsson (2000).

The standard thermodynamic properties of minerals were selected from the data set of Holland and Powell (1998) except those of pyrite and pyrrhotite which was taken from Robbie and Hemmingway (1995). Dissociation equilibriums for Al-hydroxide species were based from Arnórsson and Andrésdóttir (1999), while ferric- and ferrous hydroxide equilibriums were taken from the work of Diakonov and Tagirov (2002). The Al-Si dimer of Pokrovski et al. (1998) was incorporated into the speciation calculations (Angcoy, 2010).

Table 6.1 lists the mineral dissolution reactions and the associated equilibrium constants taken from Angcoy (2010).

6.1.1 Calcite and Anhydrite

Calcite saturation versus the selected aquifer temperature is shown in Figure 6.1.

At Hellisheidi the aquifer fluids are very close at equilibrium with calcite and when all uncertainties were considered such as analytical imprecision and selection of aquifer temperatures (e.g Angcoy (2010) and Arnorsson (2007)), departure from saturation is not significant. The average departure from calcite saturation of Hellisheidi wells is only 0.05 SI units.

Mahanagdong aquifer fluids are very close to being at equilibrium with respect to calcite. Only MG40 well showed high level of undersaturation of 2.1 SI units. MG40 has high

"excess" enthalpy and is acidic which might be affected by injected steam condensates or other acidic fluids. The average calcite saturation of Mahanagdong wells is -0.2 SI units.

Pataan wells fluids were practically at equilibrium with calcite or slightly over-saturated with an average value of 0.2 SI units. Well PT02 is the most oversaturated with 0.74 SI units.

Figure 6.2 shows calcite saturation versus total discharge enthalpy. There was no significant correlation between calcite saturation and discharge enthalpy. MG40 well is not shown. As already mentioned, the aquifer of this well is highly undersaturated.

The calculated saturation index for calcite increases with increasing value of the calculated aquifer pH (Figure 6.3). This is considered to be due to error in the calculated aquifer water pH. Many factors affect the calculated pH, including both analytical data on sample pH, total carbonate carbon and total sulfide sulfur, thermodynamic data on various dissociational equilibria, selected aquifer temperature and the model used to calculate aquifer fluid compositions from wellhead data. It is not possible to identify the main sources of their apparent variation in pH and calcite saturation index but it seems to be significant, particularly in the case of Hellisheidi.

Mahanagdong and Pataan aquifer fluids approach anhydrite equilibrium as shown in Figure 6.4 whereas Hellisheidi waters are considerably anhydrite undersaturated.

6.1.2 Magnetie, Pyrite and Pyrrhotite

Figure 6.5 shows the equilibrium curve for the redox reactions involving pyrite, magnetite, H_2S and H_2. At equilibrium this reaction gives the aqueous H_2S and H_2 molal ratios. Hellisheidi aquifer waters are quite close to equilibrium, with an average of 0.03 log units above the curve. Mahanagdong and Pataan aquifer waters are systematically with higher H_2S/H_2 ratios than those corresponding to equilibrium, by 0.2 and 0.55 log units on average, respectively.

Figure 6.6 shows the equilibrium curve for the redox reactions involving pyrite, pyrrhotite, H_2S and H_2. Hellisheidi aquifer waters are very close to equilibrium yet systematically below the equilibrium curve on average by 0.25 log units, if the degassed discharge of HE03and HE05 are excluded. Mahanagdong and Pataan aquifer waters are systematically with higher H_2S/H_2 ratios than those corresponding to equilibrium, by 0.96 and 1.3 log units on average, respectively. Clearly the H_2S/H_2 ratios in the aquifer waters in the Philippine geothermal fields are not controlled by pyrite-pyrrhotite buffer.

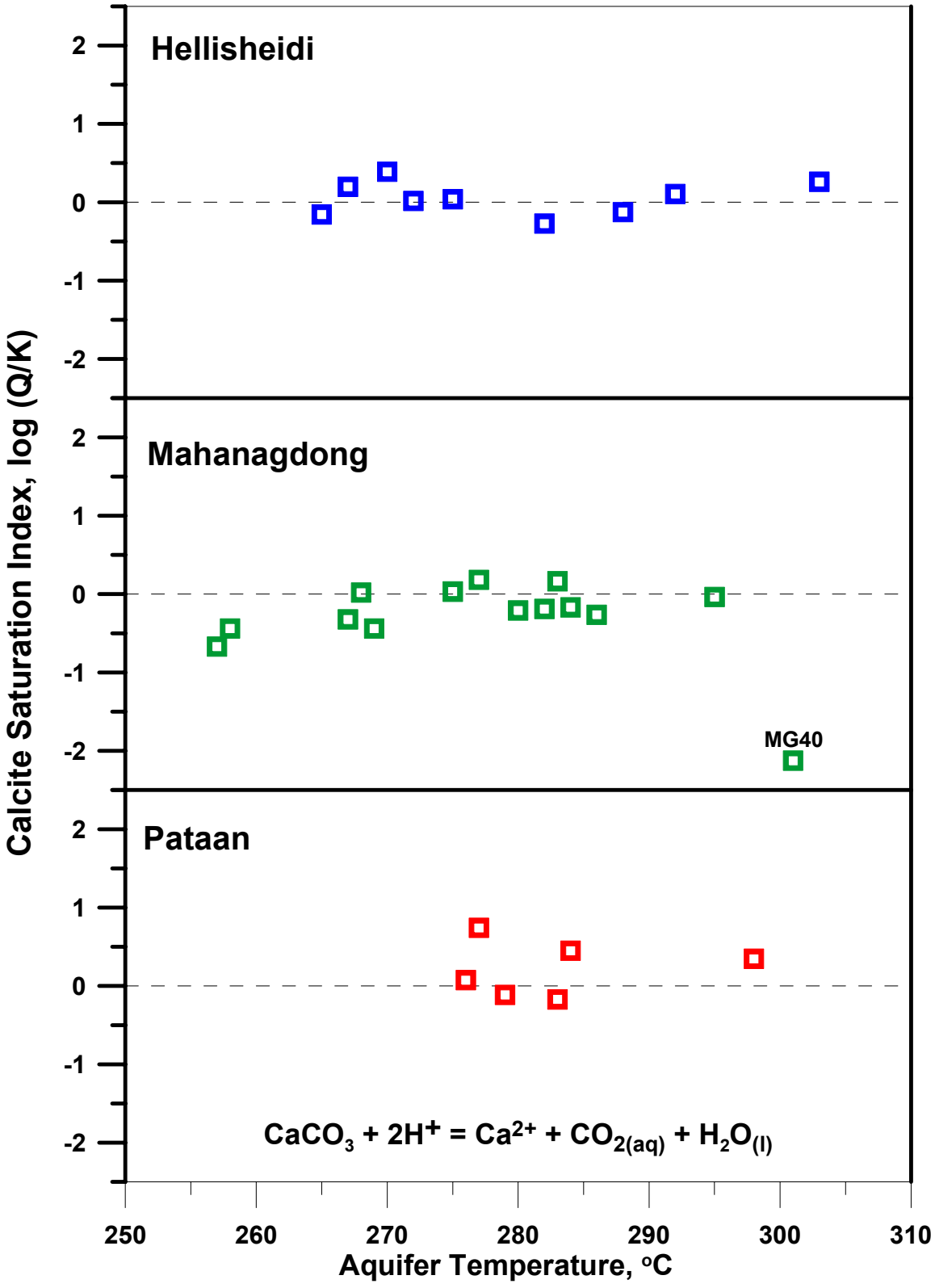

Figure 6.1 Calcite saturation index of aquifer fluid versus the selected aquifer temperature.

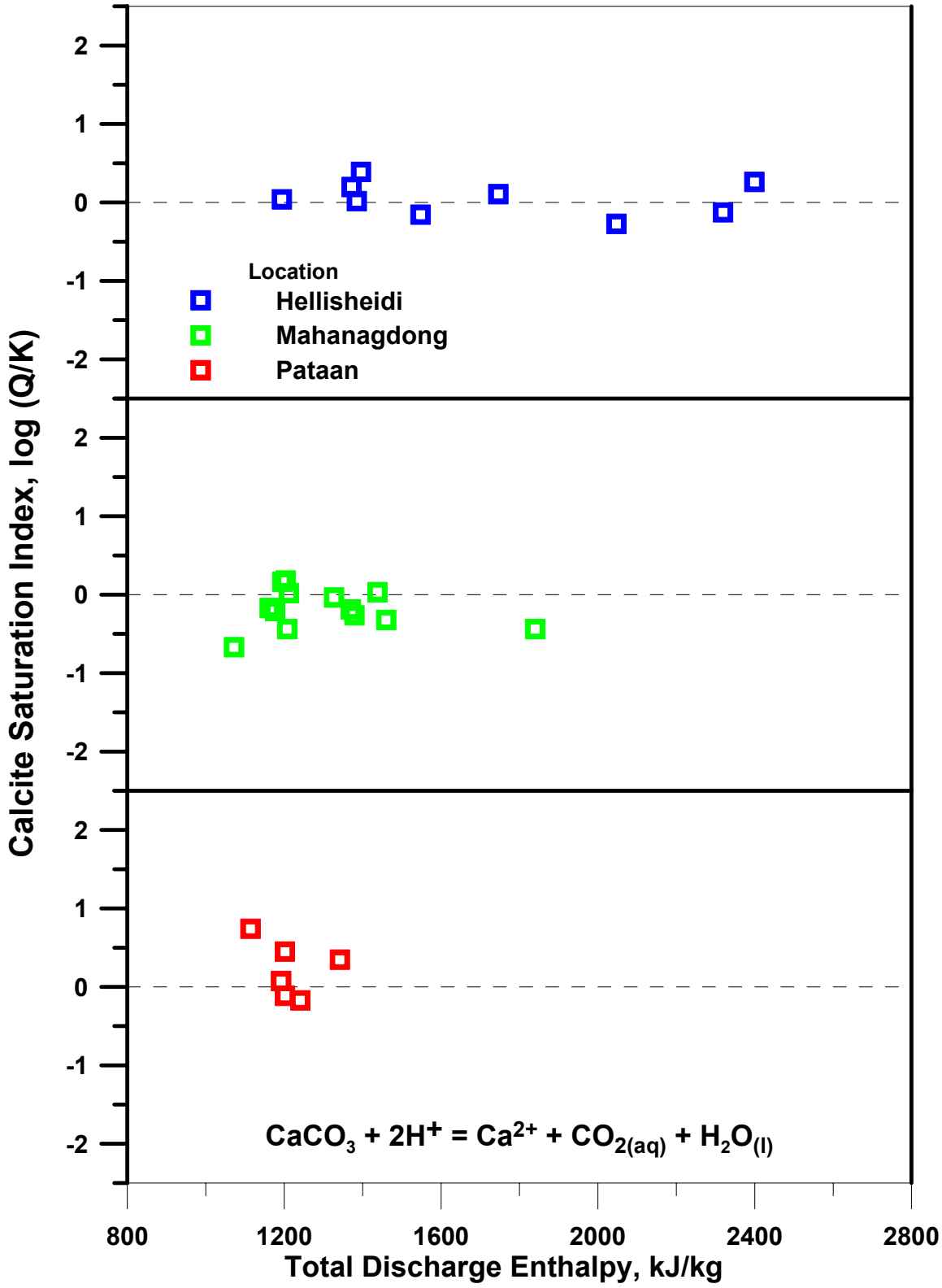

Figure 6.2 Calcite saturation index of aquifer fluid versus total discharge enthalpies.

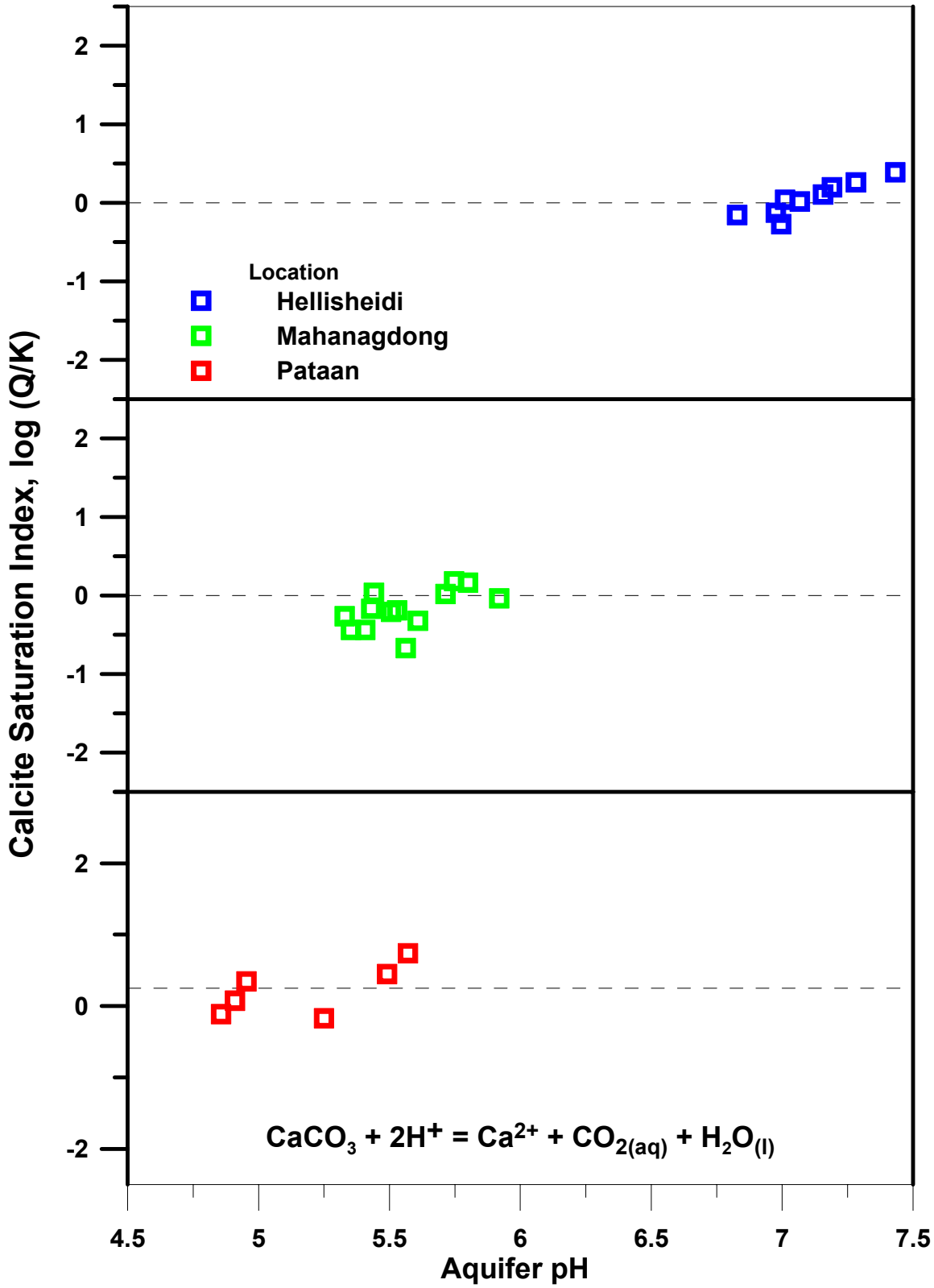

Figure 6.3 Calcite saturation index versus pH of the aquifer fluid.

Table 6.1 Log K-temperature equations of individual mineral dissolution reactions (valid at 0-350°C at P_{sat}, unit activity for all minerals and liquid water) modified after Angcoy (2010).

	Reaction	log K (T in K)
1	$cal + 2H^+ \leftrightarrow Ca^{2+} + H_2O_l + CO_{2,aq}$	$\log K = -68.271 + \frac{4385.24}{T} - 0.0075257T + 25.856 log T$
2	$wol + 2H^+ + H_2O_l \leftrightarrow Ca^{2+} + H_4SiO_4^0$	$\log K = -127.096 + \frac{8151.38}{T} - 0.029817T + 49.282 log T$
3	$gro + 4H^+ + 8H_2O_l \leftrightarrow 3Ca^{2+} + 2Al(OH)_4^- + 3H_4SiO_4^0$	$\log K = -517.662 + \frac{17623.7}{T} - 0.14343T + 203.808 log T$
4	$pre + 10H_2O_l \leftrightarrow 2Ca^{2+} + Fe(OH)_4^- + 2Al(OH)_4^- + 3H_4SiO_4^0 + 2OH^-$	$\log K = 833.95 - \frac{25642.8}{T} + 0.5035T - 2.941x10^{-4}T^2 - 369.297 log T$
5	$czo + 12H_2O_l \leftrightarrow 2Ca^{2+} + 3Al(OH)_4^- + 3H_4SiO_4^0 + OH^-$	$\log K = 36.052 - \frac{6854.78}{T} + 0.13236T - 1.3749x10^{-4}T^2 - 33.508 log T$
6	$epi + 12H_2O_l \leftrightarrow 2Ca^{2+} + Fe(OH)_4^- + 2Al(OH)_4^- + 3H_4SiO_4^0 + OH^-$	$\log K = 893.547 - \frac{27077.4}{T} - 0.54124T - 3.022x10^{-4}T^2 - 398.38 log T$
7	$mag + 4H_2O_l \leftrightarrow Fe^{2+} + 2Fe(OH)_4^-$	$\log K = 949.951 - \frac{24258.2}{T} + 0.51474T - 2.402x10^{-4}T^2 - 417.136 log T$
8	$pyr + 2H^+ + H_{2,aq} \leftrightarrow Fe^{2+} + 2H_2S_{aq}$	$\log K = -1.397 - \frac{461.3}{T} - 0.0009128T + 1.626 log T$
9	$pyrr + 2H^+ \leftrightarrow Fe^{2+} + H_2S_{aq}$	$\log K = -3.043 + \frac{1579.06}{T} + 0.001987T + 0.12 log T$
10	$qtz + 2H_2O_l \leftrightarrow H_4SiO_4^0$	$\log K = -34.188 + \frac{197.47}{T} - 5.851x10^{-6}T^2 + 12.245 log T$

cal-calcite, czo-clinozoisite, epi-epidote, gro-grossular, mag-magnetite, pre-prehnite, pyr-pyrite, pyrr-pyrrhotite, qtz-quartz, wol-wollastonite

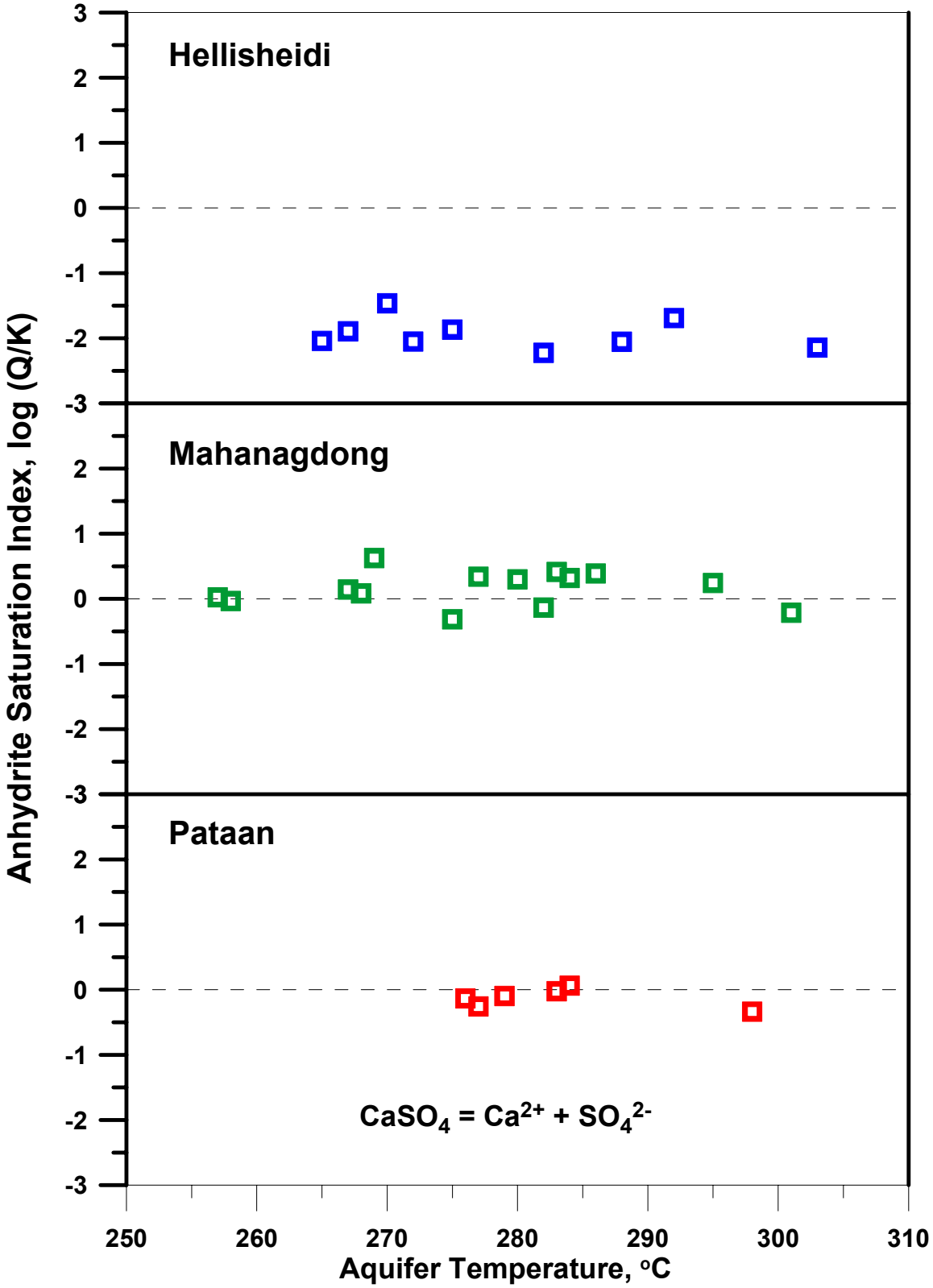

Figure 6.4 Anhydrite saturation index of aquifer fluid versus the selected aquifer temperature.

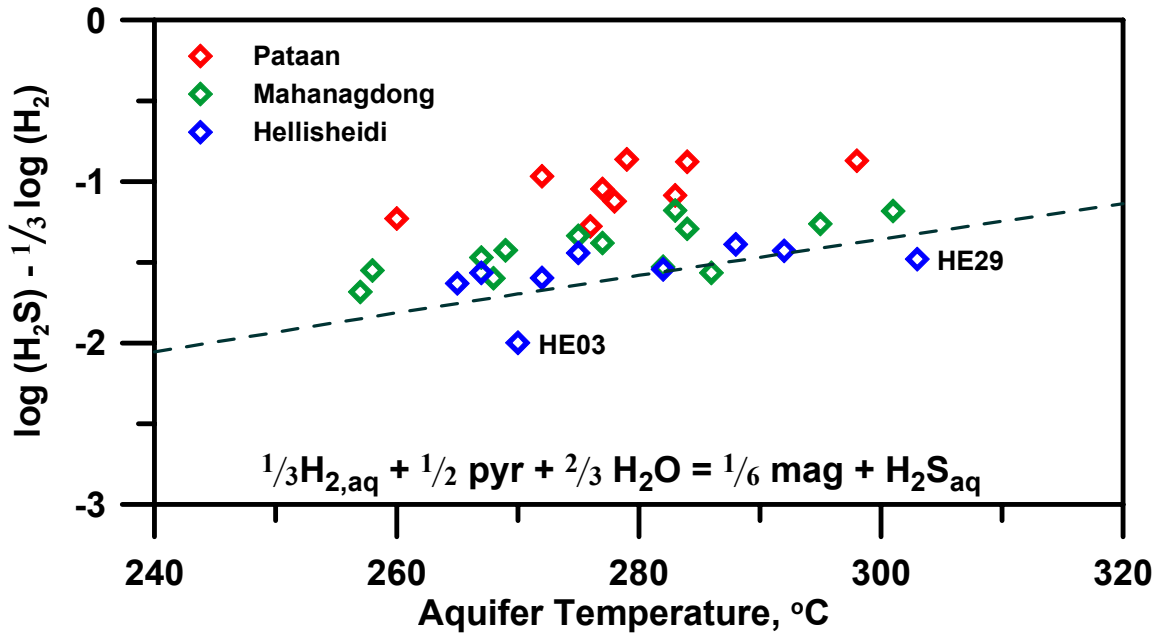

Figure 6.5 Aquifer fluid H_2S and H_2 molal ratios in relation to the equilibrium curve of pyrite-magnetite mineral assemblage.

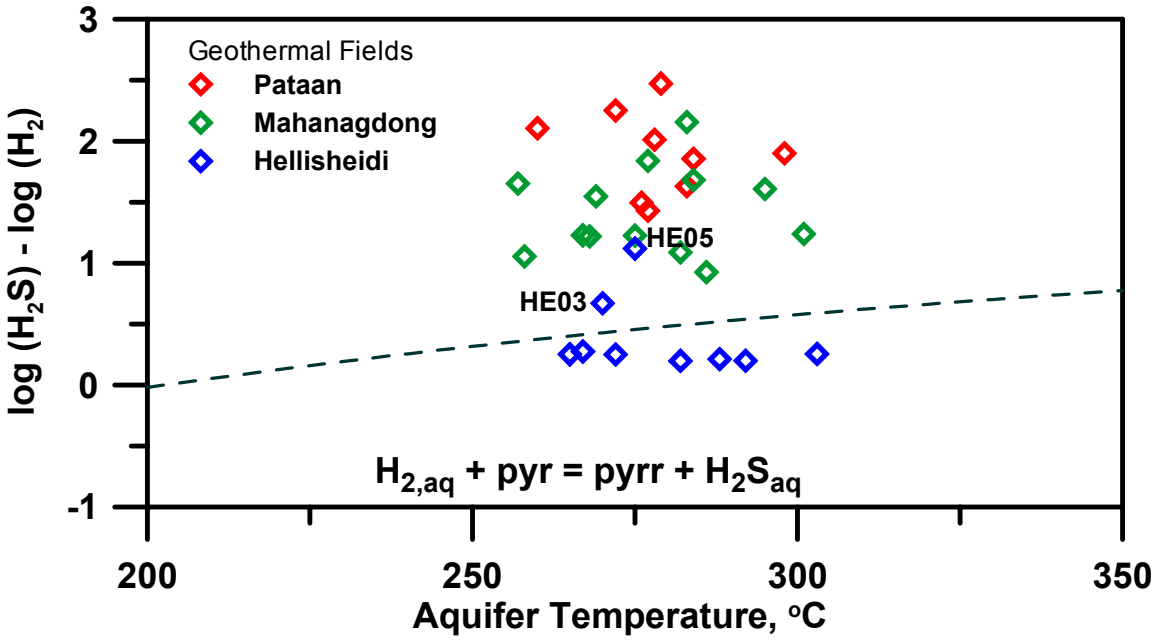

Figure 6.6 Aquifer fluid H_2S and H_2 molal ratios in relation to the equilibrium curve of pyrite-pyyrhotite mineral assemblage.

6.2 Effect of Boiling and Degassing

Mineral deposition from the boiling fluid largely occurs in response to its cooling and degassing. Cooling causes geothermal waters to become over-saturated with minerals with prograde solubility but under-saturated with those having retrograde solubility. Degassing tends to produce over-saturated water with respect to minerals whose solubility decreases with increasing pH. The quantity of minerals precipitated from solution is not only determined by the degree of over-saturation but also by the fluid composition and the kinetics of the precipitation reaction. The solubility of some minerals decreases with increasing temperature and increasing pH; an example being calcite. The combined effects of both processes, together with the rate of the precipitation reaction, determine whether or not the minerals with which the water becomes over-saturated precipitate from solution. Un-boiled geothermal liquids are typically close to being calcite-saturated as shown from this study and others (Arnórsson, 1989). Extensive degassing by boiling tends to cause an initially calcite-saturated water to become over-saturated. The cooling has the opposite effect due to the retrograde solubility of calcite with respect to temperature. The extent of degassing and cooling determine whether boiling causes an initially calcite saturated water to become over or under-saturated (Arnorsson et al., 2007).

6.2.1 Hellisheidi Wells

Figures 6.7 to 6.15 show how the degree of calcite saturation varies during adiabatic boiling at different extent of degassing for all analyzed gases (CO_2, H_2S, H_2, CH_4, N_2) in Hellishedi wells. The dots show the calculated calcite saturation in the aquifer for each well. An overall pattern in the variation of the saturation index (SI) of Hellisheidi wells with temperature is observed from all the wells except well HE03. The SI initially increases then, after it reaches a peak, decreases to negative values. The initial increase in SI reflects an increase in pH due to CO_2 and H_2S degassing. The pH increase causes a strong increase in the activity of the CO_3^{-2} species. At maximum SI values, the water has been largely degassed, and the subsequent decline in SI is caused by increased calcite solubility with decreasing temperature (Arnorsson et al., 2007). Well HE03 is an exception to the general trend because the fluid entering the well is highly degassed as reflected by the low gas content of the discharge; therefore, SI decreases immediately during adiabatic boiling.

The extent of degassing (as expressed by the degassing coefficient) increases the level of calcite SI except for degassed well HE03 which shows the opposite. The value of the degassing coefficient can be arbitrarily selected when running the WATCH program. A value of 1 represent maximum degassing, i.e. equilibrium distribution of all gases is attained between liquid and vapor. A degassing coefficient of e.g. 0.5 implies that degassing is taken to be 50% maximum. For degassing to occur during boiling, a mass transfer of gases occurs from the liquid to vapor. In reality such degassing is often incomplete as shown by analysis of CO_2 in liquid water and water in steam separators.

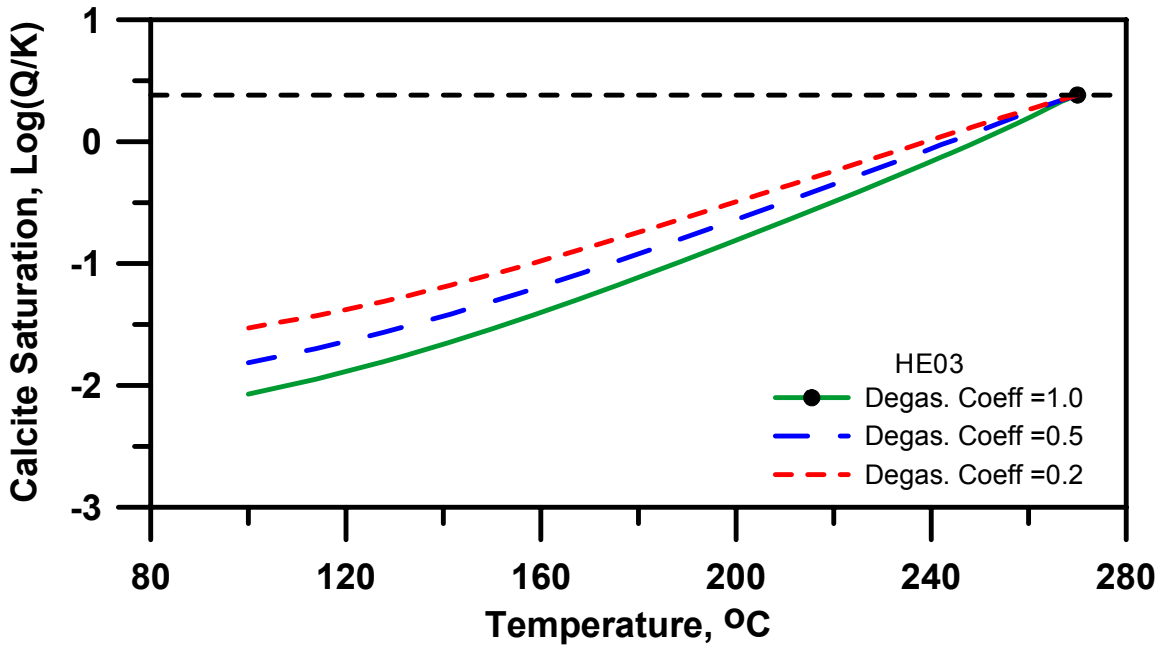

Figure 6.7 Calcite saturation of well HE03 during adiabatic boiling at different degassing coefficients.

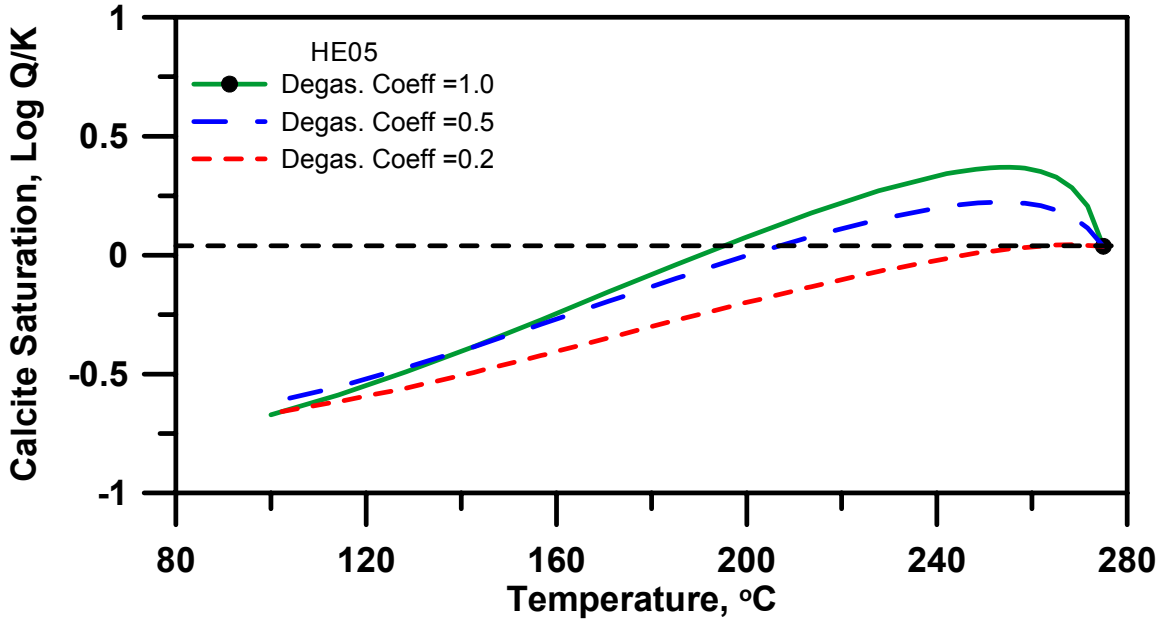

Figure 6.8 Calcite saturation of well HE05 during adiabatic boiling at different degassing coefficients.

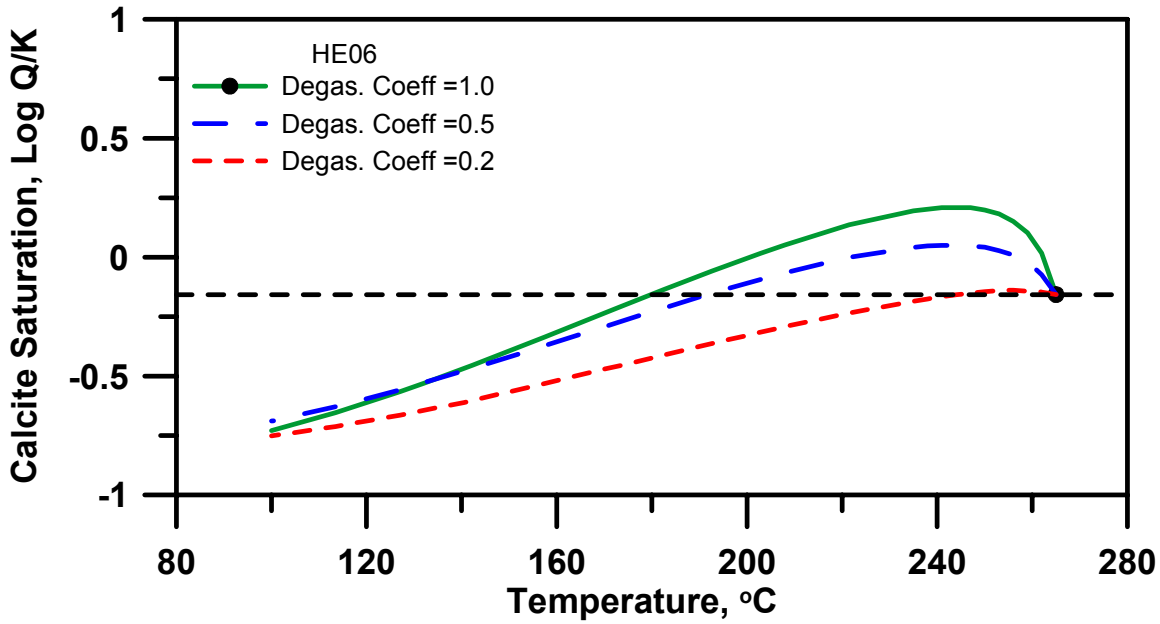

Figure 6.9 Calcite saturation of well HE06 during adiabatic boiling at different degassing coefficients.

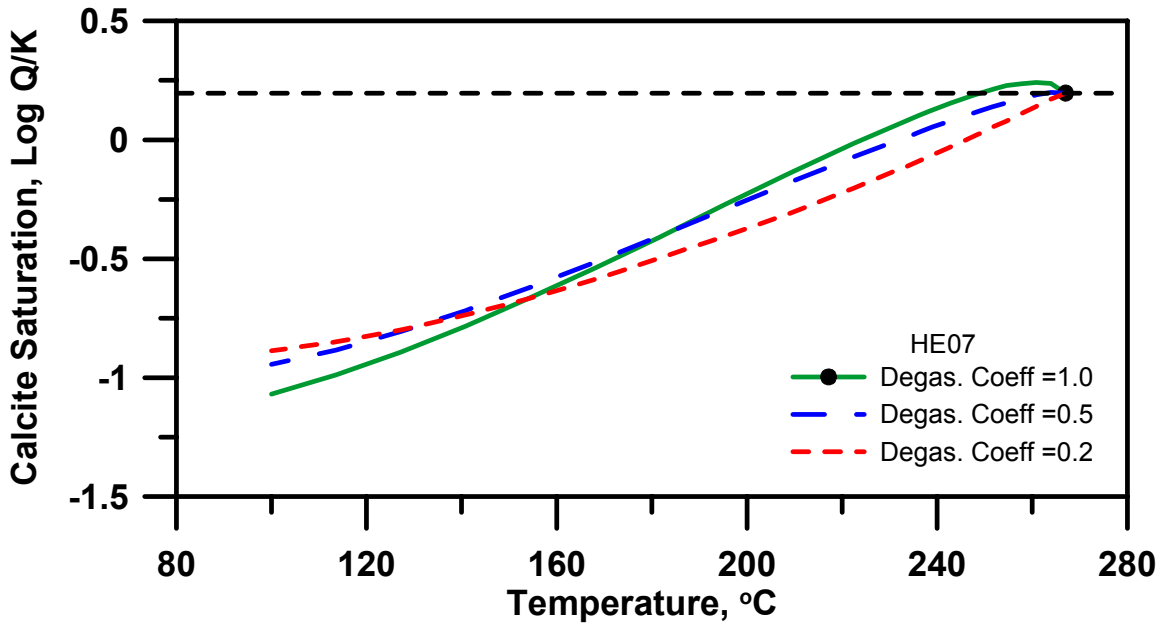

Figure 6.10 Calcite saturation of well HE07 during adiabatic boiling at different degassing coefficients.

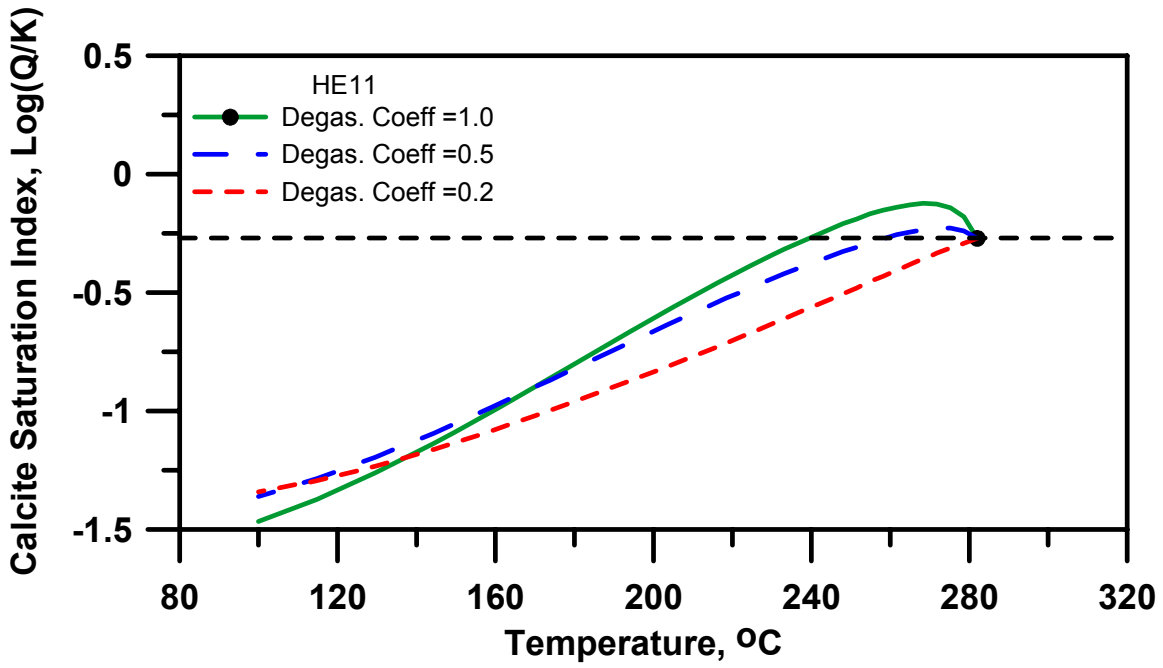

Figure 6.11 Calcite saturation of well HE11 during adiabatic boiling at different degassing coefficients.

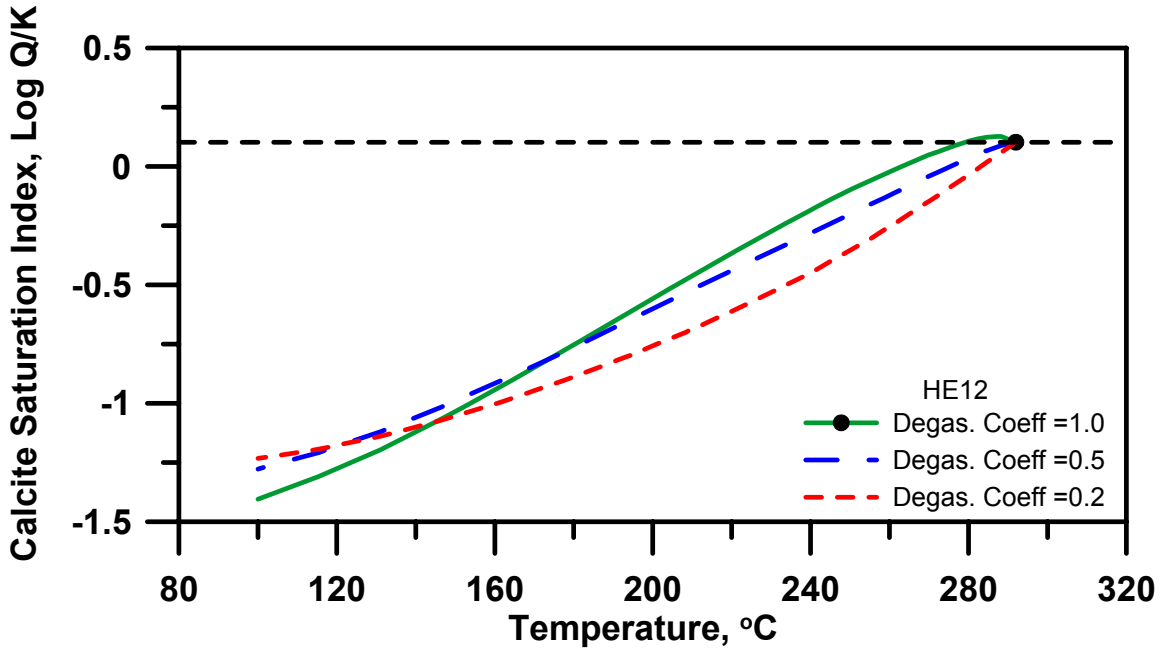

Figure 6.12 Calcite saturation of well HE12 during adiabatic boiling at different degassing coefficients.

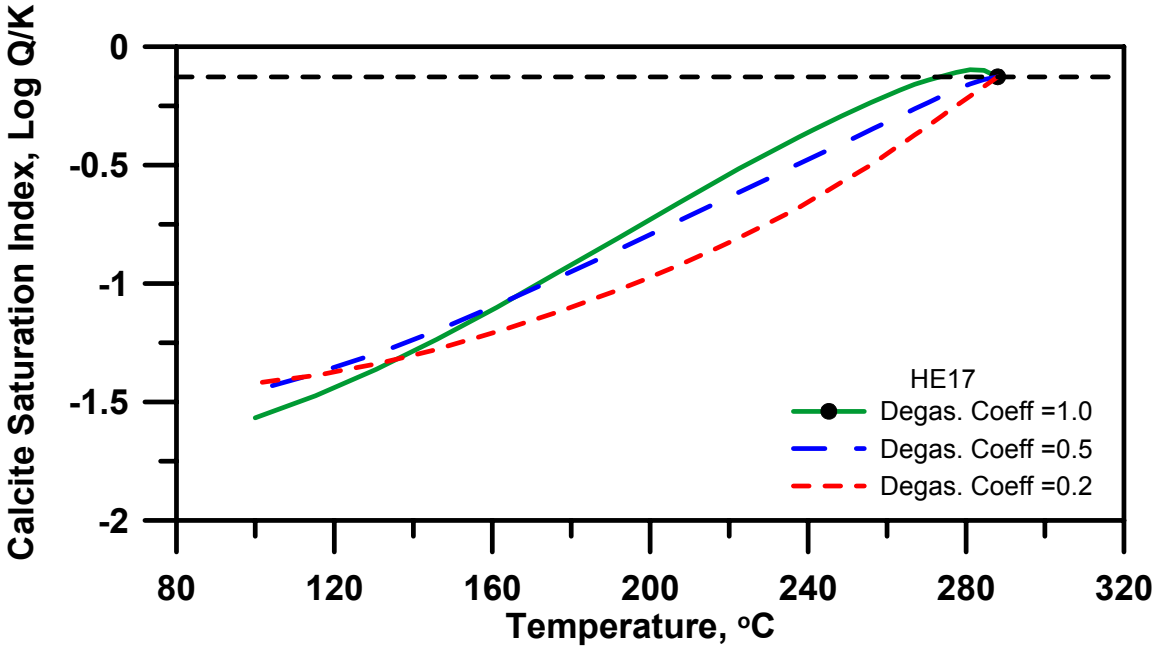

Figure 6.13 Calcite saturation of well HE17 during adiabatic boiling at different degassing coefficients.

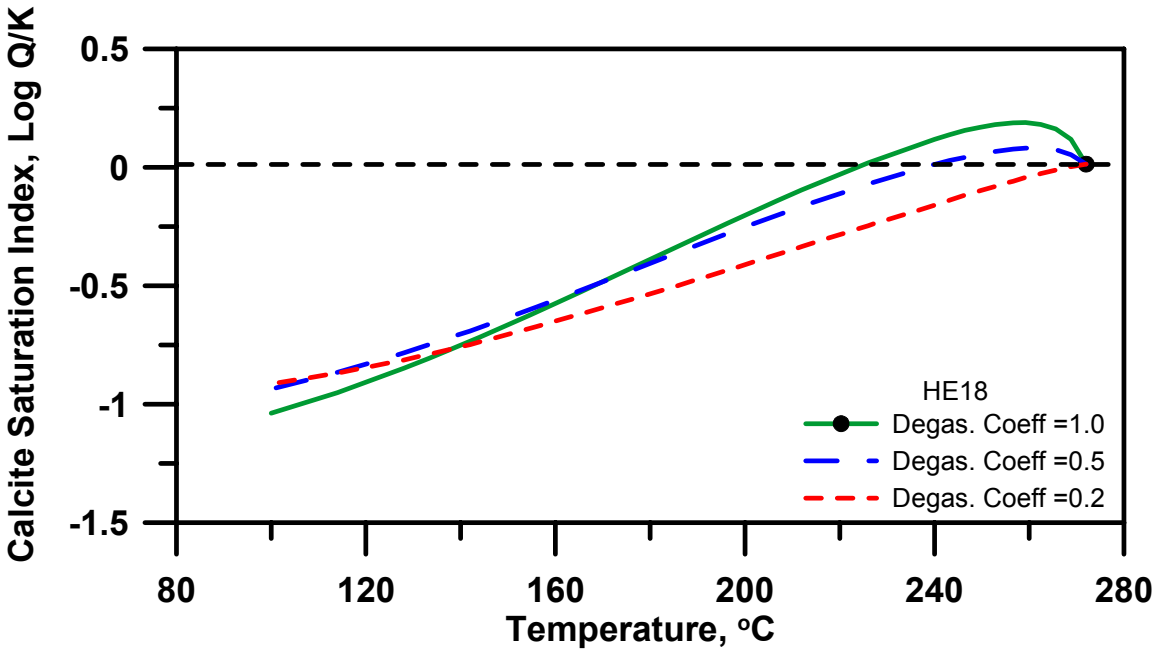

Figure 6.14 Calcite saturation of well HE18 during adiabatic boiling at different degassing coefficients.

6.2.2 Mahanagdong Wells

The majority of the wells in Mahanagdong follow the general pattern exhibited by Hellisheidi wells (Figures 6.16 to 6.31). Exception includes MG40, MG29, MG14 and MG03. MG40 is a high "excess" enthalpy and acidic well. MG03 and MG14 are postulated to be receiving fluid from the upflow zone but have been affected by brine injection returns. The reservoir chloride

levels of MG03 and MG14 are shifted towards the composition of the injected brine. The total discharge CO2 concentrations of MG03 declined and the total discharge enthalpy of MG14 declined. Well MG29, on the other hand, is located in the western periphery of the Mahanagdong geothermal system and could be affected by intrusion of cooler peripheral waters(Figure 6.32, Salonga et al., 2004).

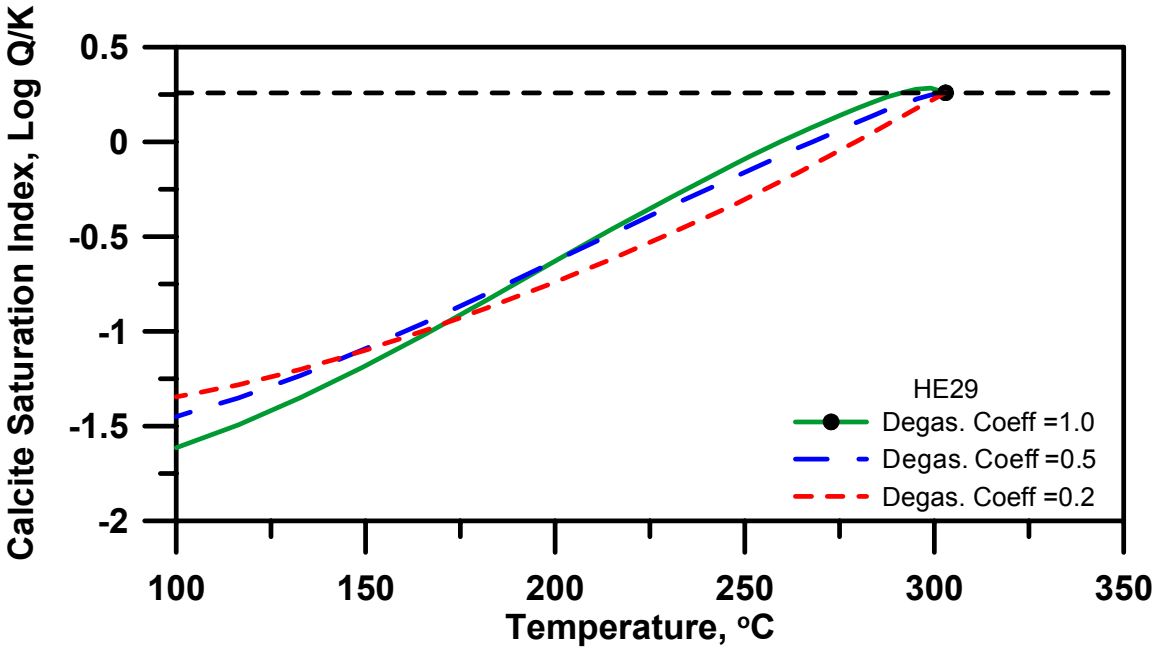

Figure 6.15 Calcite saturation of well HE29 during adiabatic boiling at different degassing coefficients.

The highest positive departure from the initial saturation in Mahanagdong is from MG19, with 0.40 (at 251 ^{o}C) SI units above the initial saturation at its most degassed state (degassing coefficient of 1.0). MG19 is known to deposit calcite scale in the well.

Figure 6.17 shows the calcite saturation of MG01 prior to production (1994 water and gas analyses). Boiling of the aquifer fluid of this well produces the highest increase in calcite over-saturation of 0.51 SI units. Comparing MG01 CO_2 and H_2S aquifer fluid concentrations on samples taken in 2009 and 1994 shows that it has been partially degassed or mixed with degassed injected brine. Aquifer fluid CO_2 concentration decreased from 8000 to 1200 ppm and H_2S concentration decreased from 92 to 15 ppm. Activity of free Ca^{2+} probably affects the calcite saturation because it partially increased (from 10 to 16 ppm) in 1994 to 2009 samples.

The case of MG19 is similar with MG01. The present fluid discharge is partially degassed or mixed with injected brine and Ca2+ concentration has increased. Aquifer fluid CO2 concentration decreased from 6900 to 3200 ppm, H2S concentration decreased from 71 to 36 ppm and Ca2+ increased from 11 to 20 ppm. Calcite mineral SI trend of MG19 practically remains the same after almost 15 years of production though the old data shows a higher departure of 0.48 SI units above the initial saturation, Figures 6.25 and 6.26.

Salonga et al (2004) inferred inflow of peripheral water into the Mahanagdong geothermal systems that could have affected the aquifer fluids feeding wells MG01 and MG19, Figure 6.32.

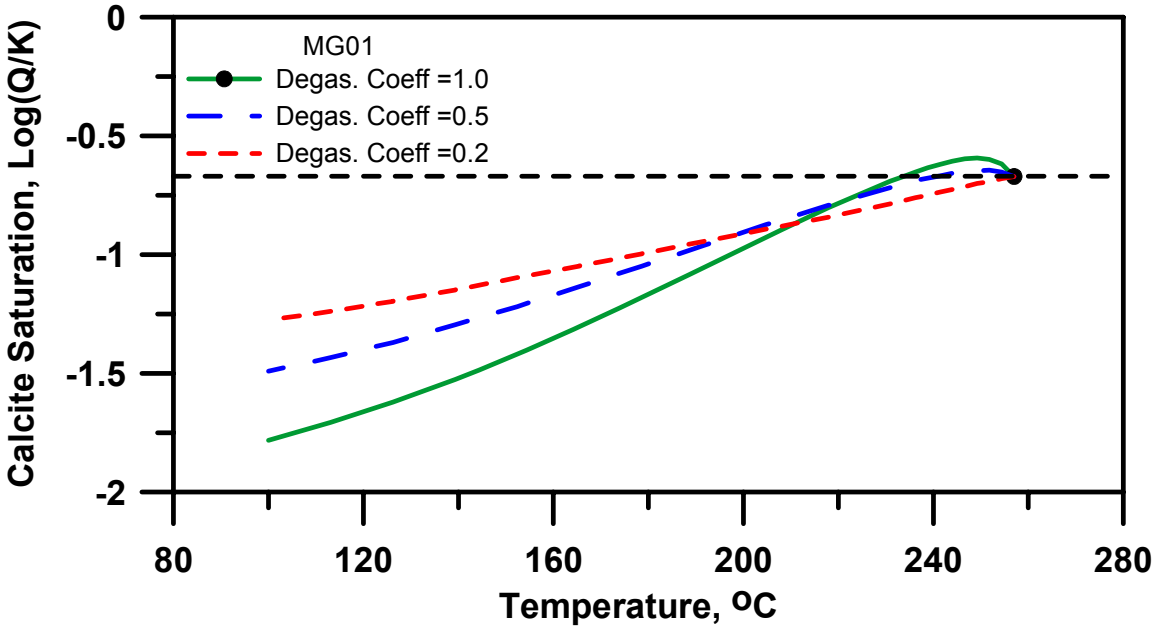

Figure 6.16 Calcite saturation of well MG01 during adiabatic boiling at different degassing coefficients.

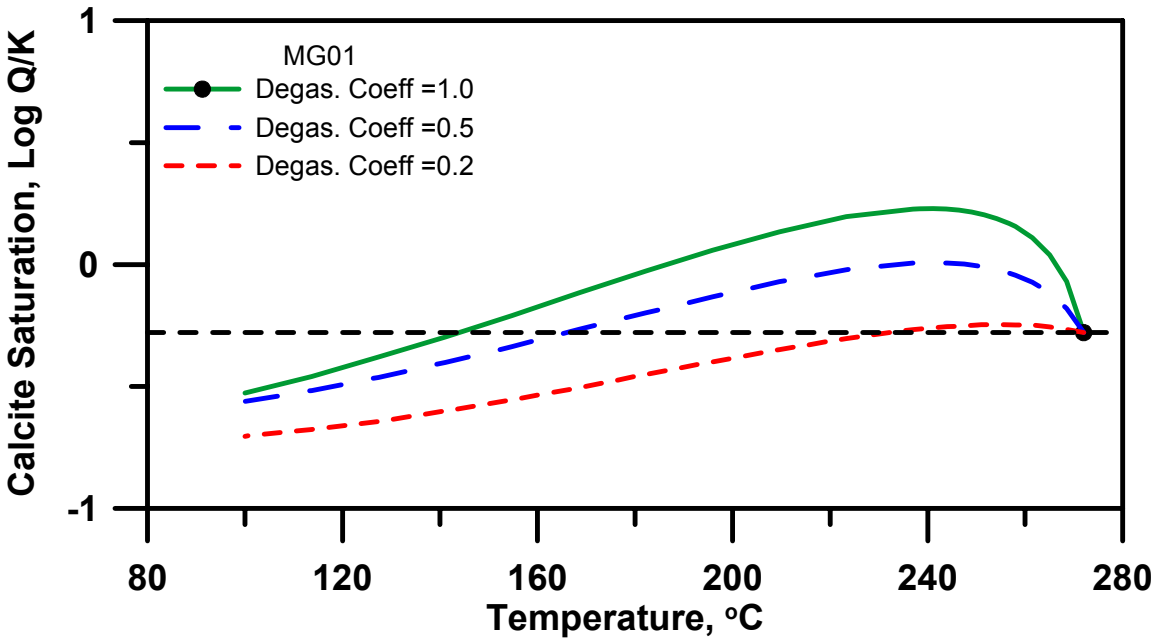

Figure 6.17 Calcite saturation of well MG01 during adiabatic boiling at different degassing coefficients. The chemistry data used in this plot is taken during fluid discharge testing (5-Nov-1994) of the well prior to production.

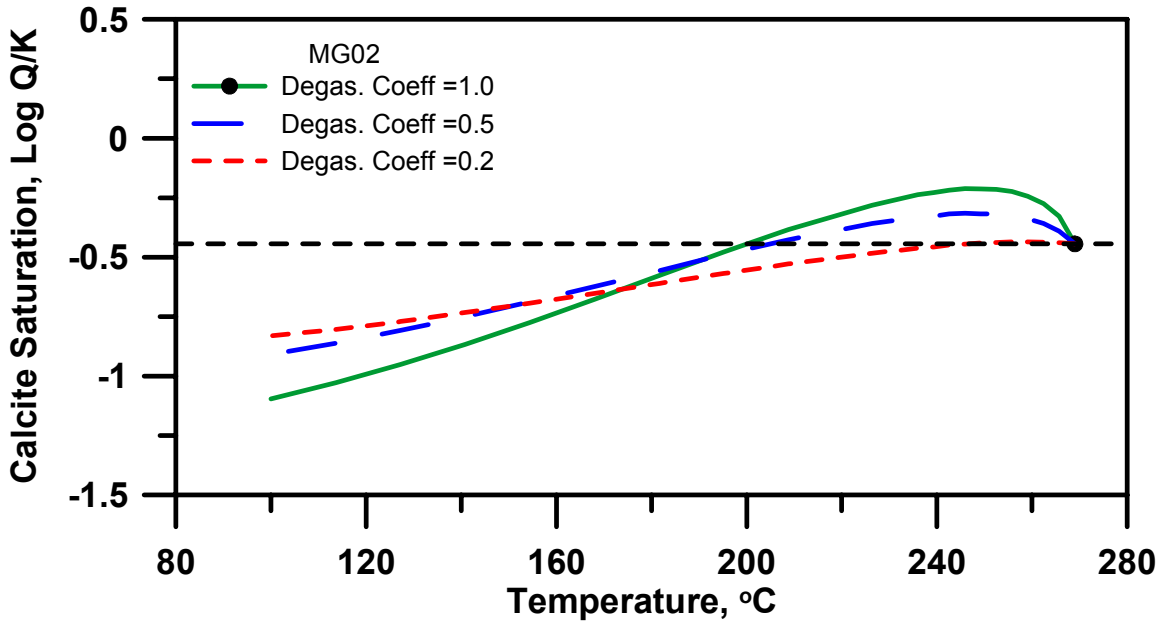

Figure 6.18 Calcite saturation of well MG02 during adiabatic boiling at different degassing coefficients.

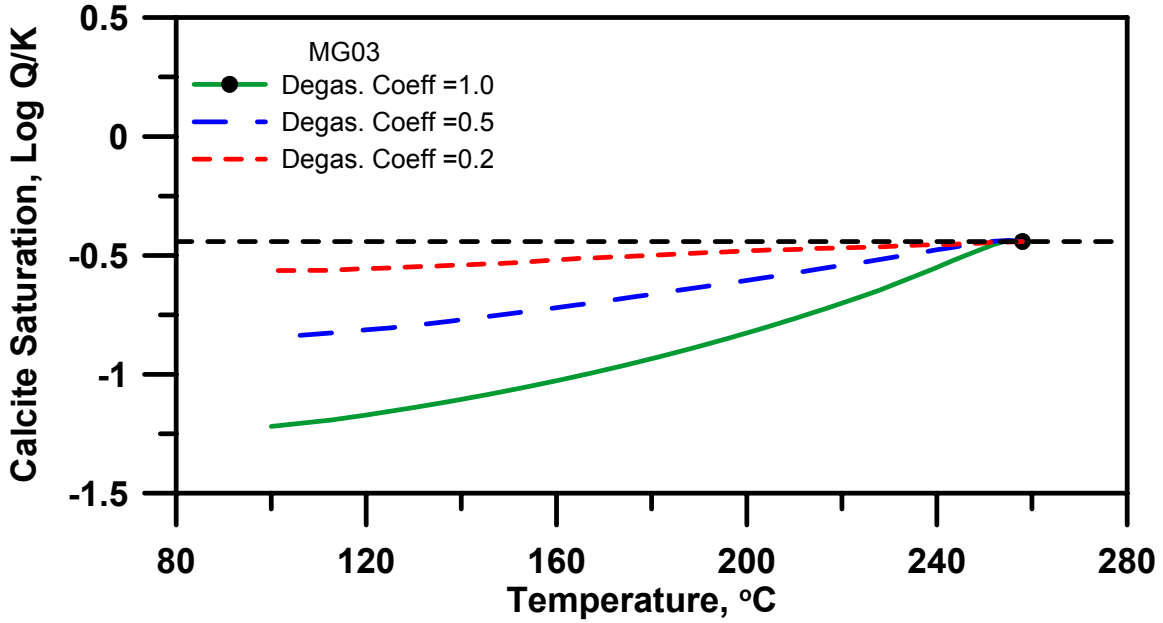

Figure 6.19 Calcite saturation of well MG03 during adiabatic boiling at different degassing coefficients.

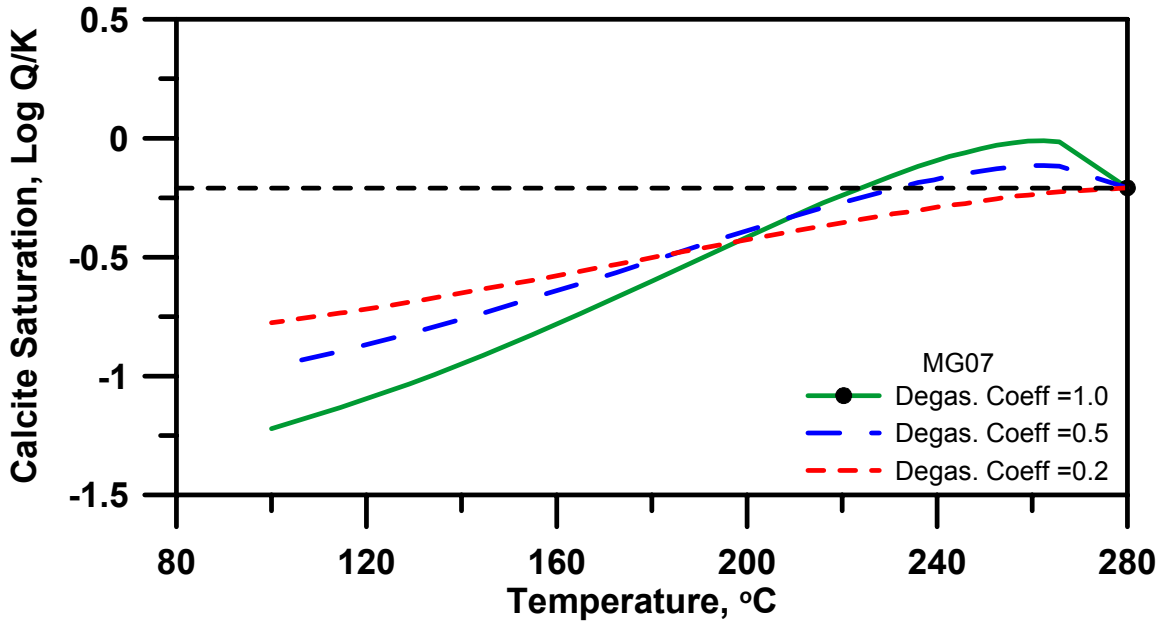

Figure 6.20 Calcite saturation of well MG07 during adiabatic boiling at different degassing coefficients.

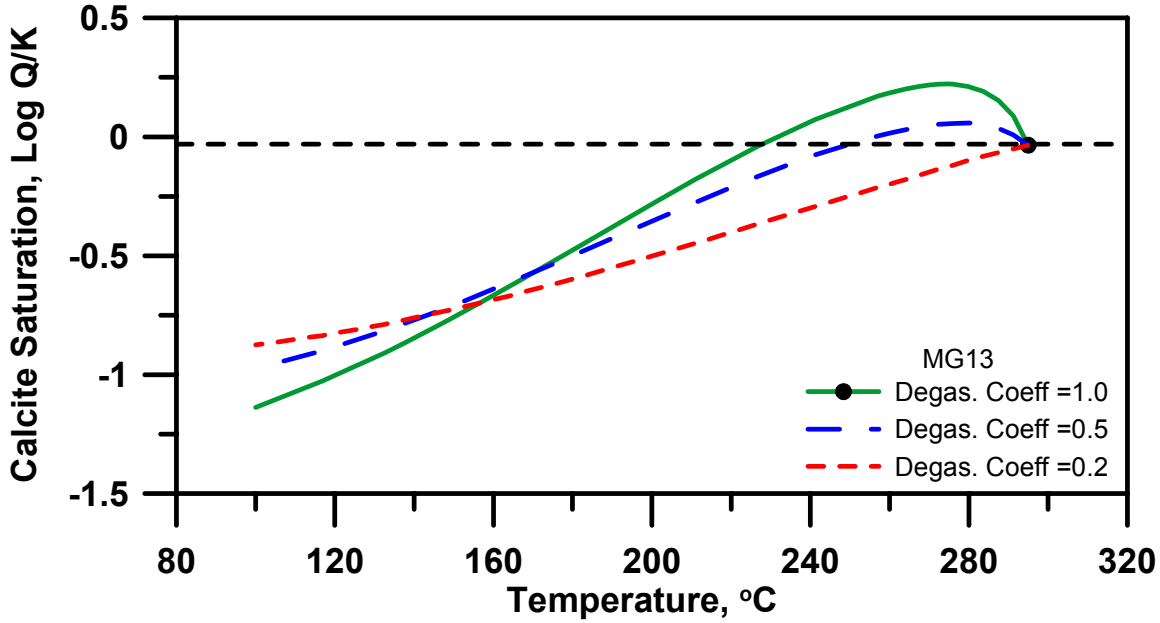

Figure 6.21 Calcite saturation of well MG13 during adiabatic boiling at different degassing coefficients.

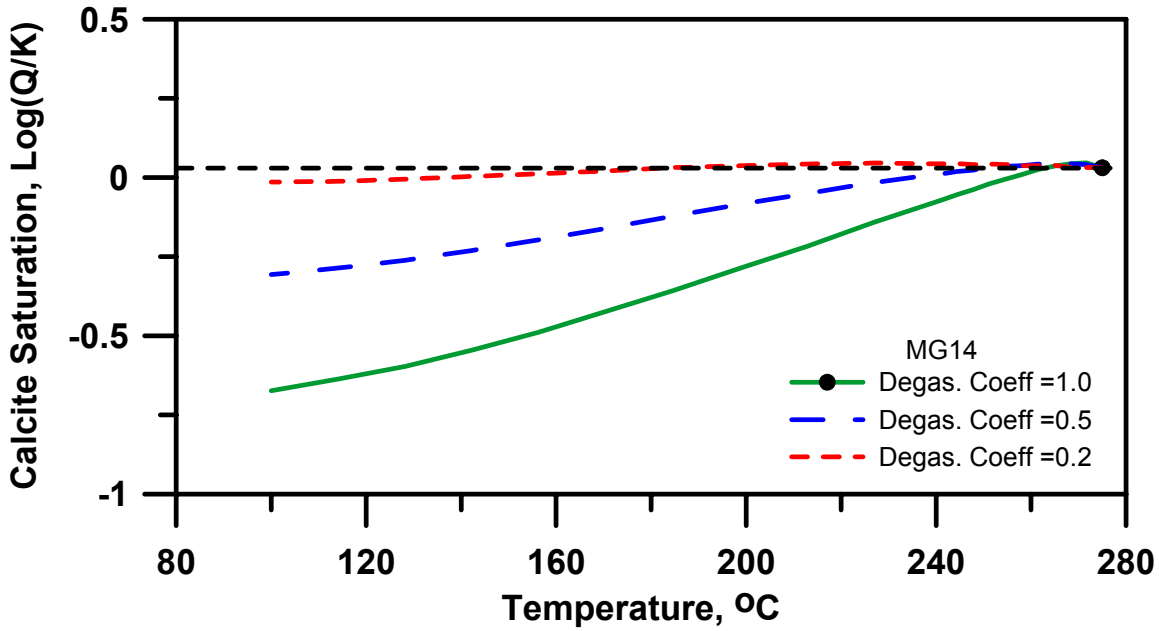

Figure 6.22 Calcite saturation of well MG14 during adiabatic boiling at different degassing coefficients.

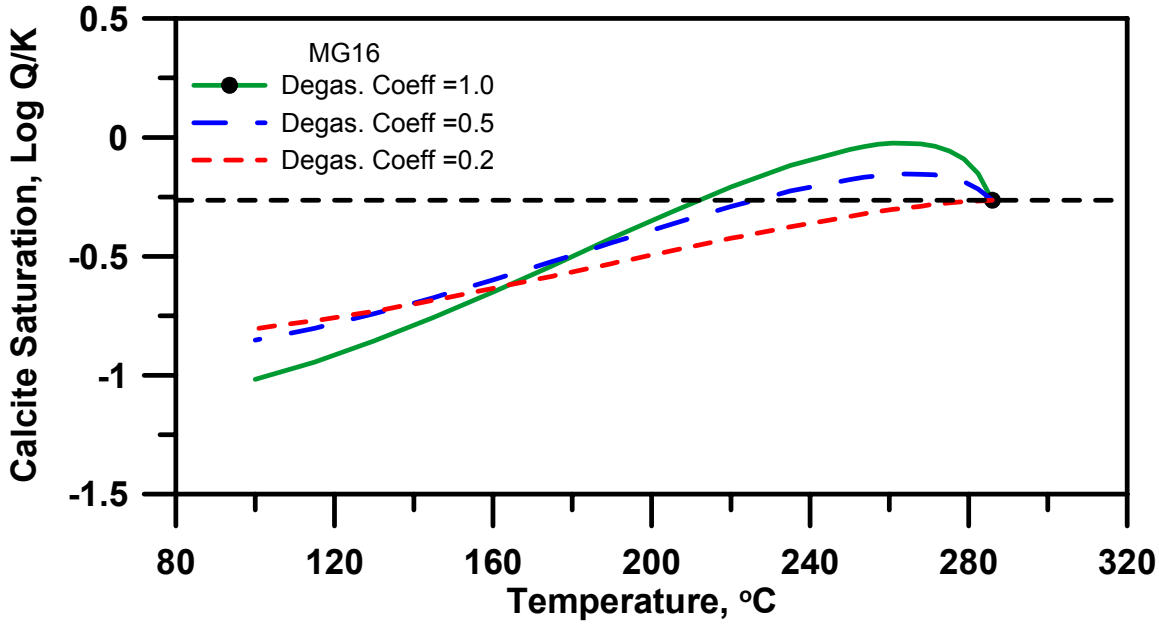

Figure 6.23 Calcite saturation of well MG16 during adiabatic boiling at different degassing coefficients.

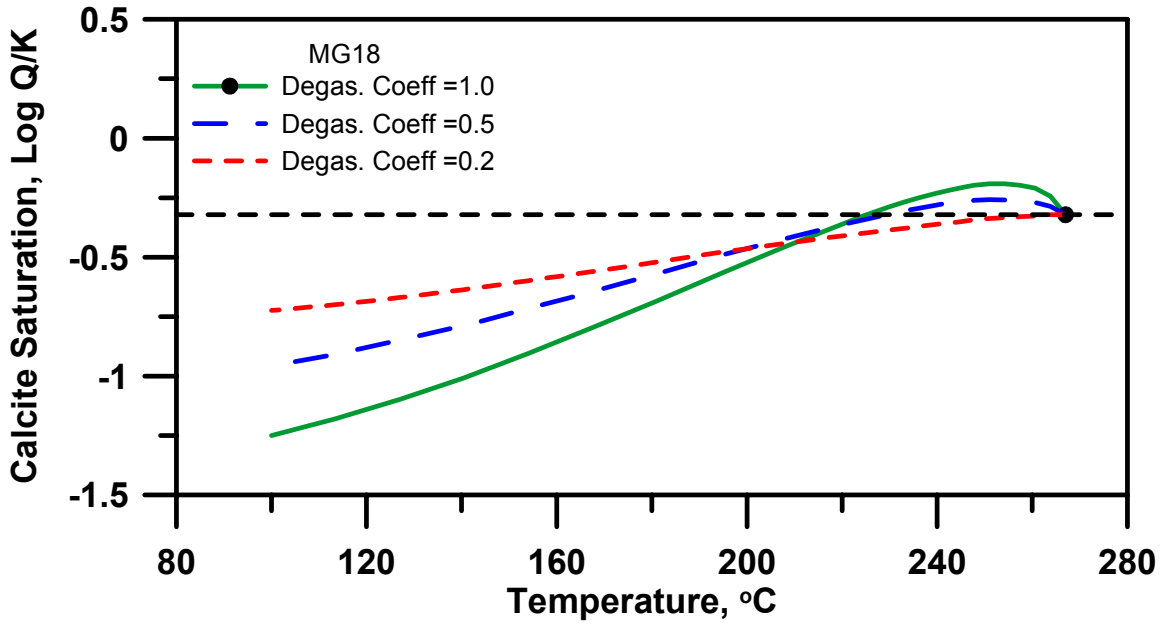

Figure 6.24 Calcite saturation of well MG18 during adiabatic boiling at different degassing coefficients.

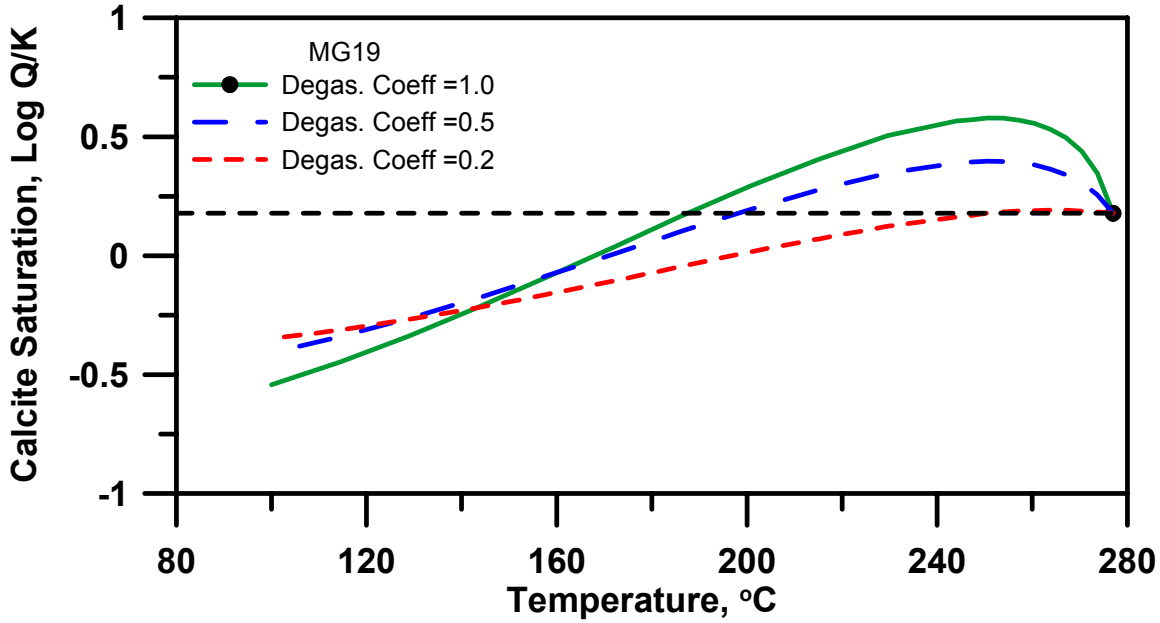

Figure 6.25 Calcite saturation of well MG19 during adiabatic boiling at different degassing coeffients.

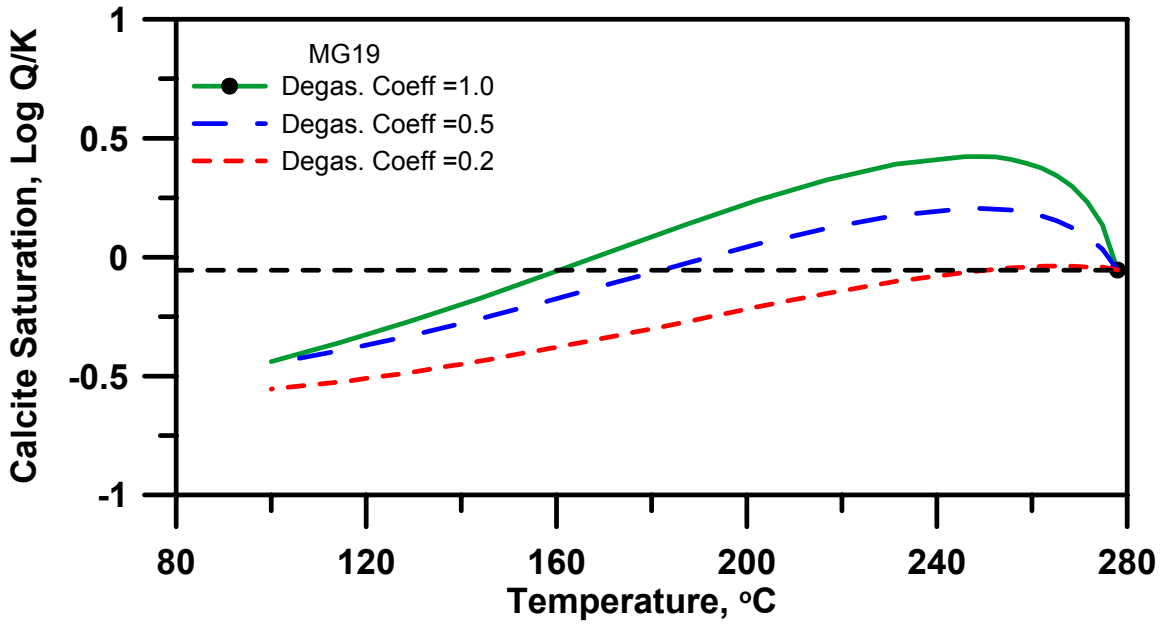

Figure 6.26 Calcite saturation of well MG19 during adiabatic boiling at different degassing coefficients. The chemistry data used in this plot is taken during fluid discharge testing (20-Dec-1995) of the well prior to production.

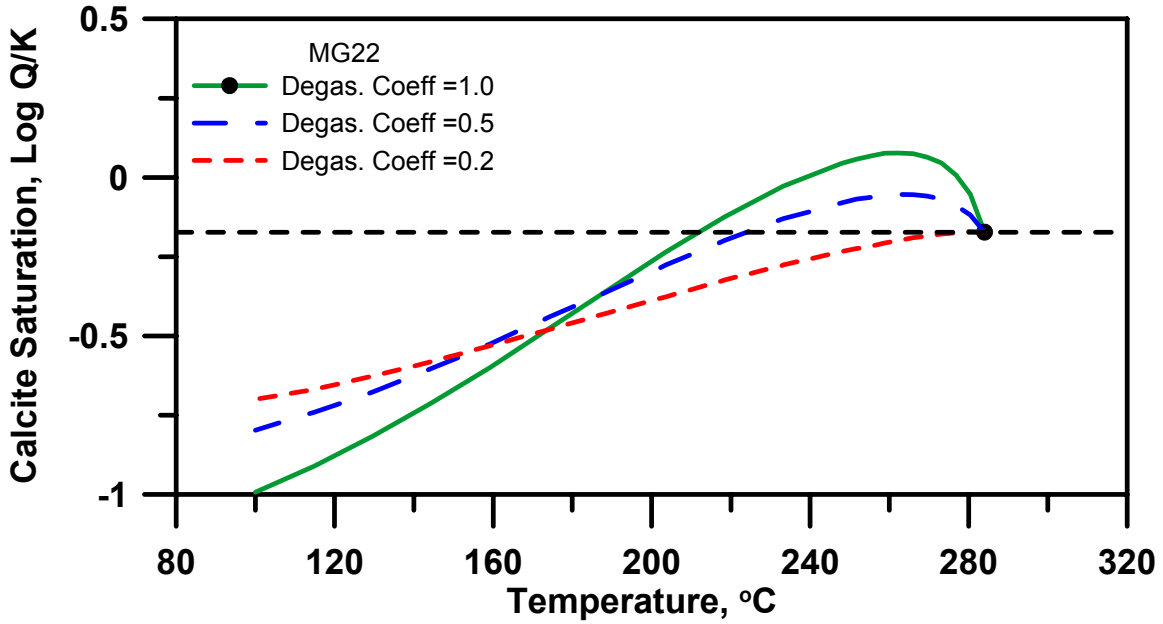

Figure 6.27 Calcite saturation of well MG22 during adiabatic boiling at different degassing coefficients.

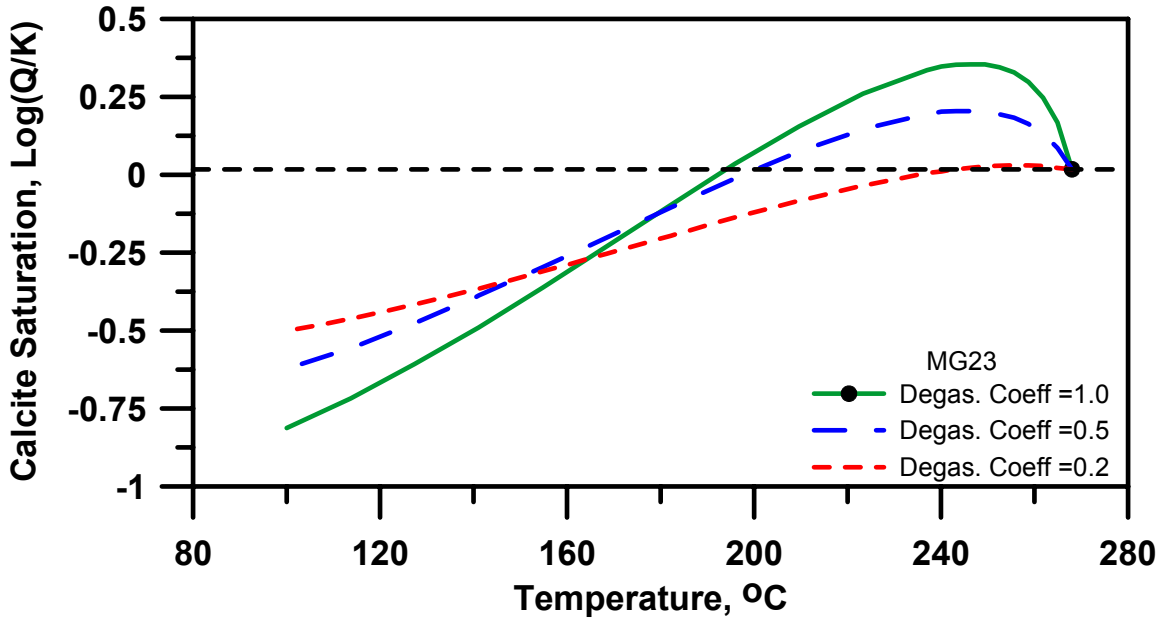

Figure 6.28 Calcite saturation of well MG23 during adiabatic boiling at different degassing coefficients.

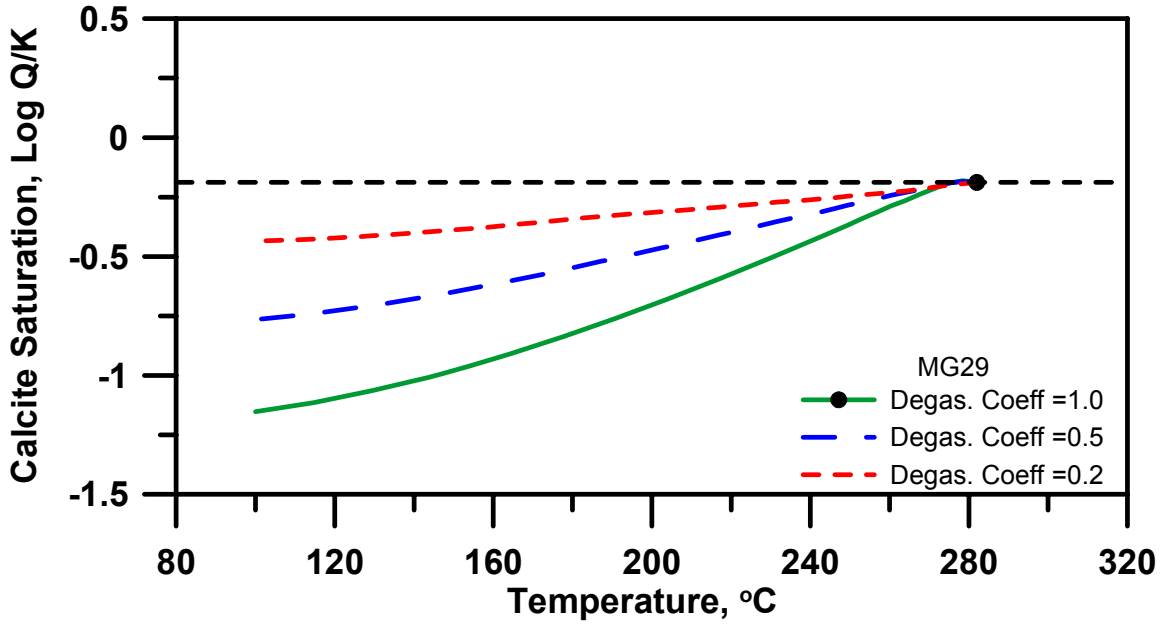

Figure 6.29 Calcite saturation of well MG29 during adiabatic boiling at different degassing coefficients.

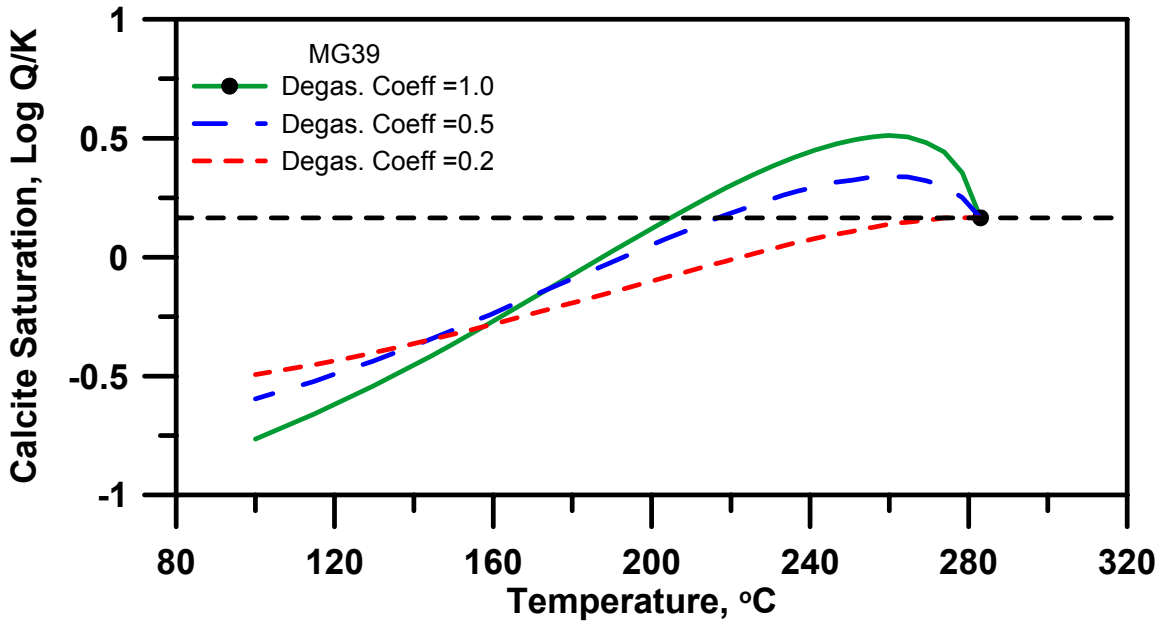

Figure 6.30 Calcite saturation of well MG39 during adiabatic boiling at different degassing coefficients.

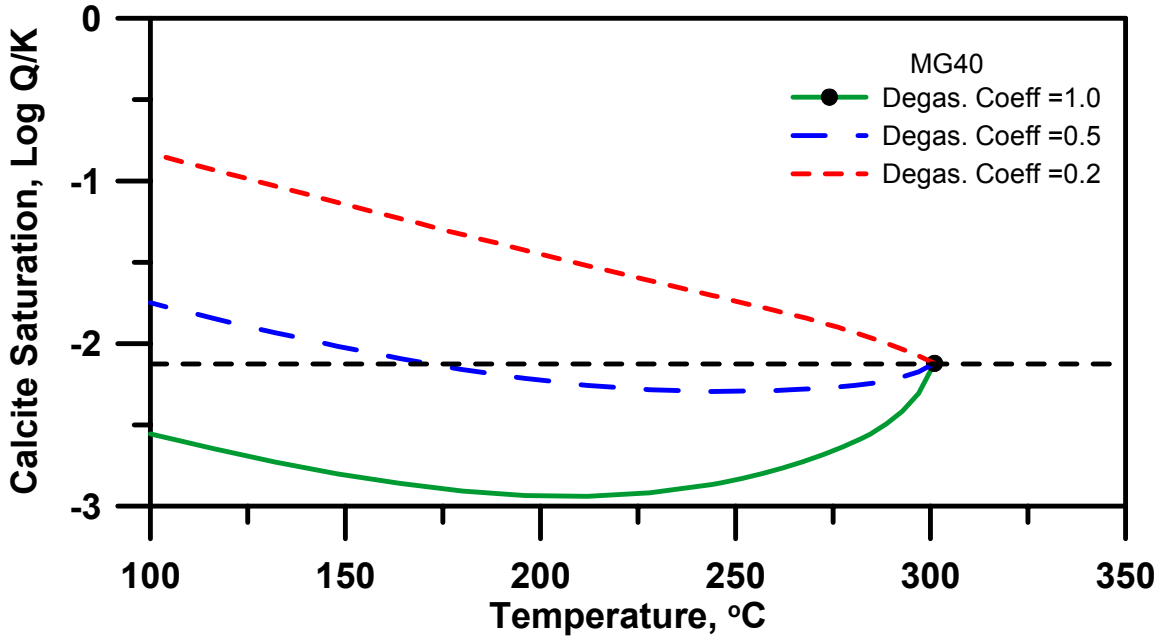

Figure 6.31 Calcite saturation of well MG40 during adiabatic boiling at different degassing coefficients.

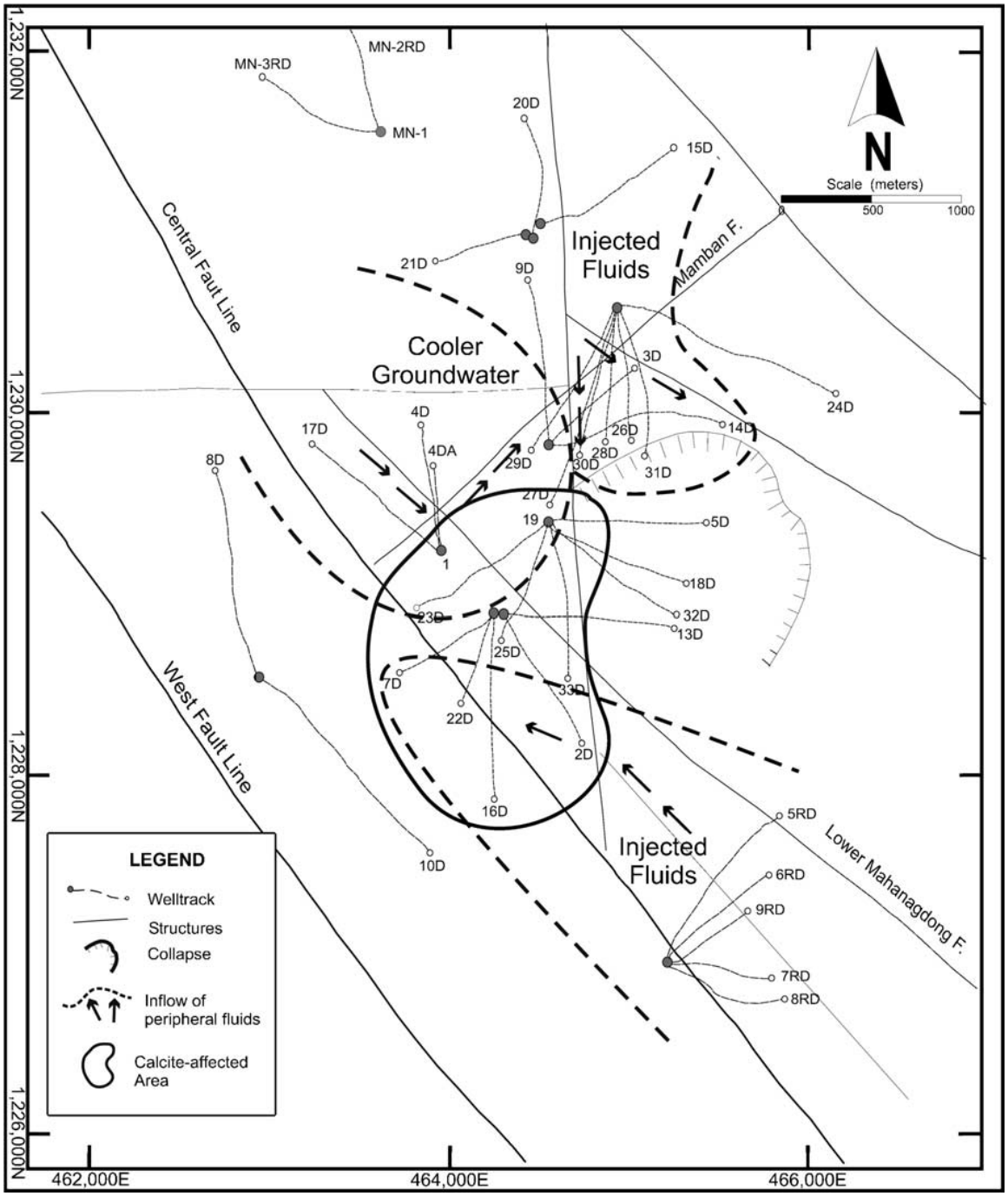

Figure 6.32 Inferred fluid flow paths at Mahanagdong geothermal field. Based on Salonga et al (2004).

6.2.3 Pataan Wells

Pataan aquifer fluids show trends similar to those of Hellisheidi and most of the Mahanagdong wells (Figures 6.33 to 6.38). During boiling the calcite saturation increases initially followed by a decline. The extent of degassing (increase in degassing coefficient) increases the degree of oversaturation. Well PT08 has the highest departure of 0.6 SI units (at 223 ^{o}C) above the initial saturation followed by PT05, PT10 and PT07 with 0.40 (at 246 ^{o}C), 0.31(at 258 ^{o}C) and 0.28 (at 252 ^{o}C) SI units above the the initial

saturation, respectively. PT05 is postulated to be nearest to the upflow region followed by PT08 and PT07 (Figure 6.39). Pataan has an observed 2 MPa "overpressure" in the area, Figure 6.40. Well PT05 has the highest dissolved aqueous CO_2 concentration at 9700 ppm followed by PT08 and PT07 at 7800 and 6700 ppm, respectively.

Wells PT02 and PT04 have the lowest positive departure from the initial saturation at 0.10 (at 262 ^{o}C) and 0.15 (at 262 ^{o}C) SI units above the initial saturation, respectively.

The implications for Pataan of the above described observations are that 1) the aquifer fluid feeding PT05 and PT08 may precipitate calcite in the immediate aquifer formation and in the well when degassing is more than 50% 2) aquifer fluids feeding PT10 and PT07 may precipitate calcite in the aquifer if sufficient over-saturation is produced and 3) aquifer fluid feeding PT02 may precipitate calcite in the well and/or in the aquifer if the degassing is less than 50% of maximum.

Olivar (2007) and Sanchez (2005) reported that PT02 is the only well that has physical evidence of calcite scale formation in the well. However, field-wide decline in total mass flow in the wells were documented during commissioning activities in 2007, Figure 6.41. Wells PT05 and PT08 total discharge enthalpies slightly increased then returned to the same level. Wells PT07 and PT10 discharge enthalpies slightly increased. Wells PT04 and PT02 total discharge enthalpies practically remained the same.

The physical evidences observed above are used to infer that Pataan geothermal area was affected by calcite precipitation in the aquifer formation during production which induces boiling and degassing of the aquifer fluids, Olivar (2007). This agrees well to the calculated calcite scaling potential of Pataan aquifer fluids as discussed above.

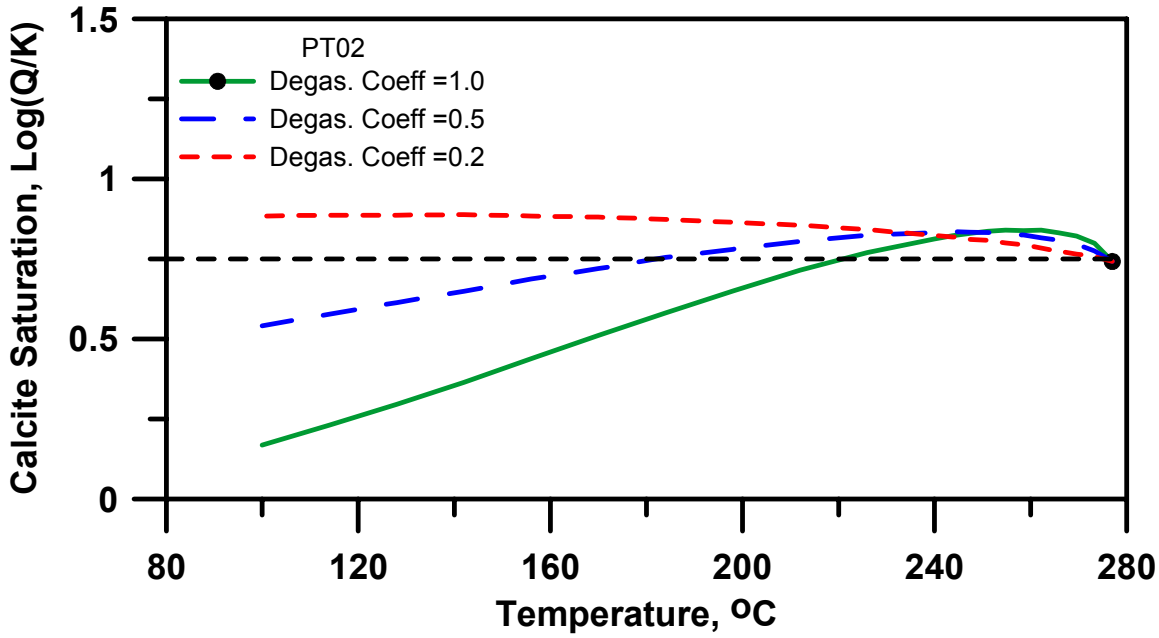

Figure 6.33 Calcite saturation of well PT02 during adiabatic boiling at different degassing coefficients.

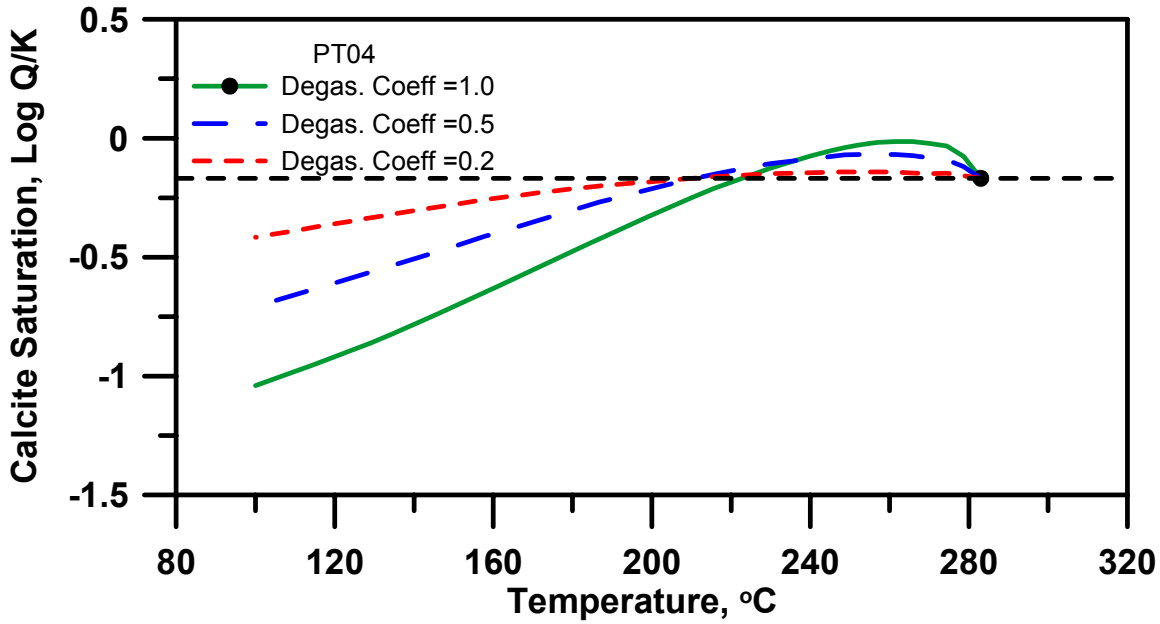

Figure 6.34 Calcite saturation of well PT04 during adiabatic boiling at different degassing coefficients.

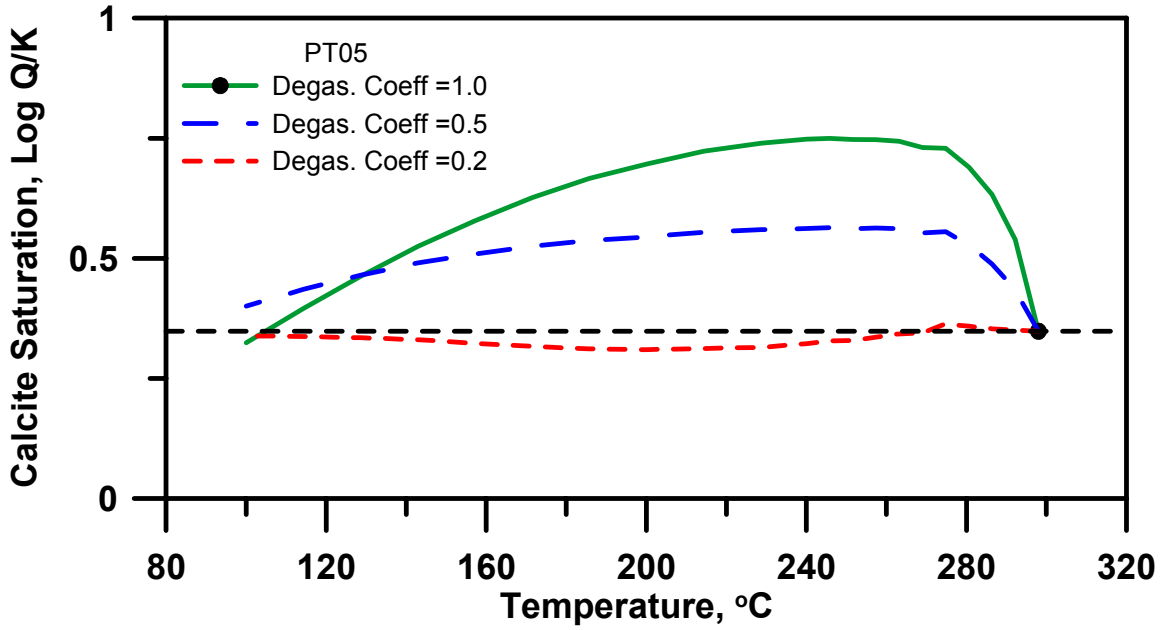

Figure 6.35 Calcite saturation of well PT05 during adiabatic boiling at different degassing coefficients.

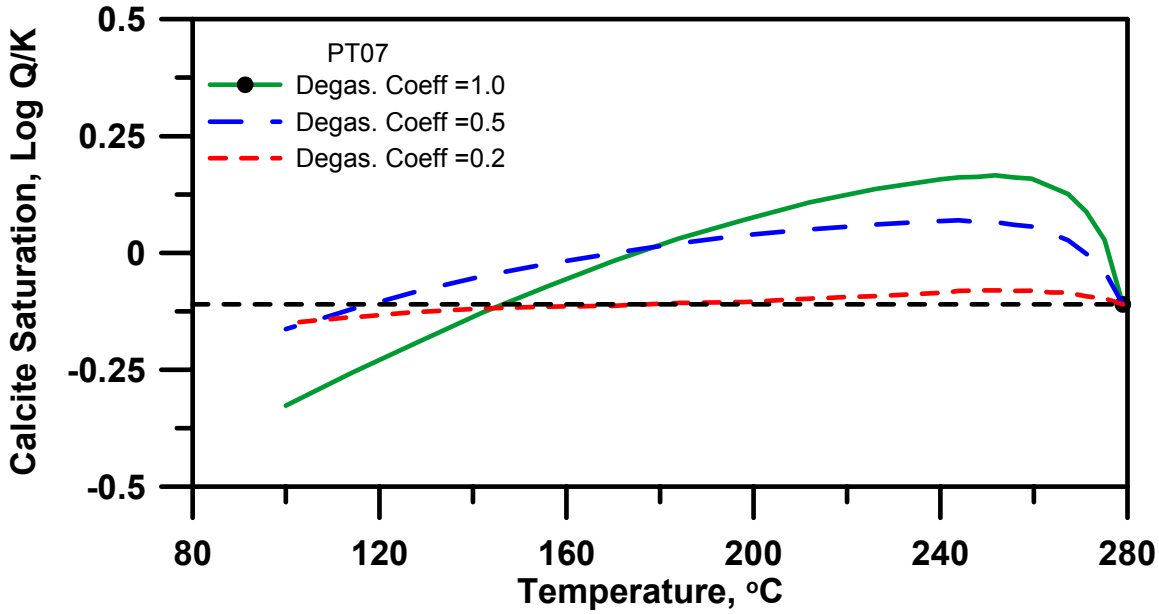

Figure 6.36 Calcite saturation of well PT07 during adiabatic boiling at different degassing coefficients.

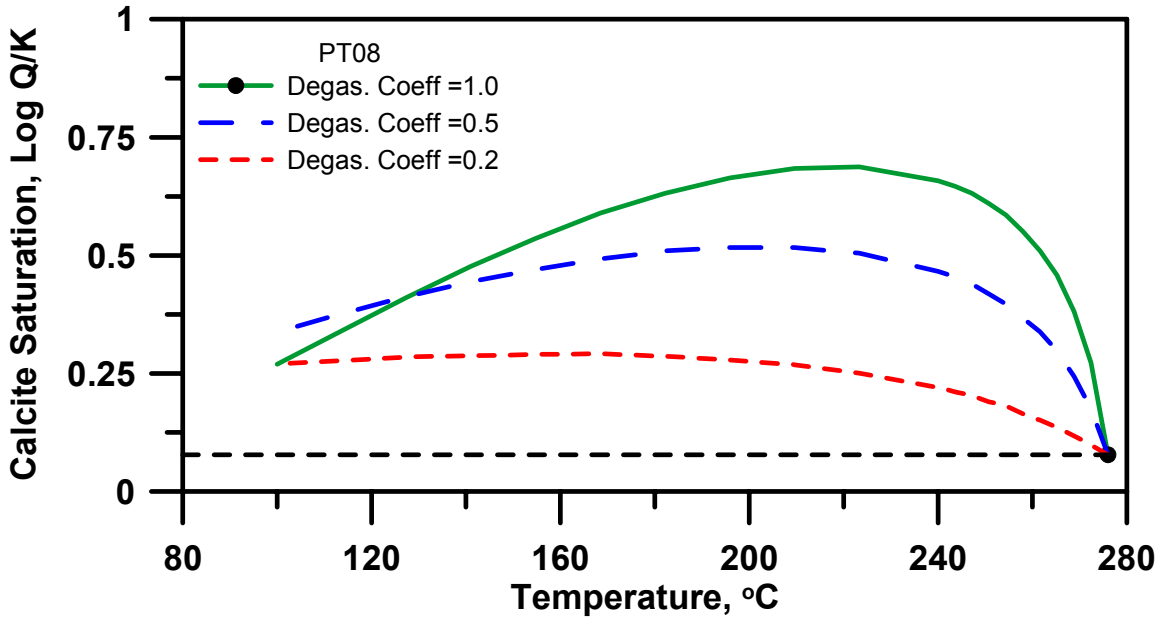

Figure 6.37 Calcite saturation of well PT08 during adiabatic boiling at different degassing coefficients.

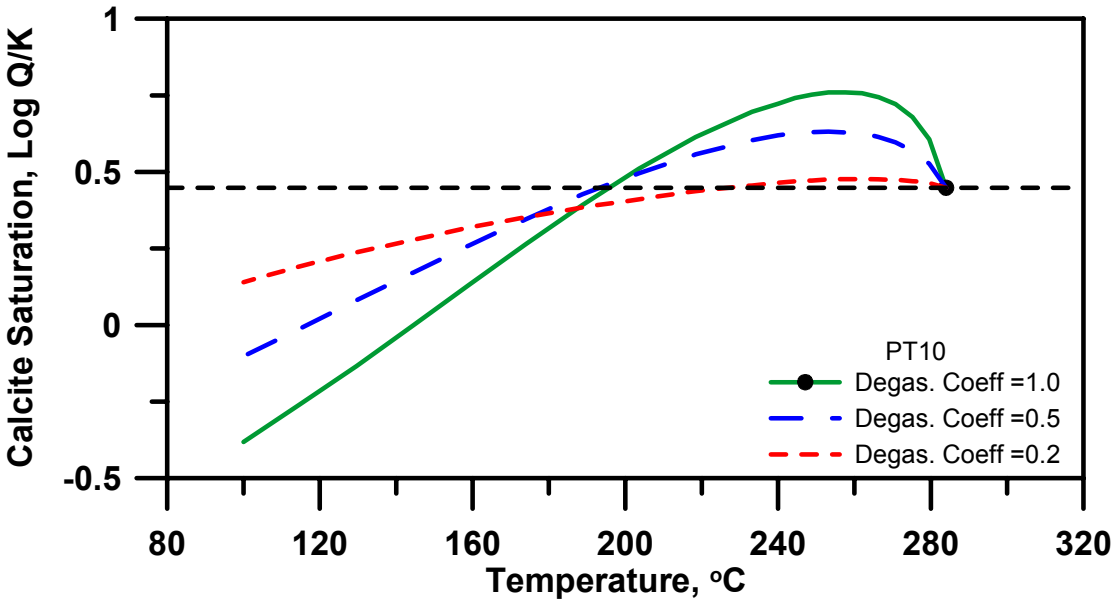

Figure 6.38 Calcite saturation of well PT10 during adiabatic boiling at different degassing coefficients.

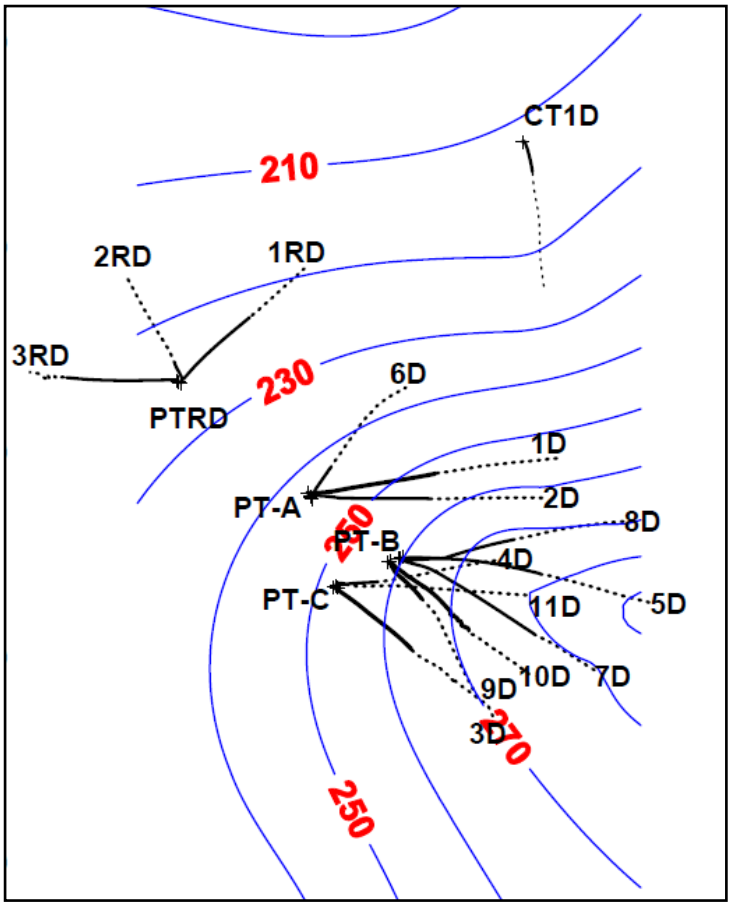

Figure 6.39 Pataan well tracks and the inferred temperature contour based on quartz geothermometer using closed system model in 2007 resource assessment. The dash line refers to the slotted liner of the well which is open for production. Modified after Olivar, 2007.

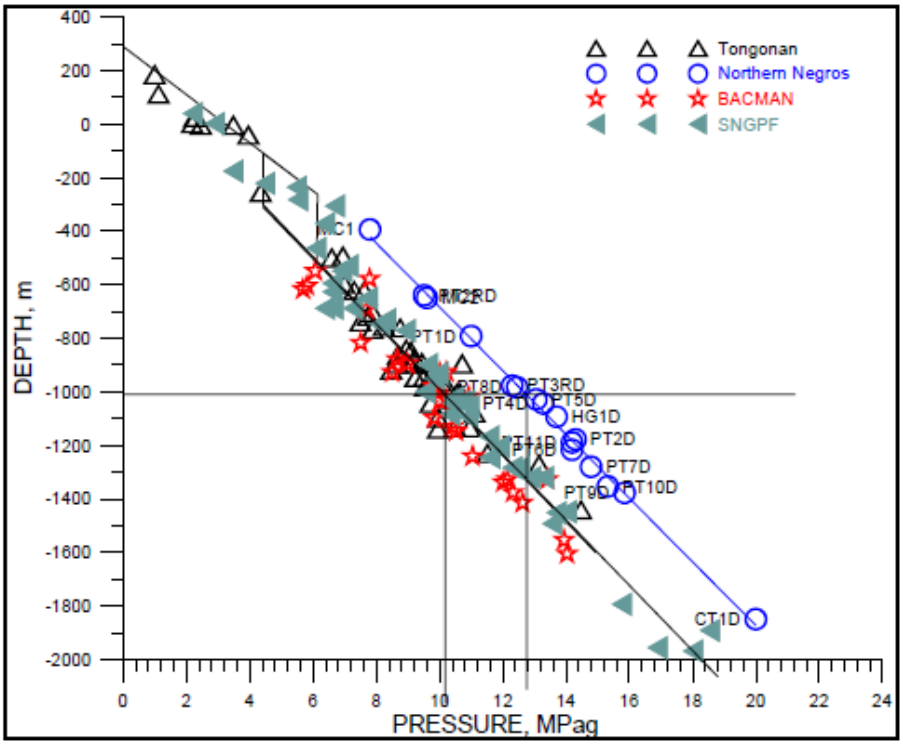

Figure 6.40 Natural stable reservoir pressure of different Philippine geothermal fields. Pataan wells are located in Northen Negros, Philippines. BACMAN refers to Bacon-Manito and SNGPF refers to Southern Negros Geothermal Production Fields. Reprint from Olivar, 2007.

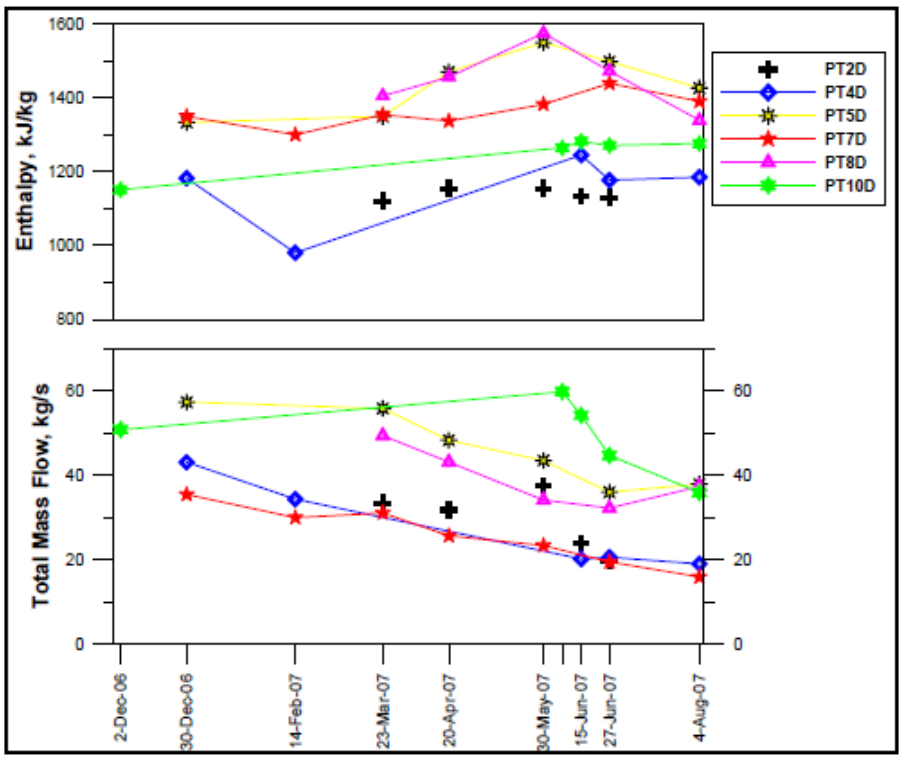

Figure 6.41 Total discharge enthalpy and mass flow of Pataan wells before and during commissioning in 2007. Reprint from Olivar (2007).

6.2.4 Well MD01

The effect of boiling and degassing for one well from Mindanao Geothermal Production Field, MD01 is plotted in Figure 6.42. This well is inferred to be affected by calcite scale formation, Olivar (personal comm.). It has similar general trend like those of Hellisheidi and Mahanagdong wells.

Well MD01 has highest departure of 0.425 SI units above the initial saturation at 241.5 ^{o}C and maximum degassing saturation. Its aquifer fluid may have the potential to precipitate calcite mineral in the surrounding aquifer formation and/or inside the well.

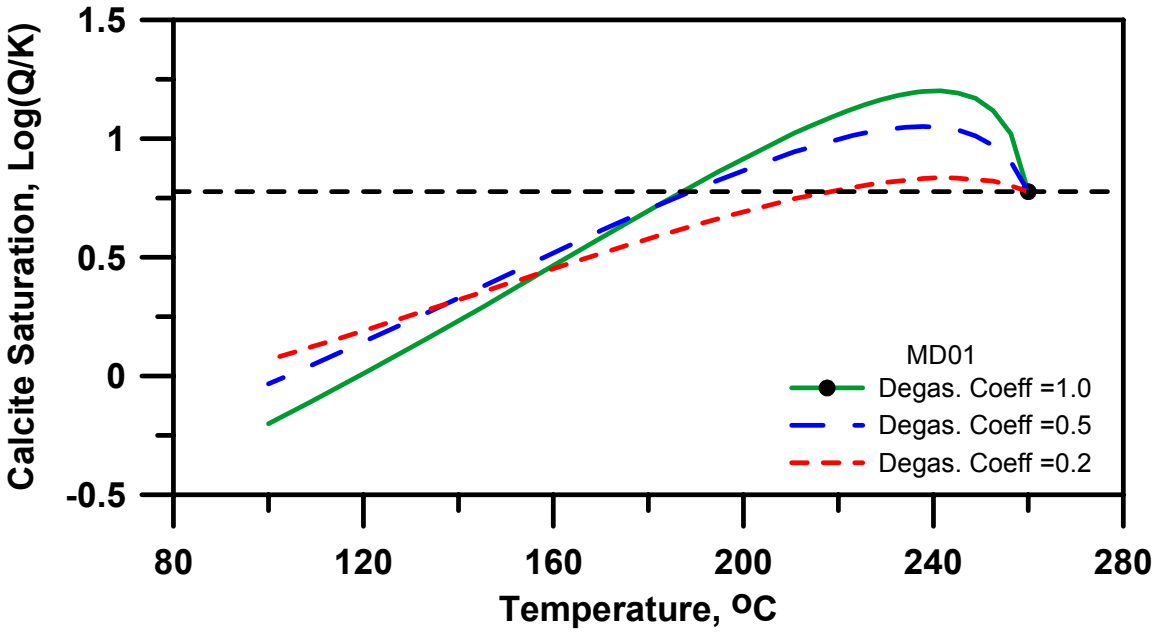

Figure 6.42 Calcite saturation of well MD01 during adiabatic boiling at different degassing coefficients.

6.3 Effect of Fluid Mixing

The effect of fluid mixing particularly that of injected separated water from the separators and aquifer fluid was investigated.

Table 6.2 summarizes the chemistry of injected separated water from the separators from Hellisheidi and Pataan wells. Pataan injected separated water is slightly acid, pH of 5.3 and higher in dissolved CO_2 than Hellisheidi. Hellisheidi in contrast is very alkaline with pH of 9.3 and has higher H_2S concentration than Pataan.

Table 6.2 Chemistry of the injected separated water from Hellisheidi and Pataan wells.

Location	Date Sampled	pH	Temp	H_2S	CO_2	NH_3	SO_4	Cl	F	SiO_2	Na	K	Ca	Mg	Fe	Al	Li	B
			°C	ppm														
Pataan	6-Jan-07	5.29	23.9	Nil	29.4	8.36	26.7	13629	5.19	675	7558	1254	702	2.54	0.85	NA	28.2	211
Hellisheidi	10-Oct-08	9.26	20	34.82	7.61	NA	10.81	198	1.34	797	200	34.3	0.42	0.0064	0.009	1.74	0.2	1.18

NA - not analyzed, Nil - negligible

The composition of the fluid mixtures are simulated using the aqueous modeling code PHREEQC-2 version 2.17.00 from the graphical interface PHREEQC for Windows develop by Vincent Post (http://www.falw.vu/~posv/phreeqc/index.html). PHREEQC is a hydrogeochemical transport model developed by D.L. Parkhurst and C.A.J Appelo (1999). The thermodynamic database used is *phreeqc.dat* which is slightly modified version of the database used in PHREEQE (Parkhurst et al., 1980). Caution must be taken into account in the interpretation of the results, however, since PHREEQC is mostly used for low-temperature aqueous geochemical speciation. An example of PHREEQC input file used in the simulation is included in Appendix A.

The mixed fluid was inputted into WATCH 2.1 to simulate boiling and degassing. Table 6.3 and 6.4 show the compositions of the mixed fluids of Hellisheidi and Pataan wells, respectively at different proportions of injected separated water. Pataan separated water from the separators is being injected at temperature of 160 ^{o}C, which is used in the simulations of both Hellisheidi and Pataan fluid mixing.

Calcite saturation indices of Hellisheidi mixed fluids are shown in Figures 6.43 to 6.51. Calcite saturation indices of the mixed fluids dropped to below the original saturation of aquifer fluids. Increasing the injected separated water proportion in the mixture decreases the calcite saturation index of the mixed fluid. Saturation indices of the mixed fluids upon boiling are below that of the initial aquifer fluids except at well HE11 where at 30% mix injected separated water, the saturation approach that of the initial aquifer fluid saturation.

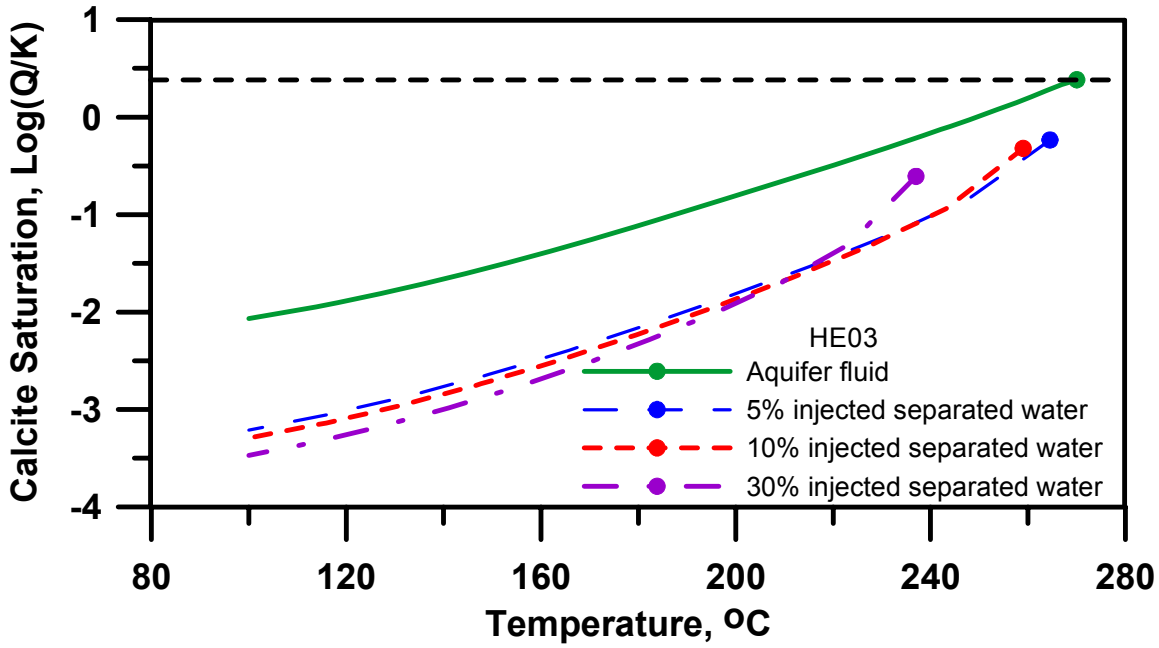

Figure 6.43 Calcite saturation of mixed fluids of well HE03 during adiabatic boiling at equilibrium degassing.

Plots of calcite mineral saturations of Pataan wells are shown in Figures 6.52 to 6.57. Calcite mineral saturation of the mixed fluids also dropped to below the original aquifer fluid saturation at low mixing proportions (5 and 10% injected separated water mixtures). However, increasing the injected separated water proportion in the mixture increases the calcite saturation index of the fluid mixtures. It seems that mixing injected separated

water by more than 30% of the initial aquifer fluids will bring the saturation to or above the initial saturation upon adiabatic boiling.

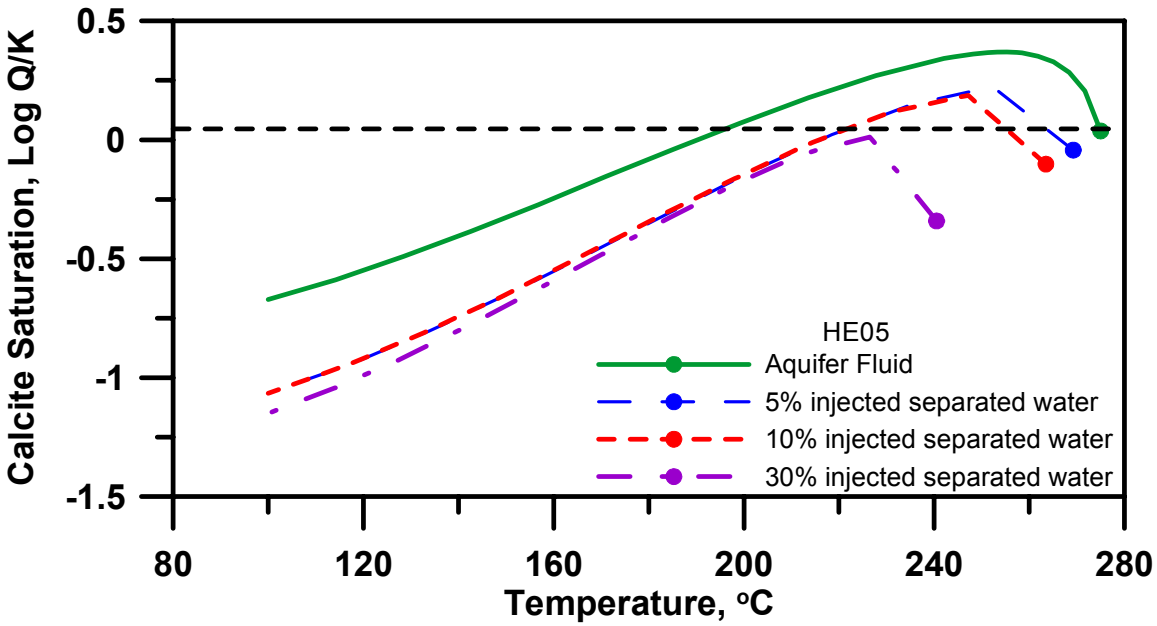

Figure 6.44 Calcite saturation of mixed fluids of well HE05 during adiabatic boiling at equilibrium degassing.

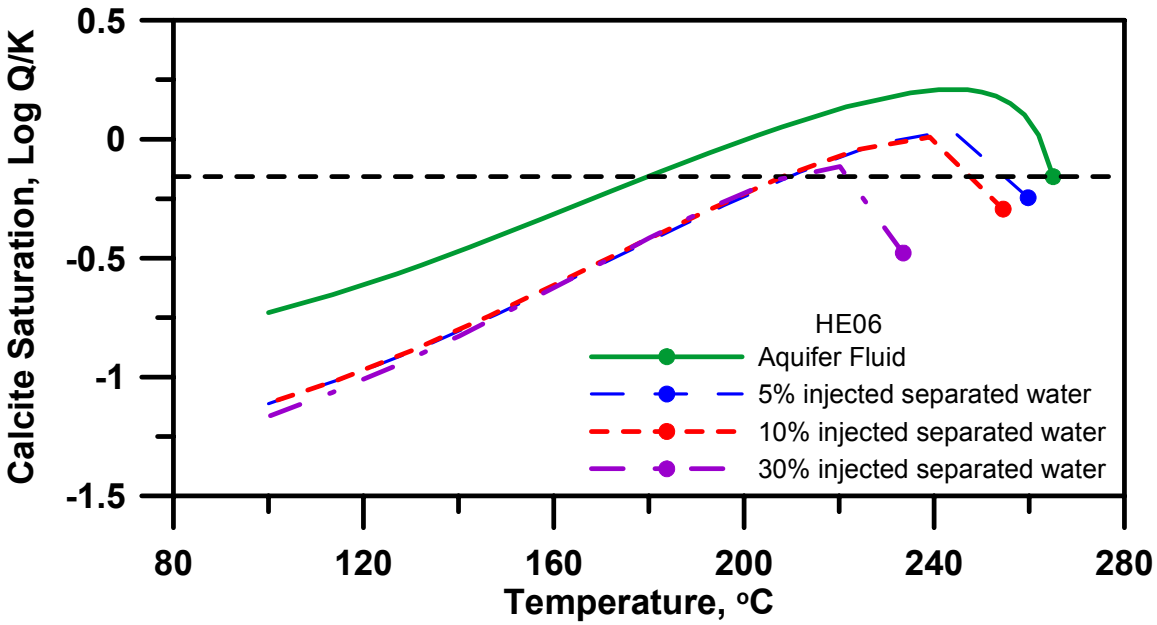

Figure 6.45 Calcite saturation of mixed fluids of well HE06 during adiabatic boiling at equilibrium degassing.

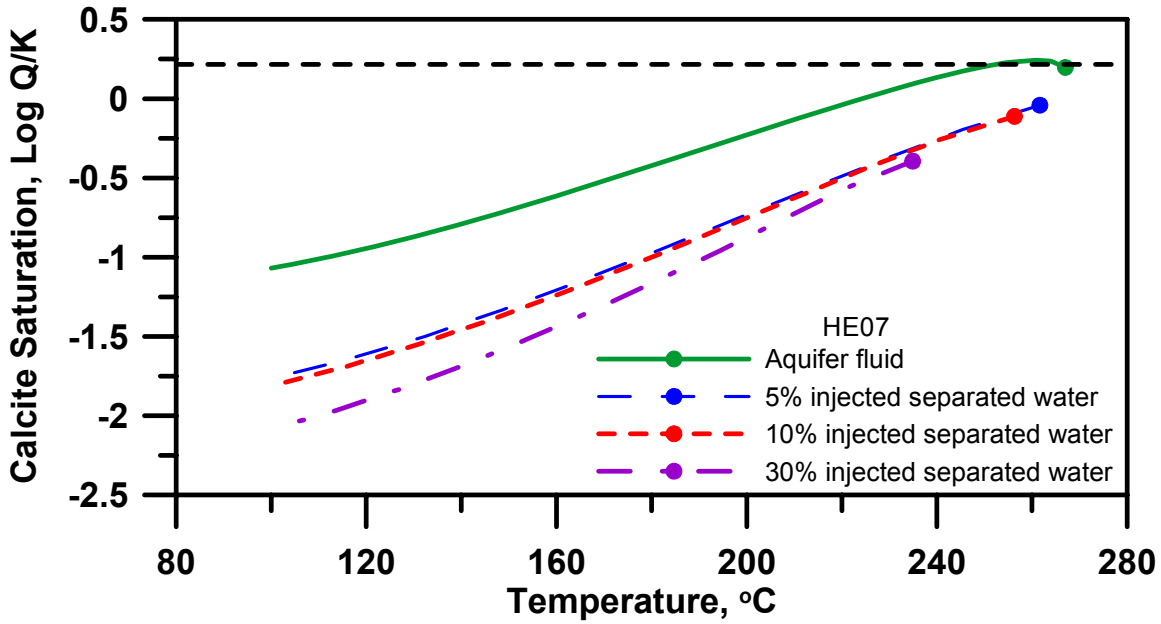

Figure 6.46 Calcite saturation of mixed fluids of well HE07 during adiabatic boiling at equilibrium degassing.

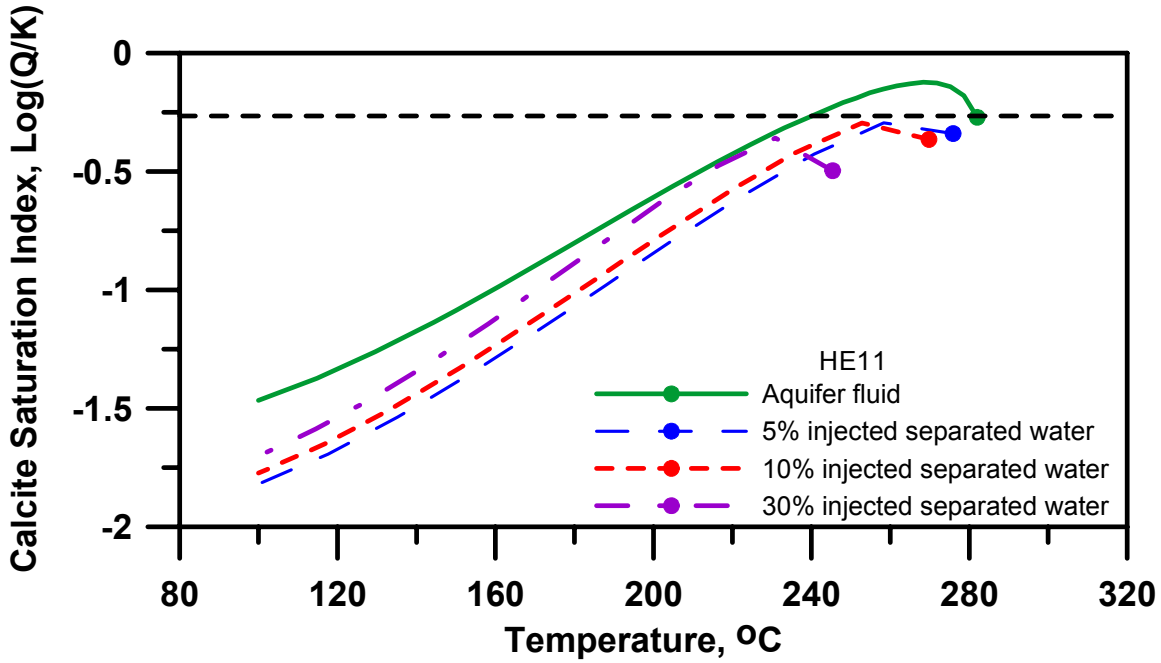

Figure 6.47 Calcite saturation of mixed fluids of well HE11 during adiabatic boiling at equilibrium degassing.

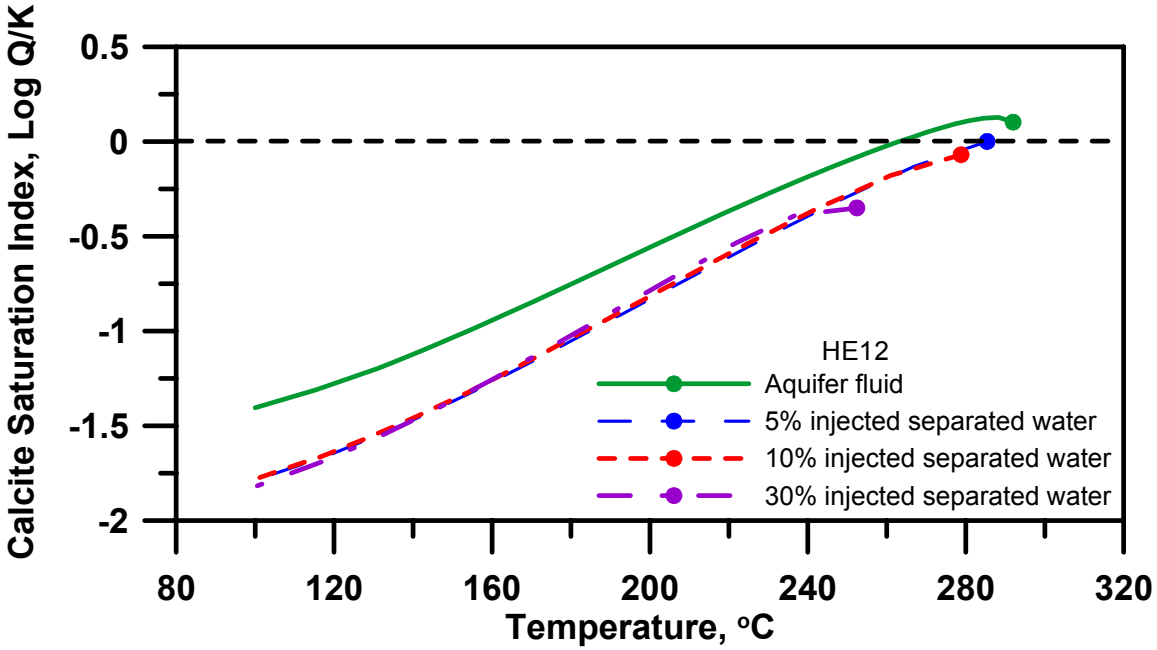

Figure 6.48 Calcite saturation of mixed fluids of well HE12 during adiabatic boiling at equilibrium degassing.

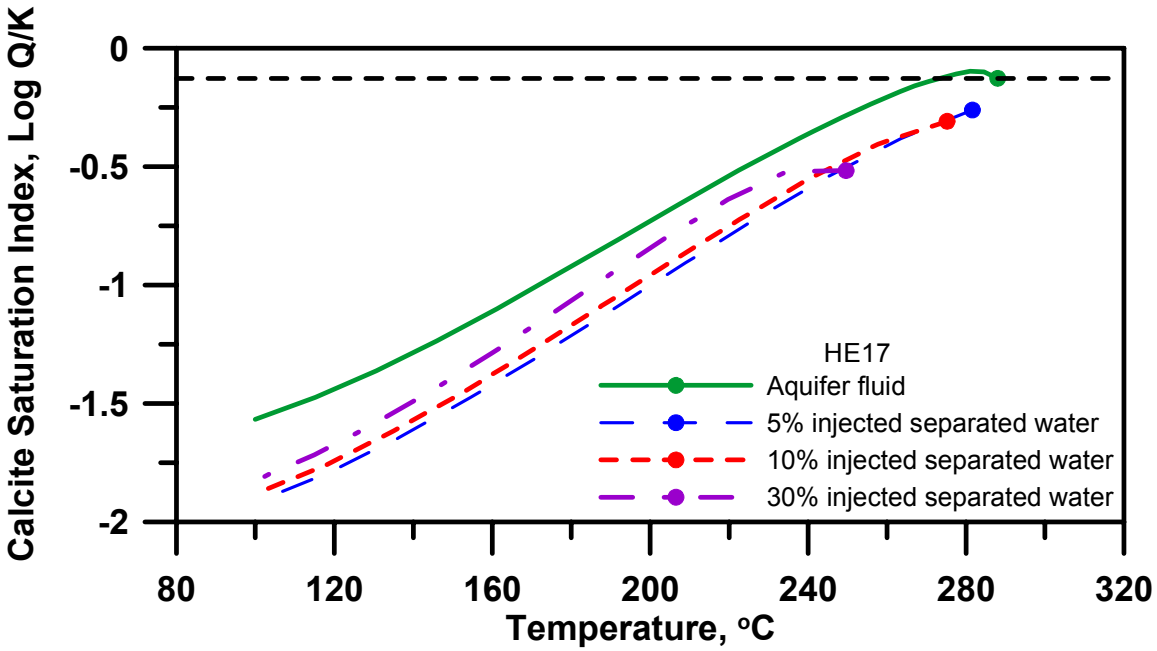

Figure 6.49 Calcite saturation of mixed fluids of well HE17 during adiabatic boiling at equilibrium degassing.

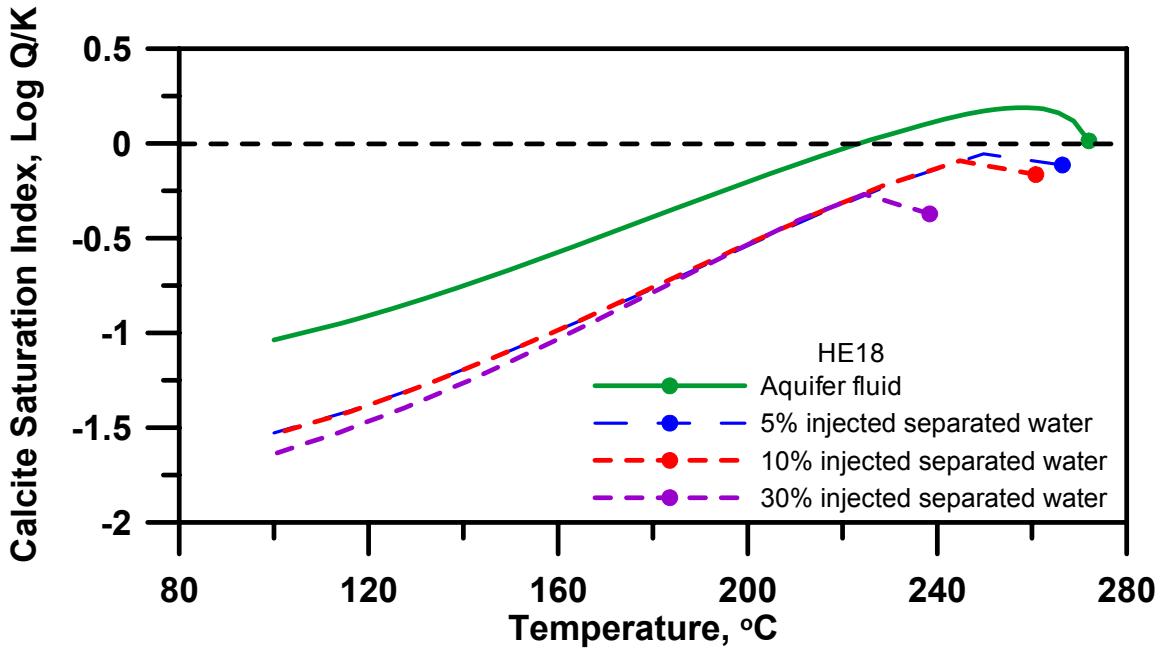

Figure 6.50 Calcite saturation of mixed fluids of well HE18 during adiabatic boiling at equilibrium degassing.

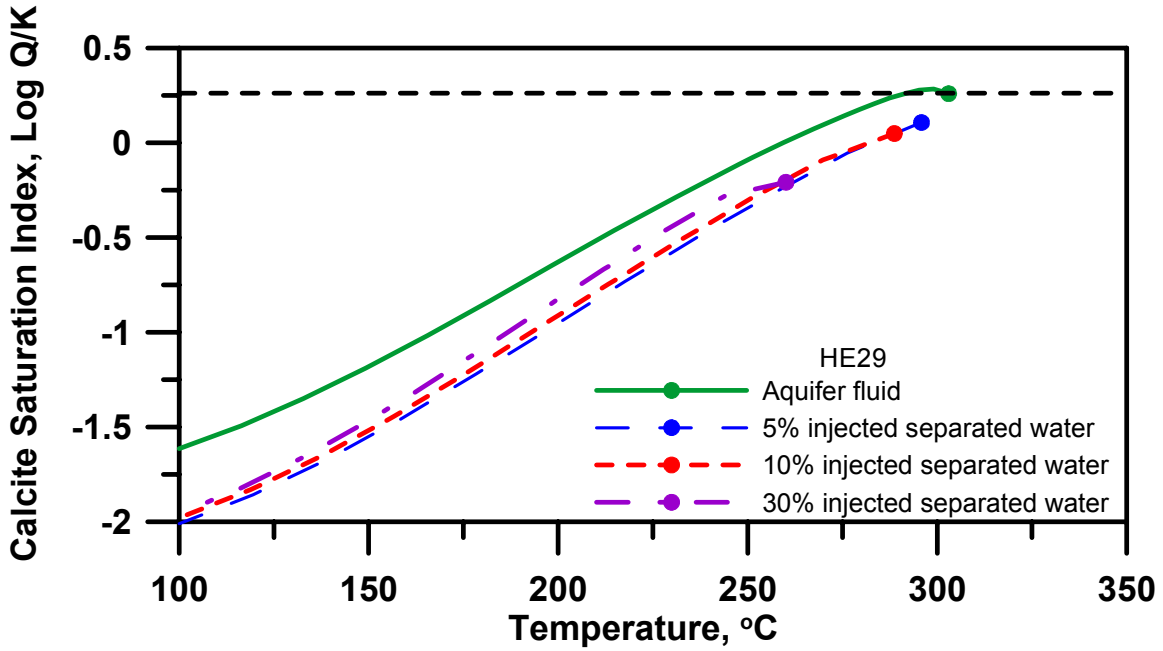

Figure 6.51 Calcite saturation of mixed fluids of well HE29 during adiabatic boiling at equilibrium degassing.

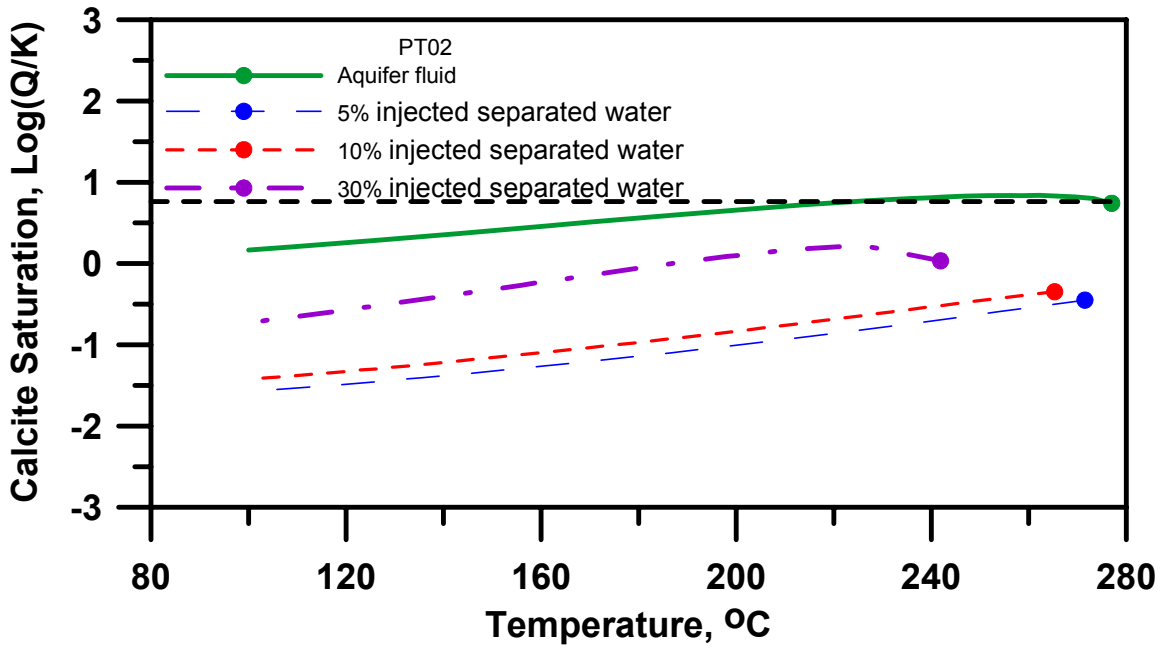

Figure 6.52 Calcite saturation of mixed fluids of well PT02 during adiabatic boiling at equilibrium degassing.

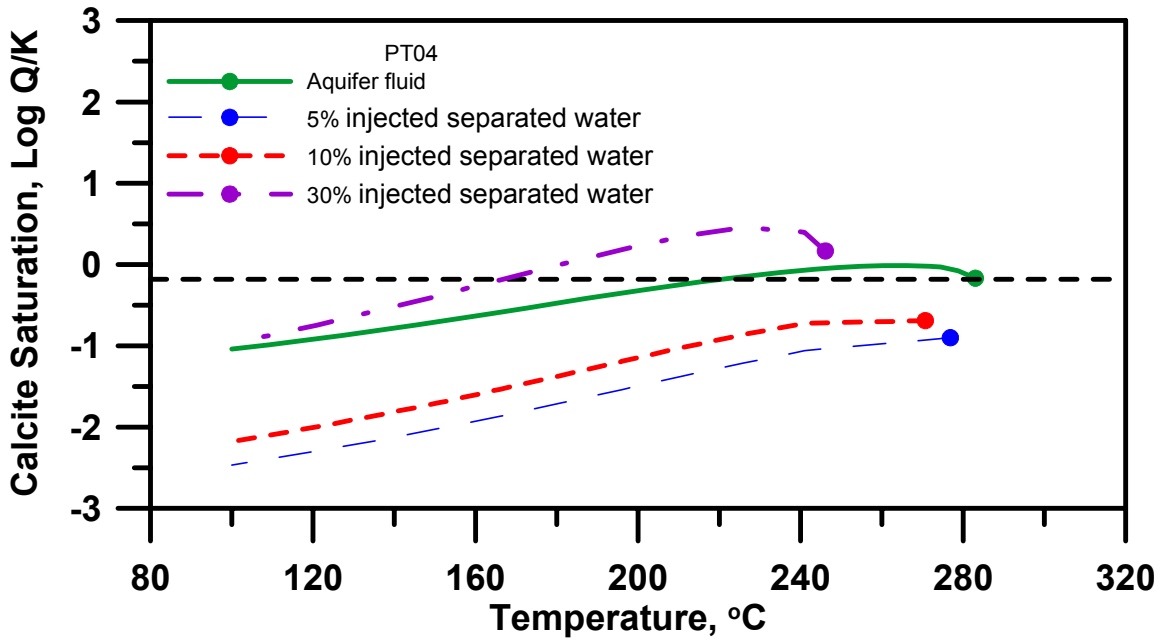

Figure 6.53 Calcite saturation of mixed fluids of well PT04 during adiabatic boiling at equilibrium degassing.

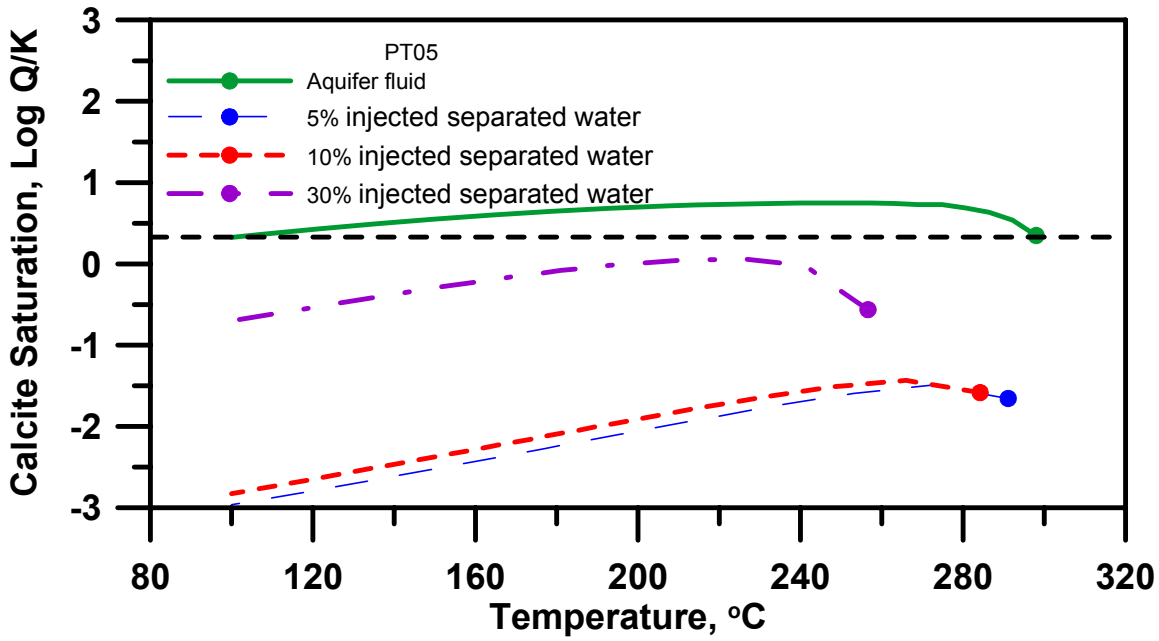

Figure 6.54 Calcite saturation of mixed fluids of well PT05 during adiabatic boiling at equilibrium degassing.

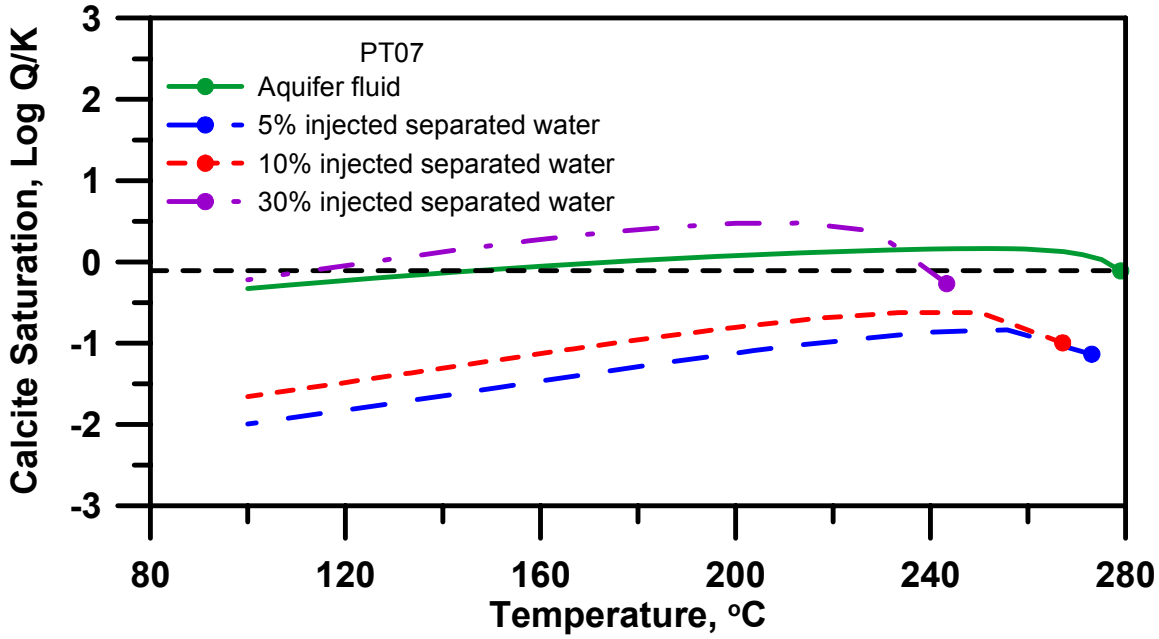

Figure 6.55 Calcite saturation of mixed fluids of well PT07 during adiabatic boiling at equilibrium degassing.

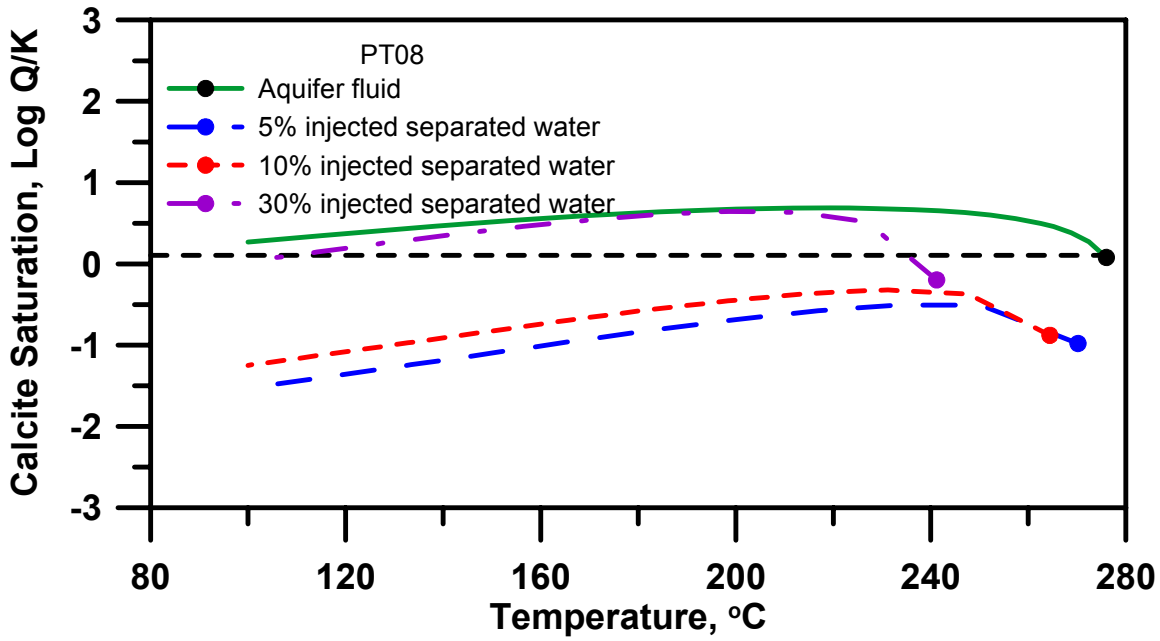

Figure 6.56 Calcite saturation of mixed fluids of well PT08 during adiabatic boiling at equilibrium degassing.

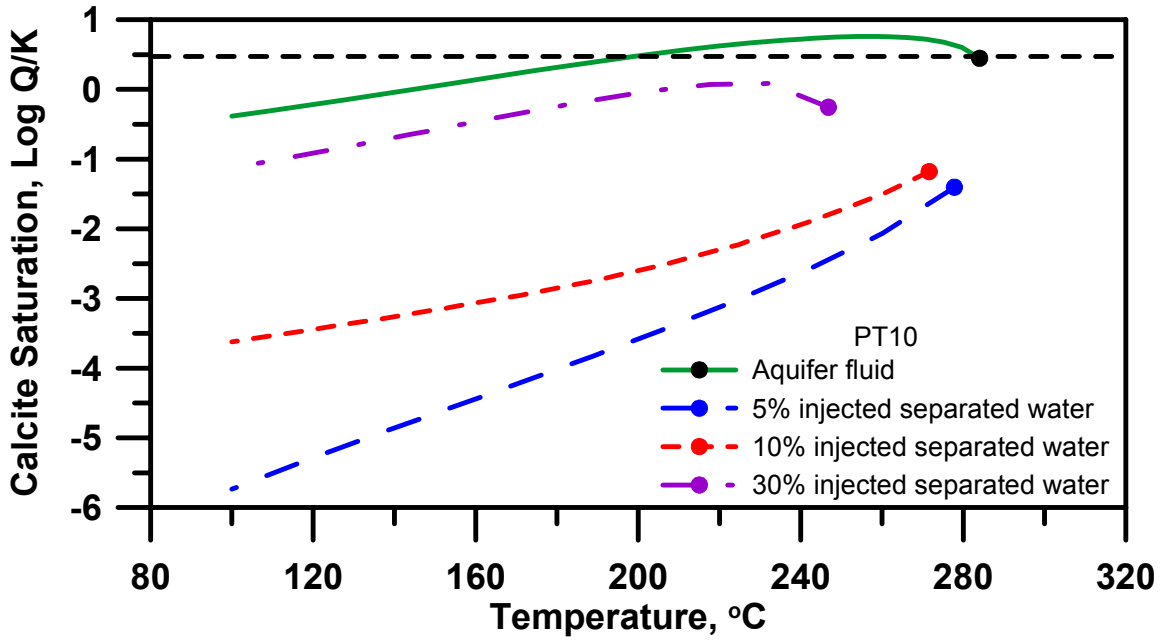

Figure 6.57 Calcite saturation of mixed fluids of well PT10 during adiabatic boiling at equilibrium degassing.

Table 6.3 Compositions of mixed fluids (aquifer fluid and injected separated waters) of Hellisheidi wells based on PHREEQC simulations.

Well	% reinjected brine	Temp	pH	Ca^{+2}	Mg^{+2}	Na+	K+	SO_4^{-2}	Cl-	F-	H_3BO_3	H_4SiO_4	Al^{+3}	Fe^{+2}	H_2S	CO_2	H_2	CH_4	N_2
		°C		mmole/kgw															
HE03	5	264.5	7.30	0.0136	1.13E-05	8.52	0.93	6.29E-02	7.83	0.0366	0.0742	8.99	7.57E-16	1.74E-06	0.35	0.43	0.0006	0.0035	0.14
HE05		269.25	7.02	0.0056	1.17E-05	5.47	0.57	1.28E-02	1.88	0.0822	0.0325	9.23	2.93E-12	1.64E-06	2.12	11.84	0.0005	0.0457	2.03
HE06		259.75	6.85	0.0068	4.83E-05	5.73	0.53	1.86E-03	2.58	0.0388	0.0529	8.67	5.42E-12	4.39E-07	2.89	10.82	0.0008	0.2927	0.17
HE07		261.65	6.39	0.0094	3.78E-04	7.02	0.67	2.34E-03	4.51	0.0465	0.0907	8.89	8.78E-14	1.15E-07	3.26	1.89	0.0013	0.3810	0.00
HE12		275.9	7.01	0.0051	1.61E-04	6.13	0.68	9.25E-04	4.13	0.0485	0.0927	10.11	1.81E-12	4.02E-07	5.78	4.19	0.0013	0.8018	1.39
HE11		285.4	7.17	0.0033	4.92E-05	5.65	0.63	9.92E-04	3.46	0.0429	0.0741	9.62	4.32E-12	1.09E-06	3.98	6.93	0.0011	0.5498	0.73
HE17		281.6	6.98	0.0050	8.77E-05	5.78	0.69	5.00E-04	4.33	0.0388	0.0996	9.84	6.31E-12	2.13E-07	6.52	4.66	0.0013	0.9224	1.14
HE18		266.4	7.07	0.0059	4.86E-05	5.80	0.57	1.92E-03	3.32	0.0482	0.0637	9.14	8.43E-13	2.22E-07	3.17	5.25	0.0010	0.3901	0.65
HE29		295.85	7.25	0.0040	4.93E-05	4.02	0.47	8.28E-04	2.17	0.0638	0.3566	10.62	2.27E-12	1.15E-07	4.51	4.44	0.0012	0.5833	0.19
HE03	10	259	7.32	0.0133	2.21E-05	8.52	0.93	6.57E-02	7.71	0.0384	0.0753	9.17	2.65E-16	1.39E-06	0.29	0.35	0.0006	0.0039	0.13
HE05		263.5	7.00	0.0057	2.33E-05	5.64	0.59	1.57E-02	2.08	0.0816	0.0365	9.44	2.02E-12	1.49E-06	2.02	11.07	0.0005	0.0410	1.93
HE06		254.5	6.84	0.0069	5.83E-05	5.88	0.55	2.26E-03	2.73	0.0405	0.0559	8.91	3.47E-12	4.25E-07	2.73	10.11	0.0008	0.2719	0.16
HE07		256.3	7.17	0.0094	3.70E-04	7.10	0.68	2.69E-03	4.56	0.0477	0.0916	9.12	5.64E-14	1.07E-07	3.01	1.74	0.0013	0.3555	0.00
HE12		269.8	7.00	0.0053	1.65E-04	6.26	0.69	1.08E-03	4.21	0.0497	0.0935	10.27	1.16E-12	3.54E-07	5.39	3.91	0.0013	0.7539	1.32
HE11		278.8	7.14	0.0036	5.94E-05	5.81	0.64	1.22E-03	3.58	0.0444	0.0759	9.81	2.59E-12	9.22E-07	3.74	6.46	0.0011	0.5152	0.69
HE17		275.2	6.97	0.0052	9.60E-05	5.93	0.70	6.17E-04	4.40	0.0405	0.1001	10.02	3.73E-12	1.87E-07	6.10	4.35	0.0013	0.8680	1.08
HE18		260.8	7.06	0.0061	5.86E-05	5.95	0.59	2.28E-03	3.44	0.0494	0.0660	9.35	5.33E-13	2.08E-07	2.97	4.87	0.0010	0.3641	0.62
HE29		288.7	7.23	0.0043	5.95E-05	4.26	0.49	1.03E-03	2.35	0.0662	0.3434	10.76	1.34E-12	1.09E-07	4.21	4.13	0.0012	0.5469	0.18
HE03	30	237	7.50	0.0125	5.66E-05	8.56	0.92	7.63E-02	7.24	0.0456	0.0772	9.79	5.18E-18	7.52E-07	0.14	0.14	0.0009	0.0047	0.10
HE05		240.5	6.93	0.0064	6.82E-05	6.32	0.65	3.21E-02	2.86	0.0794	0.0524	10.28	3.93E-13	1.03E-06	1.60	7.99	0.0005	0.0278	1.50
HE06		233.5	6.82	0.0073	9.73E-05	6.51	0.62	4.92E-03	3.37	0.0472	0.0675	9.87	5.29E-13	3.63E-07	2.11	7.29	0.0008	0.1897	0.12
HE07		234.9	7.15	0.0094	3.33E-04	7.46	0.73	4.81E-03	4.79	0.0528	0.0946	10.00	7.26E-15	8.40E-08	1.99	1.15	0.0014	0.2542	0.00
HE12		245.4	6.96	0.0063	1.81E-04	6.81	0.73	2.05E-03	4.51	0.0544	0.0966	10.92	1.72E-13	2.21E-07	3.87	2.78	0.0013	0.5625	1.03
HE11		252.4	7.05	0.0049	9.91E-05	6.46	0.69	2.66E-03	4.02	0.0503	0.0830	10.56	3.13E-13	5.11E-07	2.75	4.59	0.0011	0.3775	0.54
HE17		249.6	6.92	0.0062	1.29E-04	6.55	0.74	1.36E-03	4.66	0.0473	0.1018	10.73	4.33E-13	1.20E-07	4.41	3.13	0.0013	0.6510	0.84
HE18		238.4	7.03	0.0068	9.78E-05	6.56	0.65	4.58E-03	3.92	0.0542	0.0752	10.20	7.29E-14	1.64E-07	2.14	3.38	0.0010	0.2611	0.48
HE29		260.1	7.14	0.0055	9.95E-05	5.25	0.58	2.30E-03	3.07	0.0674	0.2903	11.30	1.50E-13	9.14E-08	3.01	2.90	0.0012	0.4019	0.14

kgw-kg water

Table 6.4 Compositions of mixed fluids (aquifer fluid and injected separated waters) of Pataan wells based on PHREEQC simulations.

Well	% reinjected brine	Temp	pH	Ca^{+2}	Mg^{+2}	Na+	K+	SO_4^{-2}	Cl-	F-	H_3BO_3	H_4SiO_4	Fe^{+2}	H_2S	NH_3	CO_2	H_2	CH_4	N_2
		°C		mmole/kgw															
PT02	5	271	5.54	0.73	0.0844	182.28	18.36	2.26E-06	209.63	0.1318	12.91	9.33	4.12E-03	5.43	1.6085	39.46	0.0861	0.6983	5.58
PT04		277	5.30	1.86	0.0679	203.29	20.93	1.26E-07	244.81	0.0064	5.63	9.70	5.82E-04	3.73	0.1328	16.66	0.1398	0.8659	2.93
PT05		291	4.71	0.53	0.0575	272.81	27.28	1.04E-07	346.17	0.0433	17.55	10.51	8.98E-03	5.82	0.0510	196.15	0.1142	0.5545	22.30
PT07		273	4.83	1.26	0.0477	225.31	23.18	3.64E-03	272.91	0.0598	15.59	9.53	1.01E-02	3.15	0.0667	135.49	0.0056	0.0000	0.38
PT08		270	4.88	1.19	0.0918	217.39	18.46	1.04E-07	256.16	0.0039	15.52	9.44	8.53E-03	2.38	0.0633	159.81	0.0707	1.5672	12.75
PT10		278	4.88	2.07	0.0526	191.28	21.75	4.64E-01	232.41	0.0034	14.12	9.72	3.81E-03	5.02	0.1069	31.47	0.0022	0.0000	5.76
PT02	10	265	5.47	1.38	0.0863	190.42	19.12	2.54E-06	219.33	0.1321	13.28	9.44	4.77E-03	5.16	1.3180	37.18	0.0680	0.6499	5.29
PT04		271	5.34	2.71	0.0698	210.32	21.56	2.40E-07	252.66	0.0143	6.38	9.79	1.16E-03	3.54	0.1341	15.81	0.1093	0.8111	2.78
PT05		284	4.55	1.34	0.0603	276.18	27.57	8.17E-08	348.69	0.0360	17.68	10.57	9.47E-03	5.53	0.0341	185.79	0.0871	0.5155	21.13
PT07		267	4.80	2.12	0.0508	231.18	23.69	1.20E-02	279.28	0.0627	15.82	9.63	1.05E-02	2.99	0.0570	128.37	0.0035	0.0000	0.36
PT08		264	4.83	2.03	0.0927	223.68	19.22	1.29E-07	263.42	0.0080	15.75	9.55	8.93E-03	2.27	0.0534	151.39	0.0560	1.4725	12.08
PT10		272	4.93	2.95	0.0552	198.93	22.33	4.73E-01	240.91	0.0083	14.43	9.81	4.30E-03	4.75	0.1065	29.89	0.0020	0.0000	5.45
PT02	30	242	5.57	5.16	0.0900	222.95	22.18	2.26E-05	258.13	0.1662	14.76	9.90	5.51E-03	4.01	0.9280	28.99	0.0254	0.4491	4.11
PT04		246	5.69	6.30	0.0762	238.44	24.07	6.80E-06	284.05	0.0614	9.37	10.17	2.89E-03	2.75	0.1749	12.54	0.0394	0.5790	2.16
PT05		257	4.83	5.15	0.0697	289.66	28.75	2.17E-06	358.74	0.0923	18.19	10.78	1.03E-02	4.35	0.0434	144.62	0.0283	0.3476	16.43
PT07		243	5.02	5.95	0.0621	254.64	25.72	5.19E-02	304.76	0.1194	16.74	10.05	1.10E-02	2.31	0.0610	100.04	0.0018	0.0000	0.28
PT08		241	5.03	5.77	0.0946	248.82	22.25	1.60E-06	292.42	0.0414	16.69	9.98	9.90E-03	1.82	0.0559	117.83	0.0215	1.0875	9.39
PT10		247	5.30	6.58	0.0650	229.54	24.65	4.54E-01	274.91	0.0492	15.64	10.19	5.78E-03	3.66	0.1377	23.58	0.0017	0.0000	4.24

kgw-kg water

7 Summary and Conclusions

The effects of calcite formation on the operation of geothermal power plants and facilities have been reported and published since the utilization of geothermal resources for power generation and space heating. The precipitation of calcium carbonate minerals (mostly calcite and rare aragonite) is enhanced by depressurization boiling. Ultimately, however, the potential for precipitation and scale formation are dependent on saturation of the initial aquifer fluid and the processes it undergoes like boiling, phase segregation and mixing.

A comparative assessment of the calcite precipitation potential of geothermal fluids from some of the Hengill-Hellisheidi geothermal wells in Iceland, Pataan wells in Northern Negros, Philippines and Mahanagdong wells in Leyte, Philippines are presented in this thesis. These include wells that were suspected and/or have been known to be affected by calcite scale formation such as wells from Pataan and wells MG01 and MG19 from Mahanagdong and well MD01 from Mindanao Geothermal Production Field. Two sets of data for wells MG01 and MG19 were compared for changes in the aquifer fluid and calcite saturation after 15 years of production. The wells from these geothermal fields should represent the varying characteristics of geothermal fluid discharges in different geological settings, ranging in composition from dilute to high salinities, and from different host rocks, i.e. basaltic and andesitic.

Webre-separator installed at the two-phase line near the wellhead was used to separate and collect steam and liquid water samples at the same sampling pressure. Steam samples were collected using double-ended gas bulbs (one evacuated containing hydroxide solution for for non-condensible (CO_2 and H_2S) and residual gases (H_2, CH_4, Ar and N_2) and one for NH_3 analysis). CO_2 and H_2S in the hydroxide solution were analyzed by titration while the residual gases in the head space of the gas sampling bulbs were analyzed on a gas-chromatograph. NH_3 in the steam condensate was analyzed by ion-selective electrode method. At Hellisheidi, CO_2 was also determined by ion chromatography.

Three sets of liquid water samples were collected for each well namely, filtered, filtered and acidified (0.5ml HNO_3 to 1000 ml sample) and unfiltered.

Water and gas analyses from Hellisheidi geothermal wells are from by Stefansson et al (2009), Mahanagdong wells were from Angcoy (2010) and Pataan wells were from Olivar (personal comm.). Water and gas samples from Hellisheidi and Mahanagdong were taken during normal production discharges of the wells whereas Pataan water and gas samples were taken before commercial production or during discharge testing of the wells.

Separated water from Hellisheidi wells are highly alkaline (8.47-9.24) while that from Pataan and Mahanagdong are slightly acidic to near-neutral. Pataan has the most saline separated water (>10,000 ppm Cl) followed by Mahanagdong (2,000<Cl< 7,500 ppm) and Hellisheidi has dilute water (< 500 ppm Cl). Dissolved H_2S is high in Hellisheidi (20 – 80 ppm) compared to Mahanagdong (0.3 -2.7 ppm) and Pataan (2-10

ppm). However, dissolved CO_2 in Hellisheidi (4-35 ppm) is lowest compared to Mahanagdong (17-74 ppm) and Pataan (30-68 ppm).

Separated vapour from Pataan wells has the highest CO2 concentration (431-1073 mmol/kg) while Hellisheidi has the lowest concentration (10-155 mmol/kg) and Mahanagdong at the middle (132-628 mmol/kg). Hellisheidi has high H2 gas concentration (up to 34 mmol/kg) compared to Mahanagdong (< 2 mmol/kg) and Pataan (<1 mmol/kg).

Separated water and gas analyses from the wells were used to calculate aquifer fluid compositions using the speciation program WATCH 2.1.

The total discharge SiO_2 approaches zero when the total fluid enthalpy approaches that of saturated steam .This is taken to indicate that the "excess" discharge enthalpy of the wells is best explained by phase segregation rather than conductive heating of the fluid by host rock. In addition, Na/K and quartz temperature agree well by the phase segregation model while Na/K temperature are generally higher than quartz for the close system model. Based from these observations it is concluded that "excess" enthalpy is mostly caused by phase segregation in the producing aquifers of Hellisheidi, Mahanagdong and Pataan wells; thus, phase segregation model was used to calculate aquifer compositions.

In this study, the phase segregation temperature was selected to correspond to the vapour saturation pressure at the midpoint between the sampling vapour pressure and the saturation vapour pressure at the selected aquifer temperature. Selected aquifer temperature is based on quartz temperature. The calculation of the aquifer fluid composition was done in two-step run by the speciation program WATCH. Separated water and gas analyses, measured discharge enthalpy and measured pH were used in the first WATCH run which used arbitrary reference temperature equal to the segregation temperature. The output of the first WATCH run was then used as input in the second WATCH run to calculate the initial aquifer fluid composition assuming the flowing fluid to have saturated liquid enthalpy corresponding to the initial aquifer temperature.

The mean percentage differences for quartz and cation geothermometers for individual wells were within 5% (13 oC) except for very high enthalpy wells HE12, HE29 and MG40 and for most of the Pataan wells. No wells exceeded 10% mean percentage differences. The mean percentage difference for all the wells is 4 %. The mean standard deviation of calculated geothermometer temperatures for the wells is 11 oC.

H_2S aquifer fluid concentrations of Hellisheidi and Pataan are close to equilibrium with the pyrite-pyrrhotite-magnetite mineral assemblage except HE03 which is significantly below the curve and was found to be highly degassed. Hellisheidi H_2S aqueous concentration can also be controlled by pyrite-pyrrhotite-prehnite-epidote mineral assemblage but aqeous H_2S concentrations at equilibrium with either of these assemblages are very similar. The data points of Mahanagdong wells are systematically above the equilibrium magnetite-hematite-pyrite mineral assemblage by about 2000J/mol which is within the limit of error according to the data on enthalpy reported by Holland and Powell (1998) on these minerals.

Na/K versus H_2S temperatures and quartz versus H_2S temperatures of the closed system and phase segregation models show inconsistency for the closed system model but not for the phase segregation model. The geothermometer results for the three

study areas substantiate the conclusion that "excess" enthalpy is mostly caused by phase segregation in producing aquifer.

Hellisheidi's H_2 aquifer fluid concentrations were found to be controlled by pyrite-pyrrhotite-magnetite or pyrite-pyrrhotite-prehnite-epidote mineral assemblage. Mahanagdong and Pataan H_2 aquifer fluid concentrations on the other hand were found to be controlled by magnetite-hematite mineral assemblage.

Hellisheidi CO_2 concentrations were consistently lower than those corresponding to equilibrium while Mahanagdong and Pataan wells were slightly above or at equilibrium with the mineral assemblage clinozoisite-calcite-quartz-prehnite or clinozoisite-calcite-quartz-grossular. One cause of the low CO_2 values at Hellisheidi may be insufficient supply of this gas to the fluid.

Aquifer fluid composition calculations show that Hellisheidi's pH range is alkaline to slightly alkaline (7-7.4) while Mahanagdong's pH is near neutral around 5.5 (5.3 – 5.9) except for MG40 (pH =4.3) which is a very high enthalpy well. MG40 could be affected by steam condensates or other acidic fluids as it also has the highest concentration of Fe and Mg in Mahanagdong. Pataan wells have slightly acidic pH (4.9 – 5.6).

Hellisheidi wells have higher concentrations of H_2 (up to 8 ppm) compared to Mahanagdong and Pataan wells (less than 0.5 ppm). Hellisheidi wells also have higher concentrations of H_2S of up to 250 ppm compared to Mahanagdong (<140 ppm) and Pataan (<200 ppm) wells. Pataan wells have the highest CO_2 concentration (up to 9700 ppm) followed by Mahanagdong (up to 5300 ppm) while Hellisheidi wells have the lowest (less than 900 ppm).

Chloride-bicarbonate-sulfate ternary diagram of all the wells under study show that Hellisheidi wells are distributed between peripheral water and mature water while most of Mahanagdong and Pataan wells are halfway towards the mature water type.

Na-K-Mg ternary diagram of the wells show that they are discharging partially mixed/ equilibrated to fully equilibrated waters with respect common hydrothermal minerals.

The aquifer fluids are close to equilibrium with calcite and when all uncertainties are taken to account, such as analytical imprecision and selection of aquifer temperatures, departure from saturation are not significant. The average departure from calcite saturation of Hellisheidi wells is only 0.05 SI units, Mahanagdong is 0.2 SI units below the equilibrium while Pataan wells is 0.2 SI units above the equilibrium. Only MG40 well showed high level of undersaturation of 2.1 SI units. MG40 has high "excess" enthalpy and is acidic. Well PT02 is the most oversaturated with 0.74 SI units.

The calculated saturation index for calcite increases with increasing value of the calculated aquifer water pH. This is considered to be due to error in the calculated aquifer water pH. Many factors affect the calculated pH and it is not possible to identify the main sources of apparent variation in pH and calcite saturation index but it seems to be significant, particularly in the case of Hellisheidi.

Mahanagdong and Pataan aquifer fluids approach anhydrite equilibrium whereas Hellisheidi waters are considerably anhydrite undersaturated.

At equilibrium, the redox reactions involving pyrite, magnetite, H_2S and H_2 fixes the aqueous H_2S and H_2 molal ratios. The Hellisheidi water are quite close to equilibrium, with an average of 0.03 log units above the curve. Mahanagdong and Pataan aquifer waters were systematically with higher H_2S/H_2 ratios than those corresponding to equilibrium, by 0.2 and 0.55 log units on average, respectively.

The redox reactions involving pyrite, pyrrhotite, H_2S and H_2 could also fix aqueous H_2S and H_2 molal ratios. The Hellisheidi aquifer waters are close to equilibrium yet systematically below the equilibrium curve on average by 0.25 log units, if the degassed discharge of HE03and HE05 are excluded. Mahanagdong and Pataan aquifer waters are systematically with higher H_2S/H_2 ratios than those corresponding to equilibrium, by 0.96 and 1.3 log units on average, respectively. Clearly the H_2S/H_2 ratios in the aquifer waters in the Philippine geothermal fields are not controlled by the pyrite-pyrrhotite buffer.

An overall pattern in the variation of the saturation index (SI) from Hellisheidi wells with temperature is observed from all the wells except well HE03 upon adiabatic boiling and degassing. The SI initially increases then, after it reaches a peak, decreases to negative values. The initial increase in SI reflects an increase in pH due to CO_2 and H_2S degassing. The pH increase caused a strong increase in the activity of the CO_3^{-2} species. At maximum SI values, the water has been largely degassed, and the subsequent decline in SI is caused by increased calcite solubility with decreasing temperature. Well HE03 is highly degassed as reflected by the low gas content of the discharge. Boiling of the degassed water causes a decrease in the value of SI. The extent of degassing (as expressed by the degassing coefficient) increases the level of calcite SI except for degassed well HE03 which showed the opposite.

The majority of the wells in Mahanagdong followed the general pattern exhibited by Hellisheidi wells except MG40, MG29, MG14 and MG03. MG40 is a high "excess" enthalpy and is acidic. MG03 and MG14 were postulated to receive fluid from the upflow zone but have been affected by brine injection returns. The reservoir chloride levels of MG03 and MG14 are shifted towards the composition of the injected brine. Well MG29, on the other hand, is located in the western periphery of the Mahanagdong geothermal system and could be affected by intrusion of cooler peripheral waters. The highest positive departure from the initial saturation in Mahanagdong is from MG19, with 0.40 (at 251 ^oC) SI units above the initial saturation at maximum degassing Calcite scale is known to form in MG19.

Boiling of MG01 aquifer fluid sampled in 1994 produces an increase in calcite saturation of 0.51 SI units above the initial saturation which is high compared to the more recent sample with only 0.07 SI units departure from the initial saturation. Comparing MG01 CO2 and H2S concentrations on samples taken in 2009 and 1994 shows that it has been partially degassed or mixed with degassed injected brine. Aquifer aqueous CO2 concentration decreased from 8000 to 1200 ppm and H2S concentration decreased from 92 to 15 ppm. Activity of free Ca2+ probably affects calcite saturation because it partially increased from 10 to 16 ppm in 1994 to 2009 samples.

The case of MG19 is similar with MG01. The present fluid discharge is partially degassed or mixed with injected brine and Ca^{2+} concentration has increased. Aquifer aqueous CO_2 concentration decreased from 6900 to 3200 ppm, aqueous H_2S

concentration decreased from 71 to 36 ppm and Ca^{2+} increased from 11 to 20 ppm. Calcite mineral SI trend of MG19 practically remains the same after almost 15 years of production, though the old data showed a higher departure of 0.48 SI units above the initial saturation compared to 0.40 SI units for the more recent sample.

Pataan aquifer fluids show trends similar to those of Hellisheidi and most of the Mahanagdong wells. Well PT08 shows the highest increase in the SI for calcite of 0.6 units (at 223 oC) above the initial saturation, followed by PT05, PT10 and PT07 with 0.40 (at 246 oC), 0.31(at 258 oC) and 0.28 (at 252 oC) SI units above the the initial saturation, respectively. PT05 was postulated to be nearest to the upflow region, followed by PT08 and PT07. Well PT05 has the highest dissolved aqueous CO2 concentration at 9700 ppm followed by PT08 and PT07 at 7800 and 6700 ppm, respectively.

Wells PT02 and PT04 have the lowest positive departure from the initial saturation at 0.10 (at 262 oC) and 0.15 (at 262 oC) SI units above the initial saturation, respectively.

The implications for Pataan of the above described observations are that 1) the aquifer fluid feeding PT05 and PT08 may precipitate calcite in the immediate aquifer formation and in the well when degassing is more than 50% 2) aquifer fluids feeding PT10 and PT07 may precipitate calcite in the aquifer if sufficient over-saturation is produced and 3) aquifer fluid feeding PT02 may precipitate calcite in the well and/or in the aquifer if the degassing is less than 50% of maximum.

It has been reported that PT02 is the only well that has physical evidence of calcite scale formation in the well. However, field-wide decline in total mass flow in the wells were documented during commissioning activities in 2007 that may be caused by calcite precipitation in producing aquifers.

The effect of boiling and degassing on calcite saturation for the one well from Mindanao Geothermal Production Field, MD01, is similar to Hellisheidi and Mahanagdong wells. It has highest departure of 0.425 SI units above the initial saturation at 241.5 oC and maximum degassing. This well is thought to be affected by calcite scaling.

The effect of fluid mixing particularly the injected separated water from the separators and aquifer fluids from Hellisheidi and Pataan areas were investigated. Pataan separated water is slightly acid, pH of 5.3 and higher in dissolved CO_2 than Hellisheidi. Hellisheidi separated water on the other hand is very alkaline with pH of 9.3 and has higher H_2S concentration than Pataan. Pataan separated water is being injected at temperature of 160 ^oC, which is used in both Pataan and Hellisheidi mixing simulations. The composition of the fluid mixtures were simulated using the aqueous modeling code PHREEQC-2 version 2.17.00 from the graphical interface PHREEQC for Windows. The mixed fluid compositions were then inputted into WATCH 2.1 to simulate boiling and degassing.

The results show that calcite saturation of the mixed fluids dropped to below the initial saturation of aquifer fluids. Increasing the injected separated water proportion in the mixture decreases the calcite saturation index of the mixed fluid for the case of Hellisheidi wells. In Pataan wells, however, increasing the separated water proportion in the mixture increases the calcite SI of the mixed fluid.

In Hellisheidi, the calcite saturation index of the mixed fluid upon boiling are below that of the initial aquifer fluid except HE11 where at 30% mix injected separated water, the saturation approach that of the initial aquifer fluid saturation. In Pataan, it seems that mixing injected separated water by more than 30% of the initial aquifer fluids will bring the saturation to or above the initial saturation upon adiabatic boiling.

References

Angcoy, Jr., E.C., 2010: Geochemical Modelling of the High-Temperature Mahanagdong Geothermal Field, Leyte, Philippines, Master's thesis, Faculty of Science, University of Iceland, pp. 130

Arnórsson, S., 1978: Precipitation of calcite from flashed geothermal waters in Iceland. *Contributions to Mineralogy and Petrology*, 66, 21-28.

Arnórsson, S., 1979: Hydrochemistry in Geothermal Investigations in Iceland Techniques and Applications. *Nordic Hydrology*, 191-224.

Arnórsson, S., 1983: Chemical equilibria in Icelandic geothermal systems--Implications for chemical geothermometry investigations. *Geothermics*, 12, 119-128.

Arnórsson, S., 1989: Deposition of calcium carbonate minerals from geothermal waters -- theoretical considerations. *Geothermics,* 18**,** 33-39.

Arnórsson, S., 1995a: Geothermal systems in Iceland: Structure and conceptual models--I. High-temperature areas. *Geothermics*, 24, 561-602.

Arnórsson, S., 1995b: Geothermal systems in Iceland: Structure and conceptual models--II. Low-temperature areas. *Geothermics*, 24, 603-629.

Arnórsson, S. (ed.), 2000: *Isotopic and chemical techniques in geothermal exploration, development and use. Sampling methods, data handling and interpretation*. International Atomic Energy Agency, Vienna, 351 pp.

Arnórsson, S., and Gunnlaugsson, E., 1983a: The chemistry of geothermal waters in Iceland II. Mineral equilibria and independent variables controlling water compositions. *Geochim. Cosmochim. Acta, 47*, 547-566.

Arnórsson, S., Grönvold, K. And Sigurdsson, S., 1978: Aquifer chemistry of four high-temperature geothermal systems in Iceland. *Geochimica et Cosmochimica Acta*, 42, 523-536.

Arnórsson, S., Gunnlaugsson, E., and Svavarsson, H., 1983b: The chemistry of geothermal waters in Iceland III. Chemical geothermometry in geothermal investigations. *Geochim. Cosmochim. Acta, 47*, 567-577.

Arnórsson, S. and Andrésdóttir, A., 1999: The dissociation constants of Al-hydroxy complexes at 0-350°C and P_{sat}. IN ÁRMANSSON, H. (Ed.) *5th International symposium on Geochemistry of the Earth's Surface.* Rotterdam, Balkema.

Arnórsson, S., Sigurdsson, S. and Svavarsson, H., 1982: The chemistry of geothermal waters in Iceland. I. Calculation of aqueous speciation from 0° to 370°C. *Geochimica et Cosmochimica Acta,* 46**,** 1513-1532.

Arnórsson, S., Stefansson, A. and Bjarnason, J. O., 2007: Fluid-Fluid Interactions in Geothermal Systems. *Reviews in Mineralogy and Geochemistry,* 65**,** 259-312.

Arnórsson, S., Geirsson, K., Andrésdóttir, A. and Sigurdsson, S., 1996: Compilation and evaluation of thermodynamic data on aqueous species and dissociational equilibria in aqueous solution I. The solubility of CO_2, H_2S, H_2, CH_4, N_2, O_2 and Ar in pure water. Reykjavik, Science Institute, University of Iceland.

Arnórsson, S., Gunnarsson, I., Stefánsson, A., Andrésdóttir, A., and Sveinbjörnsdóttir, A.E., 2002: Major element chemistry of surface- and ground waters in basaltic terrain, N-Iceland. I. Primary mineral saturation. *Geochim. Cosmochim. Acta, 66,* 4015-4046.

Arnórsson, S., Bjarnason, J.Ö., Giroud, N., Gunnarsson, I., and Stefánsson, A., 2006: Sampling and analysis of geothermal fluids, *Geofluids*, *6,* 203-216.

Arnórsson, S., Angcoy, E. C., Bjarnason, J. Ö., Giroud, N., Gunnarsson, I., Kaasalainen, H., Karingithi, C. and Stefánsson, A., 2010: Gas Chemistry of Volcanic Geothermal Systems. *2010 World Geothermal Congress.* Bali, Indonesia.

Böðvarsson, G., 1961: Physical characteristics of natural heat resources in Iceland *Jökull* 11**,** 29-38.

Bjarnason, J. Ö., 1994: The speciation program WATCH, version 2.1. Reykjavik, Iceland, Orkustofnun.

Diakonov, I. and Tagirov, B. R., 2002: Iron (III) speciation in aqueous solutions: Part 2. Thermodynamic properties of $Fe(OH)^{+2}$, $Fe(OH)^{+2}$ and $Fe(OH)_3°$ species and solubility of iron (III) oxides, and hydroxides. In preparation.

Fournier, R.O., and Potter, R.W. II, 1982: A revised and expanded silica (quartz) geothermometer. *Geoth. Res. Council Bull.,11-10*, 3-12.

Franzson, H., Kristjánsson, B. R., Gunnarsson, G., Björnsson, G., Hjartarson, A., Steingrímsson, B., Gunnlaugsson, E. and Gíslason, G., 2005: The Hengill-Hellisheiði Geothermal Field. Development of a Conceptual Geothermal Model. *Proceedings World Geothermal Congress 2005*. Antalya, Turkey.

Fernandez-Prini, R., Alvarez, J.L. and Harvey, A.H., 2003: Henry's constants and vapour-liquid distribution constants for gaseous solutes in H_2O and D_2O at high temperatures. *J. Phys. Chem. Ref. Data* 32, 903-916.

Giggenbach, W.F., 1980: Geothermal gas equilibria. *Geochim. Cosmochim. Acta*, 44, 2021-2032.

Giggenbach, W.F., 1981: Geothermal mineral equilibria. *Geochim. Cosmochim. Acta*, 45, 393-410.

Giggenbach, W. F., 1988: Geothermal solute equilibria. Derivation of Na-K-Ca-Mg geoindicators. *Geochim. Cosmochim. Acta*, 52: 2749-2765.

Gislason, S. R. and Arnórsson, S., 1993: Dissolution of primary basaltic minerals in natural waters: saturation state and kinetics. *Chemical Geology*, 105, 117-135.

Gudmundsson, B. T. and Arnórsson, S., 2005: Secondary mineral-fluid equilibria in the Krafla and Námafjall geothermal systems, Iceland. *Applied Geochemistry*, 20, 1607-1625.

Gunnarsson, I. and Arnórsson, S., 2000: Amorphous silica solubility and the thermodynamic properties of $H_4SiO_4^\circ$ in the range of 0° to 350°C at P_{sat}. *Geochimica et Cosmochimica Acta,* 64**,** 2295-2307.

Gunnarsson, I. and Arnórsson, S., 2005: Impact of silica scaling on the efficiency of heat extraction from high-temperature geothermal fluids. *Geothermics,* 34**,** 320-329.

Holland, T. J. B. and Powell, R., 1998: An internally consistent thermodynamic data set for phases of petrological interest. *J. metamorphic Geol,* 16**,** 309-344.

Karingithi, C.W., Arnórsson, S., and Grönvold, K., 2010: Processes controlling aquifer fluid compositions in the Olkaria geothermal system, Kenya. *J. Volc. Geothermal Res. (in press).*

Mutonga, M. W., 2007: The Isotopic and Chemical Characteristics of Geothermal Fluids In Hengill Area, Sw-Iceland: Hellisheidi, Hveragerdi And Nesjavellir Fields. Reykjavik, Iceland, United Nations University - Geothermal Training Programme.

Olivar, M. V. M., 2007: The Geochemistry of Northern Negros Geothermal Production Field. Taguig City, Philippines, Energy Development Corporation. *Internal report (unpublished).*

Parkhurst, D. L. and Appelo, C. A. J., 1999: User's guide to PHREEQC (Version2)-A computer program for speciation, batch-reaction, one-dimensional transport, and inverse geochemical calculations U.S.Geological Survey Water-Resources Investigations Report 99-4259.

Parkhurst, D. L., Thorstenson, D. C. and Plummer, L. N., 1980: PHREEQE--A computer program for geochemical calculations. U.S. Geological Survey Investigations Report 80-96.

Pokrovski, G. S., Schott, J., Salvi, G., Gout, R. and Kubicki, J. D., 1998: Structure and stability of aluminium-silica complexes in neutral to basic solutions. Experimental study and molecular orbital calculations. *Min. Mag.,* 62A**,** 1194-1195.

Rahmani, M. R., 2007: Assessment Of Calcite Scaling Potential In The Geothermal Wells Of The Nw-Sabalan Geothermal Prospect, Nw-Iran. Reykjavik City, Iceland, United Nations University - Geothermal Training Programme.

Robie, R.A. and Hemmingway, B.S., 1995: Thermodynamic properties of minerals and related substances at 298.15 K and 1 bar (10^5 Pascals) pressures and at higher temperatures. *USGS. Bull.* 2131, 461p.

Salonga, N. D., Dacillo, D. B. and Siega, F. L., 2004: Providing solutions to the rapid changes induced by stressed production in Mahanagdong geothermal field, Philippines. *Geothermics,* 33**,** 181-212.

Sanchez, D. R., Baltasar, A. S. J. and Candelaria, M. N. R., 2005: Evaluation of Chemical Equilibria of Calcite Deposition in a Geothermal Well at Northern Negros Geothermal Project, Philippines. *Proceedings World Geothermal Congress 2005*. Antalya, Turkey.

Satman, A., Ugur, Z. and Onur, M., 1999: The effect of calcite deposition on geothermal well inflow performance. *Geothermics*, 28, 425-444.

Siega, F. L., Herras, E. B. and Buñing, B. C., 2005: Calcite Scale Inhibition: The Case of Mahanagdong Wells in Leyte Geothermal Production Field, Philippines. *Proceedings World Geothermal Congress 2005*. Anatalya,Turkey.

Stáhl, G., Pátzay, G., Weiser, L. and Kálmán, E., 2000: Study of calcite scaling and corrosion processes in geothermal systems. *Geothermics*, 29, 105-119.

Stefánsson, A., 2001: Dissolution of primary minerals of basalt in natural waters: I. Calculation of mineral solubilities from 0°C to 350°C. *Chemical Geology*, 172, 225-250.

Stefánsson, A., Gíslason, S. R. and Arnórsson, S., 2001: Dissolution of primary minerals in natural waters: II. Mineral saturation state. *Chemical Geology*, 172, 251-276.

Stefánsson, A. and Arnórsson, S., 2002: Gas pressures and redox reactions in geothermal fluids in Iceland. *Chemical Geology*, 190, 251-271.

Stefánsson, A., Gunnarsson, I., and Giroud, N., 2007: New methods for the direct determination of dissolved inorganic, organic and total carbon in natural waters by Reagent-Free TM Ion Chromatography and inductively coupled plasma atomic emission spectrometry. *Analytical Chimica Acta, 582*, 69-72.

Tole, M. P., Ármannsson, H., Zhong-He, P. and Arnórsson, S., 1993: Fluid/mineral equilibrium calculations for geothermal fluids and chemical geothermometry. *Geothermics*, 22, 17-37.

Urbino, G.A. and Zhong-He, P., 2006: 2003 Inter-laboratory comparison of geothermal water chemistry. In: Zhong-He, P., and, Ármansson, H. (eds.), *Analytical procedures and quality assurance for geothermal water chemistry*. UNU-GTP, Reykjavik, Iceland, 131-172.

Zhong-He, P. and Ármansson, H., 2006: Analytical procedures and quality assurance for geothermal water chemistry. Reykjavik City, Iceland, United Nations University - Geothermal Training Programme.

Appendix A

Example of PHREEQC input file for mixing of aquifer fluid and injected separated water from the separators

```
Title  Pataan Aquifer Fluid and Injected Separated Water Mixing
Solution 1   Analytical results of separated water from the separators
        units       ppm
        pH          5.29
        Temp        23.9        # Temperature in °C
        Na          7558
        K           1254
        Ca          702
        Mg          2.54
        Fe          0.85
        Li          28.2
        F           5.19
        Cl          13629
        S(6)        26.7        # SO4 concentration
        B           211
        Amm         8.85        # NH3 concentration as NH4+
        Si          675         # SiO2 concentration
        C(+4)       40.09       # total carbonate carbon concentration as HCO3-
REACTION_TEMPERATURE 1
20.0 160.0 in 15 steps      # Separated water temperature is brought to 160 °C
SAVE SOLUTION 1             # Saves the simulated 160 °C separated water to Solution
1
END
Solution 2   Aquifer fluid composition of PT02
        units       ppm
        Temp        277
        pH          5.57
        B           134
        Si          545
        Cl          6975
        Na          3940
        K           677
```

```
        Mg          2.14
        Ca          329.80
        F           4.01
        S(6)        20.43           # SO4 concentration
        Fe          0.34
        C(4)        2927            # total carbonate carbon concentration as HCO3-
        S(-2)       175             # H2S concentration as HS-
        Amm         65.42           # NH3 concentration as NH4+
        H(0)        0.39            # H2 concentration
        C(-4)       36              # CH4 concentration
        N(0)        358             # N2 concentration
# 5% Separated water
MIX 1
1 0.05          # takes 0.05 fraction of solution 1
2 0.95          # adds 0.95 fraction of solution 2
END
# 10 Separated water
MIX 2
1 0.10
2 0.90
END
# 30% Separated water
MIX 3
1 0.30
2 0.70
END
```